

REVIEW ARTICLE

Progress Toward Understanding Baryon Resonances

V. Crede and W. Roberts

Florida State University, Department of Physics, Tallahassee, FL 32306, USA

E-mail: crede@fsu.edu, wroberts@fsu.edu

Abstract. The composite nature of baryons manifests itself in the existence of a rich spectrum of excited states, in particular in the important mass region 1-2 GeV for the light-flavoured baryons. The properties of these resonances can be identified by systematic investigations using electromagnetic and strong probes, primarily with beams of electrons, photons, and pions. After decades of research, the fundamental degrees of freedom underlying the baryon excitation spectrum are still poorly understood. The search for hitherto undiscovered but predicted resonances continues at many laboratories around the world. Recent results from photo- and electroproduction experiments provide intriguing indications for new states and shed light on the structure of some of the known nucleon excitations. The continuing study of available data sets with consideration of new observables and improved analysis tools have also called into question some of the earlier findings in baryon spectroscopy. Other breakthrough measurements have been performed in the heavy-baryon sector, which has seen a fruitful period in recent years, in particular at the B factories and the Tevatron. First results from the LHC indicate rapid progress in the field of bottom baryons. In this review, we discuss the recent experimental progress and give an overview of theoretical approaches.

PACS numbers: 12.39.-x Phenomenological quark models, 13.60.Le Meson production, 13.60.-r Photon and charged-lepton interactions with hadrons, 13.75.Gx Pion-baryon interactions, 25.20.Lj Photoproduction reactions

1. Introduction

A better understanding of the nucleon as a bound state of quarks and gluons as well as the spectrum and internal structure of excited baryons remains a fundamental challenge and goal in hadronic physics. In particular, the mapping of the nucleon excitations provides access to strong interactions in the domain of quark confinement. While the peculiar phenomenon of confinement is experimentally well established and believed to be true, it remains analytically unproven and the connection to quantum chromodynamics (QCD) – the fundamental theory of the strong interactions – is only poorly understood. In the early years of the 20th century, the study of the hydrogen spectrum has established without question that the understanding of the structure of a bound state and of its excitation spectrum need to be addressed simultaneously. The spectroscopy of excited baryon resonances and the study of their properties is thus complementary to understanding the structure of the nucleon in deep inelastic scattering experiments that provide access to the properties of its constituents in the ground state. However, the collective degrees of freedom in such experiments are lost.

An extensive data set of observables in light-meson photo- and electro-production reactions has been accumulated over recent years at facilities worldwide such as Jefferson Laboratory in the United States, the ELeCtron Stretcher Accelerator (ELSA), the MAInz MIcrotron (MAMI), and the GRenoble Anneau Accelérateur Laser (GRAAL) facility in Europe as well as the 8 GeV Super Photon Ring (SPRING-8) in Japan hosting the Laser Electron Photon Experiment (LEPS). The data set includes cross section data and polarisation observables for a large variety of final states, such as πN , ηN , ωN , $\pi\pi N$, $K\Lambda$, $K\Sigma$, etc. These data complement the earlier spectroscopy results from π - and K -induced reactions. For a long time, the lack of experimental data and the broad and overlapping nature of light-flavour baryon resonances has obscured our view of the nucleon excitation spectrum. These experiments therefore represent an important step toward the unambiguous extraction of the scattering amplitude in these reactions, which will allow the identification of individual resonance contributions.

Hadronic spectroscopy cannot be interpreted by applying standard perturbation theory: phenomenology as well as QCD-based models have provided much of the insight and theoretical guidance. The recent advances in lattice gauge theory and the availability of large-scale computing technology make it possible for the first time to complement these approaches with numerical solutions of QCD. Spin-parity assignments for excited states have even been successfully worked out by some groups. Some collaborations have carried out simulations with pion masses as light as 156 MeV, but the resonance nature of the states, as well as the presence of thresholds complicate the extraction of information from such calculations. In addition, to the best of our knowledge, such simulations have focused on states with lower values of angular momentum. In other simulations with larger pion masses ($m_\pi \gtrsim 400$ MeV), a rich spectrum of excited states is obtained, and the low-lying states of some lattice-QCD calculations have the same quantum numbers as the states in models based on three

quarks with wave functions based on the irreducible representations of $SU(6) \otimes O(3)$. The good qualitative agreement may be surprising since the connection between the relevant quark degrees of freedom, the constituent or dressed quarks, and those of the QCD Lagrangian is not well understood. The lattice results appear to answer the long-standing question in hadron spectroscopy of whether the large number of excited baryons predicted by quark models, but experimentally not observed, is realised in nature.

The main goals of recent experiments are the determination of the excited baryon spectrum, the identification of possible new symmetries in the spectrum, and understanding the structure of states that appear to be built of three valence quarks at a microscopic level. The fundamental questions comprise the quest for the number of relevant degrees of freedom and a better understanding of the mechanisms responsible for confinement and chiral symmetry breaking: How are the valence or dressed quarks with their clouds of gluons and quark-antiquark pairs related to the quark and gluon fields of the underlying Lagrangian of QCD? How does the chiral symmetry structure of QCD lead to dressed quarks and produce the well-known long distance behaviour? The new experimental and theoretical information bears directly on both the search for, and our current understanding of baryon resonances. This paper will review the new data, present an overview of theoretical approaches and a sampling of the phenomenological work that has been developed based on the new experimental results.

1.1. Guide to the Literature

The Particle Data Group (PDG) regularly includes minireviews on a large variety of topics in their Reviews of Particle Properties (RPP), which have been published biennially for many decades. Useful minireviews on N^* and Δ resonances as well as charmed baryons can be found in the latest edition of the RPP [1]. Owing to the lack of suitable K beams, little progress has been reported in reviews on Λ and Σ resonances in the 2010 edition of the RPP [2]. The latter also includes a very brief note on Ξ baryons based on a previous review by Meadows, published in the proceedings of the *Baryon 1980* conference [3].

A comprehensive review of baryon spectroscopy is contained in the 2009 article by Klempt and Richard [4], who discuss prospects for photo- and electroproduction experiments. Some of the open questions discussed in that review have already found answers from recent measurements. An older general article on baryon spectroscopy by Hey and Kelly [5] still provides useful information, particularly on some aspects of the theoretical data analysis. Quark model developments have been discussed by Capstick and Roberts in 2000 [6].

Further reviews were dedicated to particular aspects of experiments using electromagnetic probes. About a decade ago, Krusche and Schadmand gave a nice summary on low-energy photoproduction [7] and in 2007, Drechsel and Walcher looked at hadron structure at low Q^2 [8]. The work of Tiator *et al.* [9] and Aznauryan and Burkert [10] provide more recent reviews on the electroexcitation of nucleon resonances.

2. Baryon Spectroscopy

Baryons are strongly interacting fermions and all established baryons are consistent with a qqq configuration, so that the baryon number is $B = \frac{1}{3} + \frac{1}{3} + \frac{1}{3} = 1$. Other exotic baryons have been proposed, such as pentaquarks – baryons made of four quarks and one antiquark ($B = \frac{1}{3} + \frac{1}{3} + \frac{1}{3} + \frac{1}{3} - \frac{1}{3} = 1$), but their existence is not generally accepted. In quantum chromodynamics, heptaquarks (5 quarks, 2 antiquarks), nonaquarks (6 quarks, 3 antiquarks), etc. could also exist. Baryons which consist only of u and d quarks are called nucleons if they have isospin $I = \frac{1}{2}$ or Δ resonances if they have isospin $I = \frac{3}{2}$. Baryons containing s quarks are called hyperons and are labelled as Λ , Σ , Ξ , and Ω depending on the number of s quarks and isospin (Table 1). Baryons containing c or b quarks are labelled with an index. For example, the Λ_c^+ has isospin zero and quark content udc , the Ξ_c^+ has quark content usc and the Ξ_{cc}^{++} has quark content ucc .

2.1. Baryons Composed of u , d and s Quarks

As fermions baryons obey the Pauli principle, so the total wave function

$$|qqq\rangle_A = |\text{colour}\rangle_A \times |\text{space, spin, flavour}\rangle_S \quad (2.1)$$

must be antisymmetric (denoted by the index A) under the interchange of any two equal-mass quarks. Since all observed hadrons are colour singlets, the colour component of the wave function must be completely antisymmetric. For the light-flavour baryons, the three flavors u , d and s can be treated in an approximate SU(3) framework, in which each quark is a member of an SU(3) triplet. The flavour wave functions of baryon states can then be constructed to be members of SU(3) multiplets as

$$\mathbf{3} \otimes \mathbf{3} \otimes \mathbf{3} = \mathbf{10}_S \oplus \mathbf{8}_M \oplus \mathbf{8}_M \oplus \mathbf{1}_A. \quad (2.2)$$

The proton and neutron, of which all the matter that we see is composed, are members of both octets. The weight diagrams for the decuplet and octet representations of SU(3) are shown in Figure 1.

The total baryon spin has two possible values. The three quark spins ($s = \frac{1}{2}$) can yield a total baryon spin of either $S = \frac{1}{2}$ or $S = \frac{3}{2}$. The latter configuration yields a completely symmetric spin wave function, whereas the $S = \frac{1}{2}$ state exhibits a mixed

Table 1. Summary of baryon quantum numbers. Antihyperons have positive Strangeness +1, +2, and +3.

	N	Δ	Λ	Σ	Ξ	Ω
Isospin, I	$\frac{1}{2}$	$\frac{3}{2}$	0	1	$\frac{1}{2}$	0
Strangeness, S	0		-1		-2	-3
Number of strange quarks	0		1		2	3

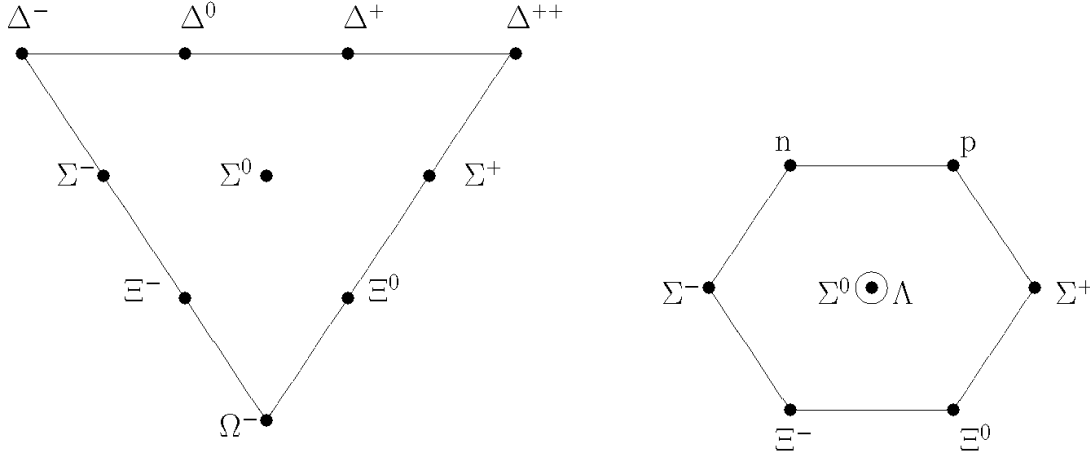


Figure 1. The symmetric **10** (left) and mixed symmetric **8** (right) of $SU(3)$.

symmetry. The flavour and spin can be combined in an approximate spin-flavour $SU(6)$, where the multiplets are

$$\mathbf{6} \otimes \mathbf{6} \otimes \mathbf{6} = \mathbf{56}_S \oplus \mathbf{70}_M \oplus \mathbf{70}_M \oplus \mathbf{20}_A. \quad (2.3)$$

These can be decomposed into flavour $SU(3)$ multiplets

$$\mathbf{56} = {}^4\mathbf{10} \oplus {}^2\mathbf{8} \quad (2.4)$$

$$\mathbf{70} = {}^2\mathbf{10} \oplus {}^4\mathbf{8} \oplus {}^2\mathbf{8} \oplus {}^2\mathbf{1} \quad (2.5)$$

$$\mathbf{20} = {}^2\mathbf{8} \oplus {}^4\mathbf{1}, \quad (2.6)$$

where the superscript $(2S + 1)$ gives the spin for each particle in the $SU(3)$ multiplet. The proton and neutron belong to the ground-state **56**, in which the orbital angular momentum between any pair of quarks is zero, and are members of the octet with spin and parity $J^P = \frac{1}{2}^+$. The Δ resonance is a member of the decuplet with spin and parity $J^P = \frac{3}{2}^+$. We refer the interested reader to the literature for the correctly symmetrized wave functions for the $SU(3)$ multiplets. The wave functions of the **70** and **20** require some excitation of the spatial part to make the overall non-colour (spin \times space \times flavour) component of the wave function symmetric. Orbital motion is accounted for by classifying states in $SU(6) \otimes O(3)$ supermultiplets, with the $O(3)$ group describing the orbital motion.

In addition to spin-flavour multiplets, it is convenient to classify baryons into bands according to the harmonic oscillator model with equal quanta of excitation, $N = 0, 1, 2, \dots$. Each band consists of a number of supermultiplets, specified by (\mathbf{D}, L_N^P) , where \mathbf{D} is the dimensionality of the $SU(6)$ representation, L is the total quark orbital angular momentum, and P is the parity. The first-excitation band contains only one supermultiplet, $(\mathbf{70}, 1_-^-)$, corresponding to states with one unit of orbital angular momentum and negative parity, whereas the second-excitation band contains

Table 2. Supermultiplets, (\mathbf{D}, L_N^P) , contained in the first three bands [1] and assignments for the ground-state octet and decuplet to known baryons.

N	Supermultiplets				
0	$(\mathbf{56}, 0_0^+)$				
$S = \frac{1}{2}^+$	$N(939)$	$\Lambda(1116)$	$\Sigma(1193)$	$\Xi(1318)$	
$S = \frac{3}{2}^+$	$\Delta(1232)$	$\Sigma(1385)$	$\Xi(1530)$	$\Omega(1672)$	
1	$(\mathbf{70}, 1_1^-)$				
2	$(\mathbf{56}, 0_2^+)$	$(\mathbf{70}, 0_2^+)$	$(\mathbf{56}, 2_2^+)$	$(\mathbf{70}, 2_2^+)$	$(\mathbf{20}, 1_2^+)$

five supermultiplets corresponding to states with positive parity and either two units of angular momentum or one unit of radial excitation. Table 2 shows the supermultiplets contained in the first three bands and the known, well-established baryons that are members of the ground-state $\mathbf{56}$. Further quark-model assignments for some of the known baryons will be discussed in Section 7.

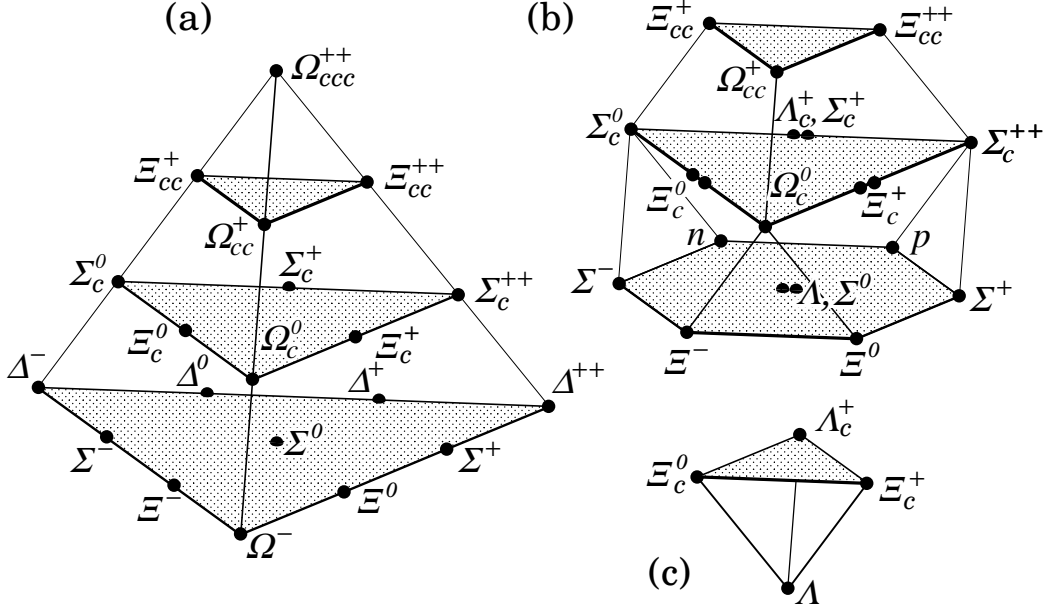
2.2. Baryons Containing Heavy Quarks

The baryons containing a single charm quark can be described in terms of SU(3) flavour multiplets, but these represent but a subgroup of the larger SU(4) group that includes all of the baryons containing zero, one, two or three charmed quarks. Furthermore, this multiplet structure is expected to be repeated for every combination of spin and parity, leading to a very rich spectrum of states. One can also construct SU(4) multiplets in which charm is replaced by beauty, as well as place the two sets of SU(4) structures within a larger SU(5) group to account for all the baryons that can be constructed from the five flavours of quark accessible at low to medium energies. It must be understood that the classification of states in SU(4) and SU(5) multiplets serves primarily for enumerating the possible states, as these symmetries are badly broken. Only at the level of the SU(3) (u, d, s) and SU(2) (u, d) subgroups can these symmetries be used in any quantitative way to understand the structure and properties of these states.

The multiplet structure for flavour SU(4) is $\mathbf{4} \otimes \mathbf{4} \otimes \mathbf{4} = \mathbf{20}_S \oplus \mathbf{20}_M \oplus \mathbf{20}_M \oplus \mathbf{4}_A$. The symmetric $\mathbf{20}$ contains the SU(3) decuplet as a subset, forming the ‘ground floor’ of the weight diagram shown in Figure 2 (a), and all the ground-state baryons in this multiplet have $J^P = \frac{3}{2}^+$. The mixed-symmetric $\mathbf{20}$ s (Figure 2 (b)) contain the SU(3) octets on the lowest level, and all the ground-state baryons in this multiplet have $J^P = \frac{1}{2}^+$. The ground-floor state of the $\mathbf{4}$ (Figure 2 (c)) is the SU(3) singlet Λ with $J^P = \frac{1}{2}^-$.

Within the flavour SU(3) subgroups, the ground-state heavy baryons containing a single heavy quark belong either to a sextet of flavour symmetric states, or an antitriplet of flavour antisymmetric states, both of which sit on the second layer of the mixed-

Figure 2. (a) The symmetric **20** of SU(4), showing the SU(3) decuplet on the lowest layer. (b) The mixed-symmetric **20**s and (c) the antisymmetric **4** of SU(4). The mixed-symmetric **20**s have the SU(3) octet on the lowest layer, while the **4** has the SU(3) singlet at the bottom. Note that there are two Ξ_c^+ and two Ξ_c^0 resonances on the middle layer of the mixed-symmetric **20**.



symmetric **20** of SU(4) of Figure 2 (b). There is also expected to be a sextet of states with $J^P = \frac{3}{2}^+$ sitting on the second floor of the symmetric **20**. The members of the two multiplets of singly-charmed baryons have flavour wave functions

$$\begin{aligned}
 \Sigma_c^{++} &= uuc, & \Sigma_c^+ &= \frac{1}{\sqrt{2}}(ud + du)c, & \Sigma_c^0 &= ddc \\
 \Xi_c^+ &= \frac{1}{\sqrt{2}}(us + su)c, & \Xi_c^0 &= \frac{1}{\sqrt{2}}(ds + sd)c, \\
 \Omega_c^0 &= ssc,
 \end{aligned} \tag{2.7}$$

for the sextet and

$$\Lambda_c^+ = \frac{1}{\sqrt{2}}(ud - du)c, \quad \Xi_c^+ = \frac{1}{\sqrt{2}}(us - su)c, \quad \Xi_c^0 = \frac{1}{\sqrt{2}}(ds - sd)c, \tag{2.8}$$

for the antitriplet. There is a similar set of flavour wave functions for baryons containing a single b quark.

For the baryons containing two charm or two beauty quarks, the flavour wave functions are

$$\Xi_{cc}^{++} = ccu, \quad \Xi_{bb}^0 = bbu, \quad \Omega_{cc}^+ = ccs, \quad \Omega_{bb}^- = bbs. \tag{2.9}$$

When the two heavy quarks are different, there are two ways of constructing their flavour wave functions. One can imagine that the two heavy quarks are members of a (pseudo-)symmetry group, $SU(2)_{bc}$, and that the pair of heavy quarks form either triplet

or singlet representations of this group. Two members of this triplet would then be the Ξ_{cc} and Ξ_{bb} , with the third member being the state

$$\Xi_{bc}^+ = \frac{1}{\sqrt{2}}(cb + bc)u. \quad (2.10)$$

The singlet state would then be

$$\Xi_{bc}'^+ = \frac{1}{\sqrt{2}}(cb - bc)u. \quad (2.11)$$

Alternatively, the flavour wave functions of these two states may be written as

$$\Xi_{bc}'^+ = \frac{1}{\sqrt{2}}(uc + cu)b \quad (2.12)$$

and

$$\Xi_{bc}^+ = \frac{1}{\sqrt{2}}(uc - cu)b. \quad (2.13)$$

The same choices of wave function need to be made when the light quark in the baryon is a down quark or a strange quark.

2.3. Naming Scheme for Light Baryons

An indispensable tool in hadron spectroscopy are of course the listings by the PDG. The group lists established baryon resonances in their Baryon Summary Table. Resonances are given a star rating based on their overall status. The ratings range from * * * * (existence is certain) and * * * (existence is likely to certain, but further confirmation is desirable) to ** (evidence of existence is only fair) and * (evidence of existence is poor) [1].

In its latest 2012 edition [1], the PDG has replaced the historical naming scheme for observed light nonstrange baryons – based on elastic πN scattering – with a more general scheme which applies to all baryons independent of the production mechanism, including those resonances that are not produced in formation experiments, e.g. Ξ or Ω resonances with $|S| > 1$ and heavy baryons. For example, the Δ resonance was observed originally in the P_{33} partial wave with $L = 1$ referring to the angular momentum between the π and the nucleon in πN scattering experiments. With the plethora of new results coming from photoproduction experiments, the resonance label has switched from the incoming πN partial wave, L_{2I2J} , to the spin-parity of the state. Consequently, the name of the Δ resonance has changed from $\Delta(1232)P_{33}$ to $\Delta(1232)\frac{3}{2}^+$.

3. Heavy-Quark Baryons

Baryons containing heavy quarks have been the focus of much attention recently, in particular since the experimental discovery of new resonances at Fermilab and the Large Hadron Collider (LHC). The heavy quark provides a ‘flavour tag’ that may give insights into the mechanism of confinement and the systematics of hadron resonances that cannot be obtained with light quarks. All of the states containing heavy quarks

are expected to be somewhat narrow, for the most part, so that their detection and isolation is relatively easy, and in general does not rely on the extensive partial-wave-analysis machinery usually necessary for identifying light baryons (most states found to date have widths of a few MeV, with the largest reported width being a few tens of MeV, but with large uncertainties). Such analyses may be required for determining the quantum numbers of the states, but even then, the procedure may still be simpler than in the case of light baryons, as it is expected to be largely free of the various interferences that arise with nearby, broad and overlapping resonances.

In addition, the heavy-quark symmetries provide a framework for understanding and predicting the spectrum of one flavour of heavy baryons, say those containing a b quark, if the spectrum of baryons containing a c quark has been obtained [11]. Used judiciously, this heavy-quark symmetry can provide some qualitative insight, and perhaps even quantitative, into the spectrum of light baryons, particularly the hyperons.

Despite the wealth of information that they can provide, and many theoretical treatises, surprisingly little is known experimentally about the heavy baryons [1]. This is largely because despite the comments above, they are difficult to produce. Unlike the heavy mesons, there are no known resonant production mechanisms, so these baryons can only be obtained by continuum production, where cross sections are small, as products in the decays of heavy mesons, or at hadron colliders. Not surprisingly, the B factories, and CLEO before that, have been the main source of these baryons.

The first observations of beauty baryons were made at the Organisation Européenne pour la Recherche Nucléaire (CERN) by the Large Electron Positron (LEP) experiments. These observations were mostly limited to a few decay modes of the Λ_b^0 baryon and some indications for other ground-state baryons based on their semileptonic decays. In recent years, the Tevatron experiments at Fermilab have observed a large number of new heavy-baryon states. In addition to direct observations of most of the ground states, the published results even include precision lifetime measurements, and several new decay modes. It is clear that future results will again come from CERN. The LHC experiments have already demonstrated their discovery potential. In 2012 alone, LHCb has announced two new Λ_b^{*0} states and the Compact Muon Solenoid (CMS) Collaboration has reported a new Ξ_b^{*0} resonance (Table 3).

3.1. The Known Baryons

In the 2012 edition of the RPP, the PDG lists 23 singly-charmed, one doubly-charmed, and six beauty baryons in its Baryon Summary Table [1]. The existence of only 23 of these ranges from likely to certain with a 3-star assignment by the PDG and only two baryons, the Λ_c^+ and $\Sigma_c(2455)$, have a 4-star assignment. The known $C = +1$ and $B = +1$ baryons with at least three stars are listed in Table 3. For most of the beauty baryons, with the exception of the Λ_b^0 , only one or two decay modes have been observed. None of the I , J , or P quantum numbers have actually been measured, but are based on quark model expectations.

Table 3. (Colour online) The heavy baryons with at least a * * * assignment as listed by the PDG indicating that existence ranges from very likely to certain [1]. Only the Λ_c^+ and the $\Sigma_c(2455)$ are considered certain with * * * * assignments. Two further states not listed in the table are well established: $\Lambda_c(2880)^+$ with a possible $J^P = \frac{5}{2}^+$ assignment and a mass of 2881.50 ± 0.35 MeV and $\Xi_c^{+(0)}$ (3080) with unknown quantum numbers and a mass of 3077.0 ± 0.4 (3079.9 ± 1.4) MeV. Masses which have changed slightly from the 2010 edition are marked with (*). Recent findings (not included in the 2012 edition) are highlighted in red with statistical errors only.

	Mass [MeV] $J^P = \frac{1}{2}^+$	Mass [MeV] $J^P = \frac{3}{2}^+$	Mass [MeV] $J^P = \frac{1}{2}^-$	Mass [MeV] $J^P = \frac{3}{2}^-$	Mass [MeV] $J^P = ??$
Λ_c^+	2286.46 ± 0.14		$2592.25 \pm 0.28^*$	$2628.11 \pm 0.19^*$	$2939.3^{+1.4}_{-1.5}$
Σ_c^{++}	$2453.98 \pm 0.16^*$	$2517.9 \pm 0.6^*$			2801^{+4}_{-6}
Σ_c^+	2452.9 ± 0.4	2517.5 ± 2.3			2792^{+14}_{-5}
Σ_c^0	$2453.74 \pm 0.16^*$	$2518.8 \pm 0.6^*$			$2806^{+5}_{-7}^*$
Ξ_c^+	$2467.6^{+0.4}_{-1.0}$	$2645.9^{+0.5}_{-0.6}$	2789.1 ± 3.2	2816.6 ± 0.9	2971.4 ± 3.3
Ξ_c^0	$2471.09^{+0.35}_{-1.00}$	2645.9 ± 0.5	2791.8 ± 3.3	2819.6 ± 1.2	2968.0 ± 2.6
$\Xi_c^{\prime+}$	2575.6 ± 3.1				
$\Xi_c^{\prime0}$	2577.9 ± 2.9				
Ω_c^0	$2695.2^{+1.8}_{-1.6}$	2765.9 ± 2.0			
Λ_b^0	$5619.53 \pm 0.13 \pm 0.45$ [12]		5911.95 ± 0.12	5919.76 ± 0.12 [13]	
Σ_b^+	$5811.3^{+0.9}_{-0.8} \pm 1.7^*$	$5832.1 \pm 0.7^{+1.7}_{-1.8}^*$			
Σ_b^-	$5815.5^{+0.6}_{-0.5} \pm 1.7^*$	$5835.1 \pm 0.6^{+1.7}_{-1.8}^*$			
Ξ_b^-	$5791.1 \pm 2.2^*$	$(5795.8 \pm 0.9 \pm 0.4$ [12])			
Ξ_b^0	$5787.8 \pm 5.0 \pm 1.3^*$	$5945.0 \pm 0.7 \pm 0.3$ [14]			
Ω_b^-	6071 ± 40	$(6046.0 \pm 2.2 \pm 0.5$ [12])			

3.2. Experimental Methods and Major Experiments

Recent experimental results on heavy-flavour baryon spectroscopy have been reported by several experiments, mostly by the so-called B factories at e^+e^- collider facilities and the experiments at the Tevatron $p\bar{p}$ collider facility. Some earlier photoproduction experiments at Fermilab, E687, E691, E791, and Focus made important contributions; technical details on these experiments can be found elsewhere in the literature. The SELEX experiment used a hadron beam and produced interesting results on charmed baryons including the possible first observation of a doubly-charmed baryon [15, 16].

Charmed baryons have been studied intensively at the Cornell Electron-positron Storage Ring (CESR) at Cornell University using the CLEO detector. Based on the CLEO-II detector, the CLEO-III detector started operation in 1999 [17]. CLEO consisted of drift chambers for tracking and dE/dx measurements and a CsI electromagnetic calorimeter based on 7800 modules inside a 1.5 T magnetic field. For CLEO-III, a silicon-strip vertex detector and a ring-imaging Čerenkov detector for particle identification were added. The integrated luminosity accumulated by the

CLEO-III detector in 1999-2003 was 16 fb^{-1} . In 2003, CLEO was upgraded to CLEO-c in order to study charmed mesons at high luminosities. The accelerator ran at significantly lower energies, mostly at the $\psi'(3770)$ charmonium state, so that charmed baryons could no longer be produced. The study of N^* states in $\psi'(3770) \rightarrow p\bar{p} + \text{mesons}$ remained a possibility, though. CLEO-c operations ended in Spring 2008. Selected results of the CLEO collaboration can be found in [18, 19, 20, 21, 22, 23, 24, 25, 26, 27, 28, 29].

In 1999, two B -factories started data-taking with the main goal of studying time-dependent CP asymmetries in the decay of B mesons: BABAR at the Stanford Linear Accelerator Center (SLAC) and Belle at the KEKB e^+e^- collider in Tsukuba, Japan. The very high luminosities of the electron-positron colliders and the general-purpose character of the detectors also made them suitable places for the study of heavy baryons. The peak cross section at the $\Upsilon(4S)$ is about 1.2 nb, which sits on approximately 3.5 nb of what is called the continuum background. Most of the information on heavy baryons comes from the reaction $e^+e^- \rightarrow \text{continuum}$ and, to a lesser extent, from B decays.

BABAR was a cylindrically-shaped detector [30] with the interaction region at its center. The electron beam of the PEP-II facility collided with a positron beam of lower energy to produce a center-of-mass energy near or at 10.58 GeV, which corresponds to the $\Upsilon(4S)$ resonance. This state decays almost instantly into two B mesons. About 10^9 B mesons were recorded. The momenta of charged particles were measured with a combination of a five-layer silicon vertex tracker and a 40-layer drift chamber in a solenoidal magnetic field of 1.5 T. The momentum resolution was about $\sigma_{p_t} \approx 0.5\%$ at $p_t = 1.0$ GeV. A detector of internally reflected Čerenkov radiation was used for charged particle identification. The electromagnetic calorimeter was a finely segmented array of CsI(Tl) crystals with an energy resolution of $\sigma_E/E \approx 2.3\% \times E^{-1/4} + 1.9\%$, where the energy is in GeV. The instrumented flux return contained resistive plate chambers for muon and long-lived neutral hadron identification. Some selected results are given in [31, 32, 33, 34, 35, 36, 37].

The Belle experiment operates at the KEKB e^+e^- accelerator, the world's highest luminosity machine with a world record in luminosity of $1.7 \times 10^{34} \text{ cm}^{-2}\text{s}^{-1}$ and with an integrated luminosity exceeding 700 fb^{-1} . The Belle detector [38] is a large-solid-angle magnetic spectrometer based on a 1.5 T superconducting solenoid. Charged particle tracking is provided by a three-layer silicon vertex detector and a 50-layer central drift chamber (CDC) surrounding the interaction point. The charged particle acceptance covers laboratory polar angles between $\theta = 17^\circ$ and 150° , corresponding to about 92% of the total solid angle in the center-of-mass system. Charged hadron identification and pion/kaon separation is provided by dE/dx measurements in the CDC, an array of 1188 aerogel Čerenkov counters (ACC), and a barrel-like array of 128 time-of-flight scintillation counters with rms resolution of 0.95 ps. Particles that produce electromagnetic showers are detected in an array of 8736 CsI(Tl) crystals of projective geometry that covers the same solid angle as the charged particle system. Results on charmed-baryon spectroscopy relevant to this review can be found in [38, 39, 40, 41, 42, 43, 44].

The large data sets available from the Tevatron $p\bar{p}$ collider at Fermilab at a center-of-mass energy of $\sqrt{s} = 1.96$ TeV have rendered possible significant progress in the field of heavy baryon spectroscopy, in particular for beautiful baryons. Both experiments, the Collider Detector at Fermilab (CDF) and DØ, collected about 10 fb^{-1} of data during the Run II period from 2001 to 2011 and could trigger on dimuon pairs so that heavy baryons decaying to J/ψ can be studied. The most relevant components of the DØ detector for the results discussed in this review are the central tracking system and the muon spectrometer. The central tracking system consists of a silicon microstrip tracker (SMT) and a central fiber tracker (CFT) that are surrounded by a 2 T superconducting solenoid. The muon spectrometer is located outside the calorimeter system and covers the pseudorapidity region $|\eta| < 2$ ($\eta = -\ln[\tan(\theta/2)]$ and θ is the polar angle). It comprises a layer of drift tubes and scintillator trigger counters in front of 1.8 T iron toroids followed by two similar layers behind the toroids. Results on heavy-baryon spectroscopy from the DØ collaboration are summarized in [45, 46, 47, 48, 49, 50].

The tracking system of the CDF II detector [51] lies within a uniform, axial magnetic field of 1.4 T surrounded by calorimeters using lead-scintillator sampling (electromagnetic calorimeters) and iron-scintillator sampling (hadron calorimeters). The inner tracking volume is comprised of 6-7 layers of double-sided silicon microstrip detectors and the remainder is occupied by an open-cell drift chamber (COT). The silicon detector provides a vertex resolution of approximately $15 \mu\text{m}$ in the transverse and $70 \mu\text{m}$ in the longitudinal direction and the COT a transverse momentum resolution of $\sigma(p_T)/p_T^2 \approx 0.1\% / (\text{GeV}/c)$. CDF was able to trigger on hadronic decays of heavy baryons which are identified by tracks displaced from the primary vertex. Recent results relevant to this review can be found in [52,].

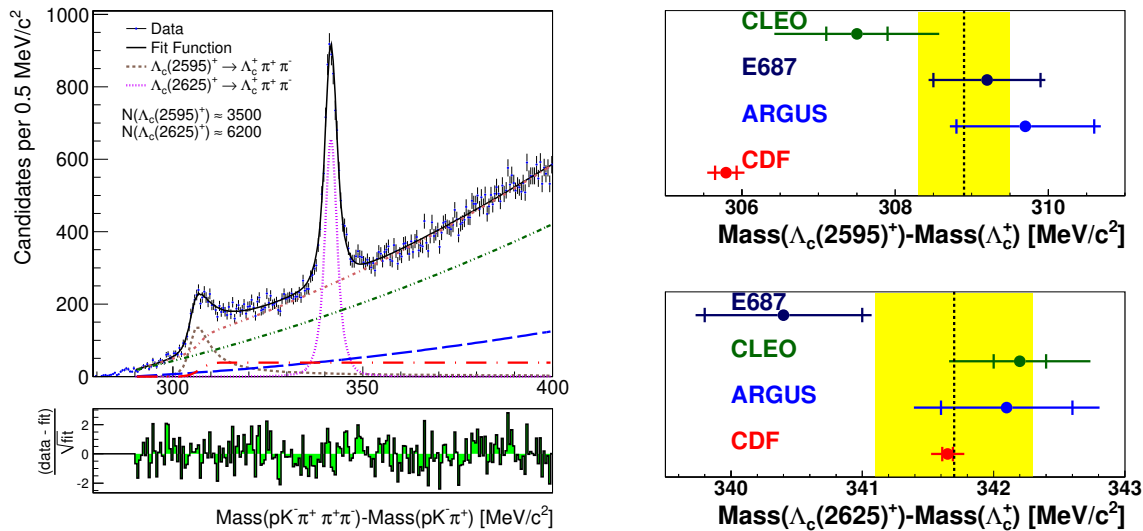
The LHC experiments, in particular LHCb and CMS, have just started to contribute significantly to hadron spectroscopy. Their most recent results on b baryons are based on the 2011 data-taking at a center-of-mass energy of $\sqrt{s} = 7$ TeV and are of unprecedented statistical quality. We refer to [66] for LHCb and [67] for CMS for more details on the experimental setups. Results relevant for this review are summarized in [12, 13, 14, 68].

3.3. Recent Results in the Spectroscopy of Charmed Baryons

3.3.1. The Λ_c^+ States The Λ_c^+ resonance (quark content udc) was the first and is now the best known charmed baryon. It was reported at Fermilab in 1976 [69] shortly after the discovery of the J/ψ meson. The PDG lists 85 different values for branching fractions for the Λ_c^+ including hadronic, semileptonic, and inclusive modes [1]. Most of the branching fractions are measured relative to the decay mode $\Lambda_c^+ \rightarrow pK^-\pi^+$ and there are no completely model-independent measurements of the absolute branching fraction for $\Lambda_c^+ \rightarrow pK^-\pi^+$. A minireview on the measurements that have been used to extract $\mathcal{B}(\Lambda_c^+ \rightarrow pK^-\pi^+)$ can be found in [2]. The most precise mass determination was reported by BABAR in 2005 based on its decay into $\Lambda K_S^0 K^+$ and $\Sigma^0 K_S^0 K^+$ [31]

$$M_{\Lambda_c^+} = 2286.4 \pm 0.14 \text{ MeV} \quad (3.1)$$

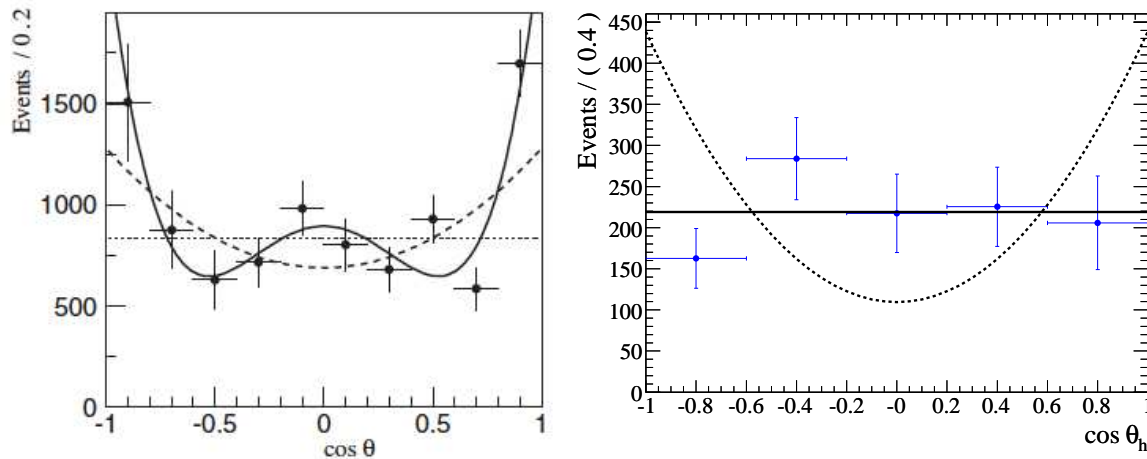
Figure 3. (Colour online) Left: The $m(pK^-\pi^+\pi^+\pi^-) - m(pK^-\pi^+)$ difference spectrum together with the fit (black solid line) from CDF [64]. The red dash-dotted line corresponds to the sum of three background contributions. The two peaks corresponding to $\Lambda_c(2595)^+ - \Lambda_c^+$ and $\Lambda_c(2625)^+ - \Lambda_c^+$ candidates are visible. Right: Comparison of Λ_c^{*+} mass difference measurements by CLEO [19], Fermilab E687 [71, 72], ARGUS [74], and CDF [64]. Pictures from [64].



and is the sole result used by the PDG for their average of the measurements. Although the spin J has not been measured directly, a $J = \frac{1}{2}$ assignment for the lowest-mass Λ_c^+ appears likely and is consistent with an analysis of $pK^-\pi^+$ decays [70].

Additional charmed baryons were discovered long after the initial observation of the Λ_c^+ ground state. In 1993, the ARGUS collaboration at the e^+e^- storage ring DORIS II at the Deutsches Elektronen-Synchrotron (DESY) discovered a first Λ_c^+ excitation, the $\Lambda_c(2625)^+$ [73]. In 1995, this sighting was confirmed by the CLEO collaboration, who also reported on the first observation of the lower-mass $\Lambda_c(2595)^+$ [19]. This second peak was later confirmed by the E687 collaboration [71, 72] at Fermilab and the ARGUS collaboration [74]. The most precise study of the $\Lambda_c(2595)/\Lambda_c(2625)$ system has been performed recently by the CDF collaboration [64], who observed a number of excited charmed baryon states. Figure 3 (left) shows the $m(pK^-\pi^+\pi^+\pi^-) - m(pK^-\pi^+)$ mass difference distribution of Λ_c^{*+} candidates decaying to $\Lambda_c^+\pi^+\pi^-$. The signals are described by a convolution of non-relativistic Breit-Wigner and Gaussian resolution functions, where the signal for the $\Lambda_c(2595)^+$ also takes into account the mass dependence of the natural width owing to the proximity of the $\Sigma_c\pi$ threshold to the $\Lambda_c(2595)^+$ mass. These finite width effects were discussed in [75] and yield a lower $\Lambda_c(2595)^+$ mass measurement than observed by previous experiments. In Figure 3 (left), a clear peak for the $\Lambda_c(2595)^+$ is visible at $\Delta m = 305.79 \pm 0.14 \pm 0.20$ MeV [64]. An additional, even stronger peak is observed at $\Delta m = 341.65 \pm 0.04 \pm 0.12$ MeV which corresponds to the $\Lambda_c(2625)^+$. Neither state has been seen in $\Lambda_c^+\pi^0$, thus ruling out an interpretation

Figure 4. (Colour online). Left: The yield of $\Lambda_c(2880)^+ \rightarrow \Sigma_c^{0,++}\pi^\pm$ decays from Belle as a function of the helicity angle [42]. The dotted, dashed, and solid curves correspond to a spin- $\frac{1}{2}$, spin- $\frac{3}{2}$, and spin- $\frac{5}{2}$ hypothesis, respectively. Right: The efficiency-corrected helicity-angle distribution for $\Sigma_c(2455)^0$ candidates from BABAR [36]. The helicity angle $\cos\theta_h$ is defined as the angle between the momentum vector of the Λ_c^+ and the momentum vector of the recoiling B -daughter \bar{p} in the rest frame of the $\Sigma_c(2455)^0$. The curves denote the spin- $\frac{1}{2}$ (solid line) and spin- $\frac{3}{2}$ (dashed line) hypothesis. Pictures from [42] and [36], respectively.



as excited Σ_c^+ states. Figure 3 (right) shows a comparison of Λ_c^{*+} mass difference measurements by various experiments. The significant shift of the $\Lambda_c(2595)^+$ mass towards lower values is attributed to the fact that the improved statistics reported by CDF [64] allows for a more detailed study of the state's line shape including the effects of the $\Lambda_c(2595)^{*+} \rightarrow \Sigma_c(2455)\pi$ threshold, which was taken into account in the fit. The proximity to the $\Sigma_c\pi$ threshold and assuming $J^P = \frac{1}{2}^+$ for the $\Sigma_c(2455)$ (lowest-mass Σ_c state) makes a $J^P = \frac{1}{2}^-$ assignment for the $\Lambda_c(2595)^+$ likely.

In 2007, BABAR reported two narrow signals observed in the invariant D^0p mass distribution which were absent in the corresponding D^+p mass spectra [34]. Consequently, the peaks were identified as Λ_c^{*+} candidates. The lower-mass peak was initially discovered in 2001 by CLEO in the $\Lambda_c\pi^+\pi^-$ final state and called $\Lambda_c(2880)^+$ [26]. Belle also studied the $\Lambda_c\pi^+\pi^-$ system and confirmed the $\Lambda_c(2880)^+$ as well as the higher-mass BABAR peak, now called $\Lambda_c(2940)^+$ [42]. Table 4 summarizes the mass and width results for both states. The decay angular distribution of $\Lambda_c(2880)^+ \rightarrow \Sigma_c(2455)^{0,++}\pi^\pm$ depends on the spin of the $\Lambda_c(2880)^+$ and is shown in Figure 4 (left) [42]. Assuming spin $\frac{1}{2}^+$ for the lowest-mass Σ_c state, a high-spin assignment for the $\Lambda_c(2880)^+$ of $J = \frac{5}{2}$ is favoured over the spin- $\frac{1}{2}$ or $\frac{3}{2}$ hypothesis. The $\Lambda_c(2880)^+$ yields were determined from fits of the $\Lambda_c^+\pi^+\pi^-$ spectrum in $\cos\theta$ bins for the $\Sigma_c(2455)$ signal region and sidebands. We note that the fit shown in [42] systematically underestimates the data points between the $\Lambda_c(2880)^+$ and $\Lambda_c(2940)^+$ signals. The paper states that this might be due to the presence of an additional resonance or due to interference and takes these possibilities into account as a systematic uncertainty. This issue needs to be

Table 4. Measurements of mass and width of the $\Lambda_c(2800)^+$ and $\Lambda_c(2800)^\pm$.

	Mass [MeV]	Width [MeV]	Decay Modes
$\Lambda_c(2880)^+$ [26]	$2882.5 \pm 1 \pm 2$	< 8	$\Lambda_c^+ \pi^+ \pi^-$
$\Lambda_c(2880)^+$ [34]	$2881.9 \pm 0.1 \pm 0.5$	$5.8 \pm 1.5 \pm 1.1$	pD^0
$\Lambda_c(2880)^+$ [42]	$2881.2 \pm 0.2 \pm 0.4$	$5.8 \pm 0.7 \pm 1.1$	$\Sigma_c(2455)^{0,++} \pi^\pm$
$\Lambda_c(2940)^+$ [34]	$2939.8 \pm 1.3 \pm 1.0$	$17.5 \pm 5.2 \pm 5.9$	pD^0
$\Lambda_c(2940)^+$ [42]	$2938.0 \pm 1.3_{-4.0}^{+2.0}$	$13_{-5}^{+8+27}_{-7}$	$\Sigma_c(2455)^{0,++} \pi^\pm$

further addressed in the future in order to reduce the uncertainty in this rare attempt of measuring the J quantum number of a heavy baryon. The authors also determined the ratio of $\Lambda_c(2880)^+$ partial widths [42]

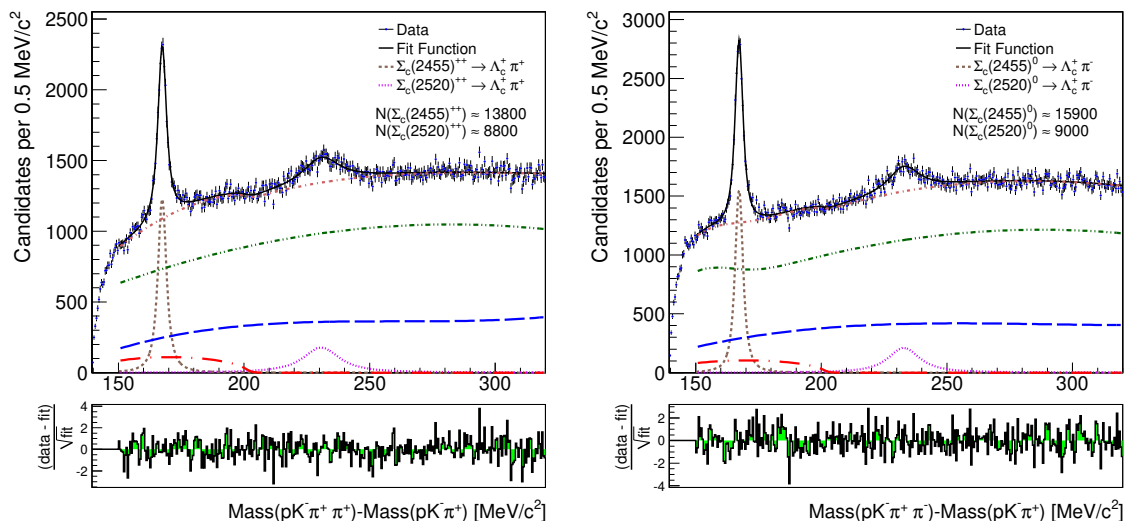
$$\Gamma(\Sigma_c(2520)\pi) / \Gamma(\Sigma_c(2455)\pi) = 0.225 \pm 0.062 \pm 0.025, \quad (3.2)$$

which favours a spin-parity assignment of $\frac{5}{2}^+$ over $\frac{5}{2}^-$ in various models [11, 76, 77]. It is interesting to note that the favoured $J^P = \frac{5}{2}^+$ assignment for the $\Lambda_c(2880)^+$ requires a large decay angular momentum of $L = 3$ for all observed decays, into $\Sigma_c(2455)\pi$, $\Sigma_c(2520)\pi$ and pD^0 . However, a lower angular momentum may be sufficient for the $\Lambda_c(2880)^+$ decay into $\Sigma_c(2520)\pi$ and it remains a mystery why the $L = 1$ decay into $\Sigma_c(2520)$ should be suppressed. It is also worth pointing out that the original CLEO analysis [26] observes $\Lambda_c(2880)^+$ decays via $\Sigma_c\pi$ and nonresonantly to $\Lambda_c^+\pi^+\pi^-$, but not via Σ_c^* . This analysis suffers from significantly lower statistics and thus, does not contradict the Belle results.

We finally mention the $\Lambda_c(2765)^+$, which is listed as a (*) state in the RPP [1], but its quantum numbers are unknown. The state was observed as a broad, statistically significant peak by the CLEO collaboration in $\Lambda_c^+\pi^+\pi^-$ [26], but is not even fully identified as a Λ_c resonance. It should be studied further in $\Lambda_c^+\pi^+\pi^0$ events, for example by the BABAR or Belle collaboration.

3.3.2. The Σ_c States Σ_c states are expected to occur in triplets: Σ_c^{++} , Σ_c^+ and Σ_c^0 , with quark content uuc , udc and ddc , respectively. The two lowest-lying Σ_c resonances, $\Sigma_c(2455)$ and $\Sigma_c(2520)$, are well established and both have been confirmed in several experiments [1]. Their masses allow strong decays only into $\Lambda_c^+\pi$. In 2001, the CLEO collaboration published mass and width measurements for the Σ_c^+ and Σ_c^{*+} states based on their decays into $\Lambda_c^+\pi^0$ [27]. The CLEO results for the Σ_c^{*++} and Σ_c^{*0} states decaying into $\Lambda_c^+\pi^\pm$ [28] have been much improved upon statistically by recent Tevatron results [64]. The CDF collaboration used a data sample corresponding to 5.2 fb^{-1} of integrated luminosity from $p\bar{p}$ collisions at $\sqrt{s} = 1.96 \text{ TeV}$ and selected $\Lambda_c^+ \rightarrow pK^-\pi^+$ decays. Figure 5 (left) shows the $m(pK^-\pi^+\pi^-) - m(pK^-\pi^+)$ and Figure 5 (right) the $m(pK^-\pi^+\pi^+) - m(pK^-\pi^+)$ mass difference spectrum. The signals are

Figure 5. (Colour online). The difference spectra $m(pK^-\pi^+\pi^-) - m(pK^-\pi^+)$ (right) and $m(pK^-\pi^+\pi^+) - m(pK^-\pi^+)$ (left) together with the fits (black solid line) from CDF [64]. The red dash-dotted line corresponds to the sum of all three background contributions including reflections from Λ_c^{*+} decays. The two peaks corresponding to $\Sigma_c^{0(++)} - \Lambda_c^+$ and $\Sigma_c^{*0(++)} - \Lambda_c^+$ candidates are visible. Pictures from [64].



described by a convolution of non-relativistic Breit-Wigner and Gaussian resolution functions. Two peaks corresponding to Σ_c^{*++} and Σ_c^{*0} are clearly visible in both distributions.

BABAR observed the resonant decay $B^- \rightarrow \Sigma_c(2455)^0 \bar{p}$ but reported a negative result for $B^- \rightarrow \Sigma_c(2520)^0 \bar{p}$ [36]. The absence of the $\Sigma_c(2520)^0$ in B decays appears to be in conflict with a 2.9σ signal (13_{-5}^{+6} events) based on $152 \times 10^6 B\bar{B}$ events reported by Belle [40]. Figure 4 (right) shows the helicity-angle distribution from BABAR for $\Sigma_c(2455)^0$ candidates [36]. The data points correspond to efficiency-corrected $B^- \rightarrow \Sigma_c(2455)^0 \bar{p}$ events and the curves denote the spin- $\frac{1}{2}$ (solid line) and spin- $\frac{3}{2}$ (dashed line) hypotheses. From this angular distribution, the spin of the $\Sigma_c(2455)^0$ was determined to be $\frac{1}{2}$ as predicted by quark model calculations. Neither J nor P has been measured for the $\Sigma_c(2520)$ but $J^P = \frac{3}{2}^+$ appears natural rendering this resonance the charm counterpart of the $\Sigma(1385)$ [1].

A third triplet of Σ_c resonances, $\Sigma_c(2800)$, was seen in the $\Lambda_c^+ \pi$ mass spectra and first reported by Belle in 2005 [39]. The results for the mass difference and width measurements are summarized in Table 5. BABAR tentatively confirmed the neutral state in the resonant decay $B^- \rightarrow \Sigma_c(2800)^0 \bar{p} \rightarrow \Lambda_c^+ \pi^- \bar{p}$ and determined its mass and width to be $(2846 \pm 8 \pm 10)$ MeV and (86_{-22}^{+33}) MeV, respectively [36]. The widths are consistent in both experiments, whereas the masses are 3σ apart. This discrepancy may indicate that the two observed signals are not the same state. Based on the mass of the $\Sigma_c(2800)^+$, Belle suggested a spin- $\frac{3}{2}$ assignment, while BABAR observes weak evidence for spin $J = \frac{1}{2}$. The authors conclude that B decays to higher-spin baryons might be suppressed [36].

Table 5. Mass differences and widths of the $\Sigma_c(2800)$ reported by Belle [39].

	Mass [MeV]	Width [MeV]
$m(\Sigma_c(2800)^{++}) - m(\Lambda_c^+)$	$514.5_{-3.1-4.9}^{+3.4+2.8}$	75_{-13-11}^{+18+12}
$m(\Sigma_c(2800)^+) - m(\Lambda_c^+)$	$505.4_{-4.6-2.0}^{+5.8+12.4}$	62_{-23-38}^{+37+52}
$m(\Sigma_c(2800)^0) - m(\Lambda_c^+)$	$515.4_{-3.1-6.0}^{+3.2+2.1}$	61_{-13-13}^{+18+22}

Table 6. Masses and widths of the Ξ_c states with $J^P = \frac{1}{2}^+$ quoted by the PDG [1].

	Mass [MeV]	Mean Life [fs]		Mass [MeV]	Decay Mode
Ξ_c^0	$2471.09_{-1.00}^{+0.35}$	112_{-10}^{+13}	$\Xi_c'^0$	2577.9 ± 2.9	$\Xi_c^0 \gamma$
Ξ_c^+	$2467.6_{-1.0}^{+0.4}$	442 ± 26	$\Xi_c'^+$	2575.6 ± 3.1	$\Xi_c^+ \gamma$

3.3.3. *The Ξ_c States* The two states, Ξ_c^+ and Ξ_c^0 , form an isospin doublet with quark content usc and dsc , respectively. The first evidence for the Ξ_c^+ ground state was reported in 1983 by experiments studying Σ^- nucleon collisions at the CERN SPS hyperon beam [78]. The $\Lambda K^- \pi^+ \pi^+$ mass distribution showed an excess of 82 events and the signal had a 6σ statistical significance. CLEO discovered the isospin partner a few years later in its decay to $\Xi^- \pi^+$ in the reaction $e^+ e^- \rightarrow \Xi^- \pi^+ + X$ [18]. According to the PDG, none of the $I(J^P)$ quantum numbers has been measured, but the spin-parity assignment $\frac{1}{2}^+$ appears likely from quark-model calculations.

In 1999, CLEO published evidence for a further Ξ_c doublet, $\Xi_c'^+$ and $\Xi_c'^0$, which was observed to decay via low-energetic photon emission to $\Xi_c^{+(0)}$ [22]. The mass differences were determined to be

$$m(\Xi_c'^+) - m(\Xi_c^+) = 107.8 \pm 1.7 \pm 2.5 \text{ MeV} \quad (3.3)$$

$$m(\Xi_c'^0) - m(\Xi_c^0) = 107.0 \pm 1.4 \pm 2.5 \text{ MeV}, \quad (3.4)$$

which kinematically do not permit the transitions $\Xi_c' \rightarrow \Xi_c \pi$; radiative decays are the only allowed decay modes. The two Ξ_c' states have been interpreted as the partners of Ξ_c , where the light-quark pairs sd and su are symmetric with respect to interchange of the light quarks, i.e. the light-quark pair forms mostly a spin-triplet, $S = 1$. The masses and widths of the resonances quoted by the PDG are summarized in Table 6.

Several additional excited Ξ_c states were discovered by CLEO. A narrow state decaying into $\Xi_c^+ \pi^-$, $\Xi_c(2645)^0$, was observed with a mass difference $m(\Xi_c^+ \pi^-) - m(\Xi_c^+)$ of $178.2 \pm 0.5 \pm 1.0$ MeV, and a width of < 5.5 MeV [20]. The quantum numbers of this state have not been measured but a $J^P = \frac{3}{2}^+$ assignment seems natural. The isospin partner, $\Xi_c(2645)^+$, was also discovered by CLEO with a mass difference of $m(\Xi_c^0 \pi^+) - m(\Xi_c^0)$ of $174.3 \pm 0.5 \pm 1.0$ MeV, and a width of < 3.1 MeV [21]. A confirmation of these states and the most precise mass measurements were reported by Belle [44] and are

Table 7. Masses and widths of the $\Xi_c(2645)$, $\Xi_c(2790)$, and $\Xi_c(2815)$ resonances.

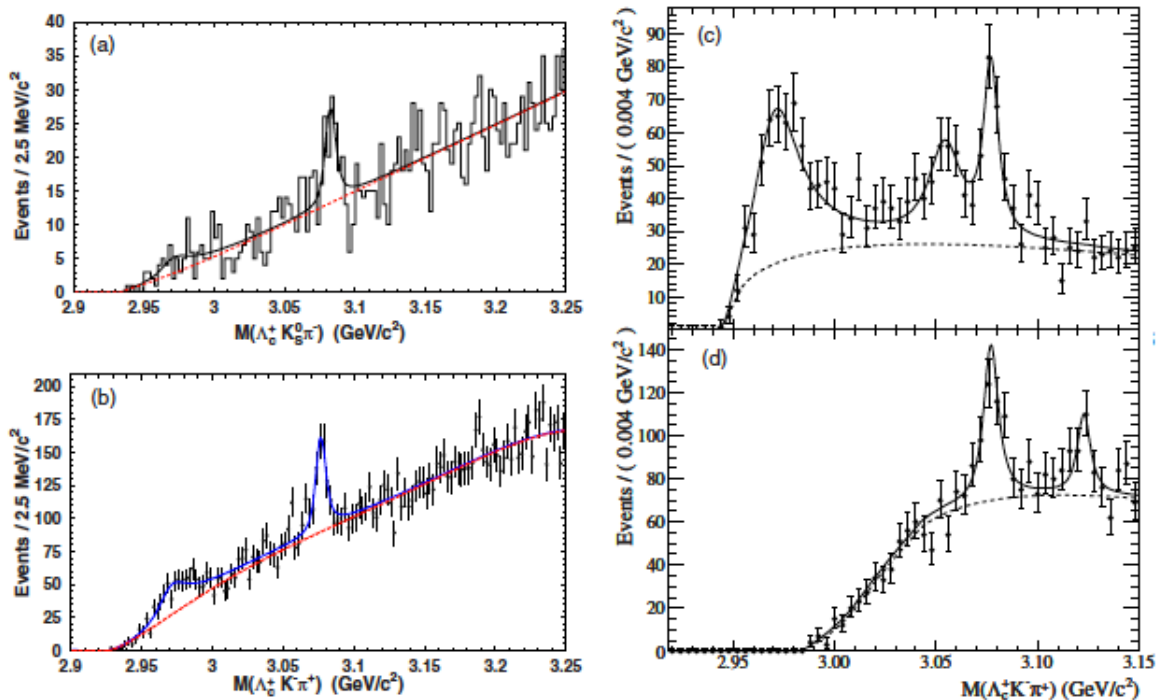
	$\Xi_c(2645)^{+,0}$	$\Xi_c(2790)^{+,0}$	$\Xi_c(2815)^{+,0}$
Mass [MeV]	$2645.6 \pm 0.2_{-0.8}^{+0.6}$ [44]	2789.1 ± 3.2 [25]	$2817.0 \pm 1.2_{-0.8}^{+0.7}$ [44]
	$2645.7 \pm 0.2_{-0.7}^{+0.6}$ [44]	2791.8 ± 3.3 [25]	$2820.4 \pm 1.4_{-1.0}^{+0.9}$ [44]
Width [MeV]	< 3.1 [21]	< 15 [25]	< 3.5 [23]
	< 5.5 [20]	< 12 [25]	< 6.5 [23]

almost identical to the numbers quoted by the PDG. In the same publication [44], Belle reported on a further Ξ_c state, $\Xi_c(2815)$, decaying into $\Xi_c(2645)^{+(0)}\pi^\mp$ [44]. This state was originally discovered by CLEO [23] and both experiments observed it in the decay into $\Xi_c\pi\pi$ via an intermediate $\Xi_c(2645)$. The quantum numbers were not measured, but the states were interpreted as $J^P = \frac{3}{2}^-$ resonances, the charmed-strange analogs of the $\Lambda_c(2625)^+$. Finally about a decade ago, CLEO reported on a doublet of states, $\Xi_c(2790)$, decaying to $\Xi_c'\pi$ [25]. The Belle collaboration confirmed the state [44], but did not determine its parameters. Based on the properties (mass, width, and decay mode), the simplest interpretation of these states is as a pair of $J^P = \frac{1}{2}^-$ resonances, the charmed-strange partners of the $\Lambda_c(2595)^+$. Mass and width measurements of the three states, $\Xi_c(2645)$, $\Xi_c(2790)$, and $\Xi_c(2815)$ are summarized in Table 7.

In the last few years, even more Ξ_c states have been observed at and above 3 GeV. Belle observed two new states, $\Xi_c(2980)$ and $\Xi_c(3080)$, decaying into $\Lambda_c^+K^-\pi^+$ and $\Lambda_c^+K_S^0\pi^-$ [41]. The $\Xi_c(2980)$ resonance was later confirmed by Belle in its decay into $\Xi_c(2645)\pi$ [44], though with a somewhat lower mass. It is important to note that, in contrast to all previous Ξ_c states, the masses of these states are above the threshold for decays into $\Lambda_c^+K\pi$. In these processes, the charm and strangeness of the initial state are carried away by two different final state particles, a charmed baryon and a strange meson. The SELEX collaboration has reported a doubly-charmed baryon decaying into $\Lambda_c^+K^-\pi^+$ inspiring further investigation of this promising decay mode [15]. However, the claim has still not been confirmed by other experiments. A similar flavour separation occurs in the decay mode ΛD^+ , which is allowed above 3 GeV, but no observation of such a decay has yet been reported.

Figure 6 shows various $\Lambda_c^+K\pi$ mass distributions. Results from Belle are given in (a) for the invariant $\Lambda_c^+K_S^0\pi^-$ mass and in (b) for the invariant $\Lambda_c^+K^-\pi^+$ mass with the overlaid fitting curve [41]. The dashed line is the background component of the fitting function, and the solid curve is the sum of the background and signal (Breit-Wigner function convolved with a Gaussian detector resolution function). In (a), a clear signal around 3080 MeV is observed corresponding to the $\Xi_c(3080)^0$. In addition, a broad enhancement near the threshold of the mass distribution is visible, which reveals weak evidence for the $\Xi_c(2980)$. The distribution in (b) provides more information on the origin of the states and confirms both signals. The narrow peak at 3080 MeV and the

Figure 6. (Colour online) Signals for charmed-strange Ξ_c states in the invariant $\Lambda_c^+ \bar{K} \pi$ mass: (a) $\Lambda_c^+ K_S^0 \pi^-$ mass and (b) $\Lambda_c^+ K^- \pi^+$ mass published by the Belle collaboration [41]; (c) and (d) show the corresponding $\Lambda_c^+ K^- \pi^+$ mass from BABAR [35] with the $\Lambda_c^+ \pi^+$ mass consistent with $\Sigma_c(2455)$ and the $\Sigma_c(2520)$, respectively.



broad enhancement at threshold are clearly visible.

The latest confirmation of both states and weak evidence for additional Ξ_c states above 3 GeV were reported by BABAR [35]. Figure 6 (c) and (d) show invariant $\Lambda_c^+ K^- \pi^+$ mass distributions. In (c), the corresponding invariant $\Lambda_c^+ \pi^+$ mass is consistent with the $\Sigma_c(2455)^{++}$ mass (within 3.0 natural widths) and in (d), the $\Lambda_c^+ \pi^+$ mass is consistent with the $\Sigma_c(2520)^{++}$ mass (within 2.0 natural widths). The very broad and the narrow signal for the two states observed by Belle, $\Xi_c(2980)$ and $\Xi_c(3080)^0$, are clearly visible. Mass and width measurements of these states are summarized in Table 8. Moreover, two further signals are observed in the BABAR mass distributions. One signal sits at $(3054.2 \pm 1.2 \pm 0.5)$ MeV with a significance of 6.4σ in the $\Sigma_c(2455)^{++} K^- \rightarrow \Lambda_c^+ K^- \pi^+$ mass spectrum (Figure 6 (c)). The other signal sits at $(3122.9 \pm 1.3 \pm 0.3)$ MeV with a significance of 3.8σ in the $\Sigma_c(2520)^{++} K^- \rightarrow \Lambda_c^+ K^- \pi^+$ mass spectrum (Figure 6 (d)). Neither state, $\Xi_c(3055)^+$ and $\Xi_c(3123)^+$, has been confirmed by any other experiment. The PDG has omitted these two states from its summary table.

3.3.4. The Ω_c States The Ω_c^0 baryon is the heaviest known singly-charmed hadron that decays weakly. The quark content is ssc where the ss pair is in a symmetric state.

Table 8. Mass and width measurements of the charmed-strange resonances $\Xi_c(2980)$ and $\Xi_c(3080)$ in MeV from Belle and BABAR.

	Mass	Width	Experiment
$\Xi_c(2980)^+$	$2969.3 \pm 2.2 \pm 1.7$	$27 \pm 8 \pm 2$	BABAR [35]
	$2967.7 \pm 2.3^{+1.1}_{-1.2}$	$18 \pm 6 \pm 3$	Belle [44]
	$2978.5 \pm 2.1 \pm 2.0$	$43.5 \pm 7.5 \pm 7.0$	Belle [41]
$\Xi_c(2980)^0$	$2972.9 \pm 4.4 \pm 1.6$	$31 \pm 7 \pm 8$	BABAR [35]
	$2965.7 \pm 2.4^{+1.1}_{-1.2}$	$15 \pm 6 \pm 3$	Belle [44]
$\Xi_c(3080)^+$	$3077.0 \pm 0.4 \pm 0.2$	$5.5 \pm 1.3 \pm 0.6$	BABAR [35]
	$3076.7 \pm 0.9 \pm 0.5$	$6.2 \pm 1.2 \pm 0.8$	Belle [41]
$\Xi_c(3080)^0$	$3079.3 \pm 1.1 \pm 0.2$	$5.9 \pm 2.3 \pm 1.5$	BABAR [35]
	$3082.8 \pm 1.8 \pm 1.5$	$5.2 \pm 3.1 \pm 1.8$	Belle [41]

In addition to the ground-state Ω_c with $J^P = \frac{1}{2}^+$, a further excited state is fairly well established. The observation of the ground state was first reported in 1985 by the WA62 collaboration based on a cluster of three events in one out of four modes studied in Σ^- -nucleus interactions using the SPS charged hyperon beam at CERN [79]. Since then, the resonance has been seen and some of its properties measured by a large variety of experiments, e.g. at CERN by the WA89 collaboration in its decay into $\Xi^- K^- \pi^+ \pi^+$ and $\Omega^- \pi^+ \pi^- \pi^+$ [80], at Fermilab by the E687 collaboration [81], and CLEO [24]. The most precise and consistent study was reported in 2009 by Belle via the decay into $\Omega^- \pi^-$ [43]. The average mass value given by the PDG is [1]

$$M_{\Omega_c^0} = 2695.2^{+1.8}_{-1.6} \text{ MeV}. \quad (3.5)$$

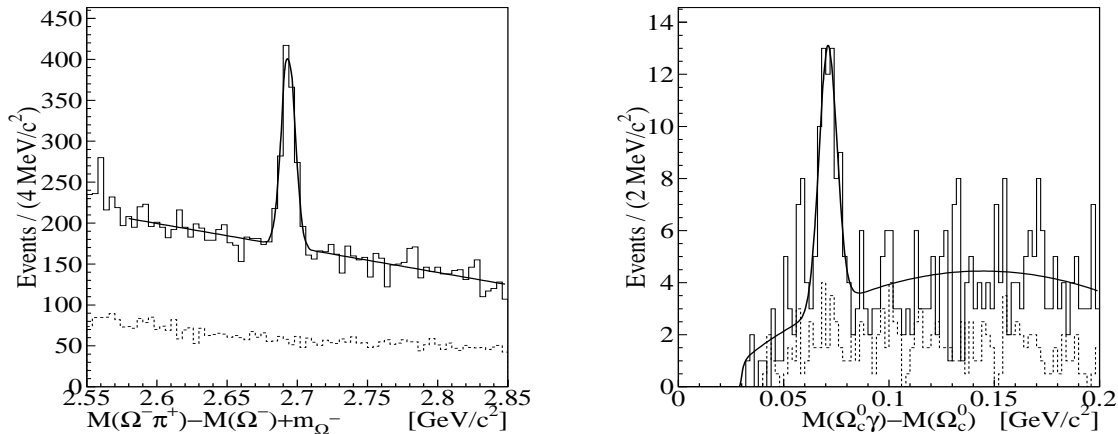
An excited Ω_c baryon was first proposed by BABAR [32] in the radiative decay $\Omega_c^{*0} \rightarrow \Omega_c \gamma$ and in 2009 confirmed by Belle in the same decay with a significance of 6.4σ [43]. The mass difference relative to the ground state, $M_{\Omega_c^{*0}} - M_{\Omega_c^0}$, was measured to be 70.7 ± 0.9 (stat.) $^{+0.1}_{-0.9}$ (syst.) MeV, which is in excellent agreement with the BABAR result. Figure 7 presents the results from Belle. The left side shows the Ω_c^0 signal in the invariant $\Omega^- \pi^+$ mass and the right side shows the signal associated with the Ω_c^{*0} in the $M(\Omega_c^0 \gamma) - M(\Omega_c^0)$ mass difference. The average mass of the Ω_c^{*0} quoted by the PDG in the most recent edition of the RPP is [1]

$$M_{\Omega_c^{*0}} = 2765.9 \pm 2.0 \text{ MeV}. \quad (3.6)$$

The J^P quantum numbers have not been measured, but the natural assignment is $J^P = \frac{3}{2}^+$, which makes the Ω_c^{*0} a partner of the $\Sigma_c(2520)$ and $\Xi_c(2645)$ baryons.

3.3.5. The Status of Doubly-Charmed Baryons The lightest doubly-charmed baryons can exist with either quark content ccu , Ξ_{cc}^{++} , or ccd , Ξ_{cc}^+ . Models generally predict a mass range of 3.516-3.66 GeV for the $J^P = \frac{1}{2}^+$ ground state and 3.636-3.81 GeV for

Figure 7. Results on the Ω_c^0 and Ω_c^{*0} charmed baryons from Belle [43]. Left: Invariant $M(\Omega^- \pi^+) - M(\Omega^-) + m_{\Omega^-}$ mass, where the latter refers to the 2008 PDG mass [82] of the Ω^- state. Right: $M(\Omega_c^0 \gamma) - M(\Omega_c^0)$ mass difference. The solid line represents a fit using a Crystal Ball function for the signal and a second-order polynomial for the background. Pictures from [43].



the $J^P = \frac{3}{2}^+$ excited state. In 2002, the SELEX collaboration at Fermilab reported weak evidence for a Ξ_{cc}^+ candidate decaying into $\Lambda_c^+ K^- \pi^+$ with a statistical significance of 6.3σ using a 600 MeV beam of Σ^- hyperons [15]. The state was later confirmed by SELEX in the decay into $p D^+ K^-$ [16] with an averaged mass from both results of 3518.7 ± 1.7 MeV. The observed lifetime of less than 33 fs is significantly shorter than that of the Λ_c^+ , in contradiction with model calculations based on heavy quark effective theory (see [16] and further references therein).

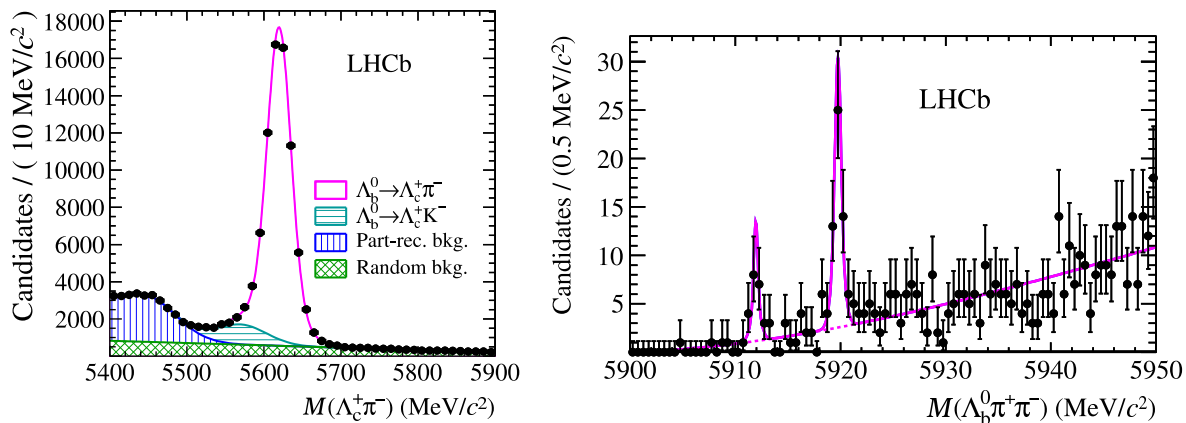
The observation of doubly-charmed baryons is not undisputed. The two B factories, BABAR and Belle, have found no evidence for a Ξ_{cc}^+ state in the $\Lambda_c^+ K^- \pi^+$ decay mode [33, 41]. Other experiments with large samples of charmed baryons, e.g. FOCUS with about $12\times$ more Λ_c^+ events in photoproduction or E791 at Fermilab with about $5\times$ as many Λ_c^+ events as SELEX, have not confirmed the Ξ_{cc}^+ signal. It is interesting to note though that SELEX reported the observation only in baryon-induced reactions (using Σ^- and proton beams), but not in π^- -induced reactions, and none of the other experiments used a baryon beam. Moreover, only SELEX covers the forward hemisphere with baryon beams where the doubly-charmed events are observed.

Some evidence for the doubly-charged partner of the Ξ_{cc}^+ as well as for a higher-mass state was presented by members of the SELEX collaboration at conferences, but BABAR again could not confirm these claims. No evidence for a Ξ_{cc}^{++} state was found in the $\Lambda_c^+ K^- \pi^+ \pi^+$ and $\Xi_c^0 \pi^+ \pi^+$ modes [33] studied by SELEX. Given the weak experimental evidence for doubly-charm baryons, we will not discuss these observations further.

3.4. Recent Results in the Spectroscopy of Beautiful Baryons

Beautiful or bottom baryons are composed of two light quarks and one heavy b quark, qqb ($q = u, d, s$). Prior to 2007, only one bottom baryon, the Λ_b with quark content

Figure 8. (Colour online) Mass spectra from LHCb [13]. Left: Invariant mass spectrum of $\Lambda_c^+\pi^-$ combinations showing a prominent Λ_b^0 signal. Right: Discovery of two excited Λ_b^0 states, Λ_b^{*0} , in the invariant $\Lambda_b^0\pi^+\pi^-$ mass. The fit yields 17.6 ± 4.8 events for the lower-mass peak, $\Lambda_b(5912)^{*0}$, and 52.5 ± 8.1 events for the higher-mass peak, $\Lambda_b(5920)^{*0}$. Pictures from [13].



udb , had been observed directly. It was first discovered at the CERN ISR [83, 84] and later studied in more details by the LEP collaborations, ALEPH, DELPHI, and OPAL. Only indirect observations were reported for the other known bottom baryon at that time, the Ξ_b baryon, by ALEPH [85] and DELPHI [87] via an excess of same-sign $\Xi^\mp l^\mp$ events as compared to those with an opposite-sign $\Xi^\mp l^\pm$ pair. Many new resonances have been discovered in recent years, but none of the quantum numbers, I , J , or P has been experimentally determined. All assignments are based on quark model predictions.

3.4.1. The Λ_b States The isosinglet Λ_b^0 baryon has been known for about 20 years, but the observation of two new excited Λ_b^{*0} baryons has been the most recent discovery of a new heavy baryon. While the original discovery at CERN was based on just 90 events of the reaction $\Lambda_b^0 \rightarrow \Lambda_c^+ \pi^+ \pi^- \pi^-$ in pp collisions at $\sqrt{s} = 62$ GeV [84], LHCb has used pp collision data collected in 2011 at a center-of-mass energy $\sqrt{s} = 7$ TeV. The left side of Figure 8 shows $(70\,540 \pm 330)$ Λ_b^0 signal events reconstructed from the $\Lambda_c^+ \pi^-$ decay mode [13]. The most precise mass measurement has been reported by LHCb to be [12]

$$M_{\Lambda_b^0 \rightarrow J/\psi \Lambda} = 5619.53 \pm 0.13 \text{ (stat)} \pm 0.45 \text{ (syst)} \text{ MeV} . \quad (3.7)$$

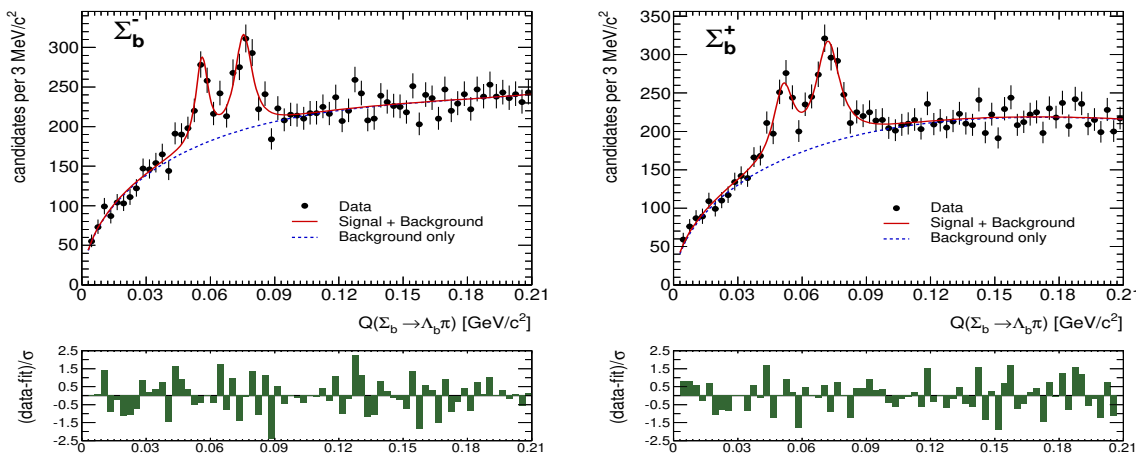
The right side of Figure 8 shows the invariant $\Lambda_b^0 \pi^+ \pi^-$ mass. A higher-mass peak with a significance of 10.2 standard deviations is visible around 5920 MeV and a less significant lower-mass peak with a significance of 5.2 standard deviations is claimed around 5912 MeV [13]. The masses have been determined to be

$$M_{\Lambda_b^{*0}(5912)} = 5911.97 \pm 0.12 \pm 0.02 \pm 0.66 \text{ MeV} \quad (3.8)$$

$$M_{\Lambda_b^{*0}(5920)} = 5919.77 \pm 0.08 \pm 0.02 \pm 0.66 \text{ MeV} , \quad (3.9)$$

where the first uncertainty is statistical, the second is systematic, and the third is the uncertainty due to the the knowledge of the Λ_b^0 mass. The two peaks are associated

Figure 9. (Colour online) Observation of $\Sigma_b^{(*)}$ states in Q -value spectra from CDF where $Q = M_{\Lambda_b^0 \pi^\pm} - M_{\Lambda_b^0} - M_{\pi^\pm}$ [65]. Left: Q -value spectrum for $\Sigma_b^{(*)-}$ candidates. Right: Q -value spectrum for $\Sigma_b^{(*)+}$ candidates. The solid and dashed lines represent the projections of an unbinned likelihood fit. The bottom of each plot shows the pull distributions of each fit. Picture from [65].



with two orbitally excited Λ_b^0 states with the quantum numbers $J^P = \frac{1}{2}^-$ and $\frac{3}{2}^-$.

3.4.2. The Σ_b States Only the CDF collaboration has studied baryons with quark content qqb ($q = u, d$) other than the Λ_b^0 . In the quark model, the three states, Σ_b^+ , Σ_b^0 , and Σ_b^- , form an (uub, udb, ddb) isotriplet. Of the two observed $\Sigma_b^{\pm,0}$ triplets – presumably the ground-states with $J^P = \frac{1}{2}^+$ and the lowest-mass excitations with $J^P = \frac{3}{2}^+$ – only the charged states, $\Sigma_b^{(*)\pm}$, have been observed so far via their decays to $\Lambda_b^0 \pi^\pm$. The resonances were discovered in 2007, but the most precise measurements of their properties were reported by CDF in 2012 using a data sample corresponding to an integrated luminosity of 6.0 fb^{-1} [65]. Figure 9 shows the signals for the $\Sigma_b^{(*)}$ states dependent on $Q = M_{\Lambda_b^0 \pi^\pm} - M_{\Lambda_b^0} - M_{\pi^\pm}$. Masses and widths were determined to be

$$M_{\Sigma_b^+} = 5811.3_{-0.8}^{+0.9} \pm 1.7 \text{ MeV}, \quad \Gamma = 9.7_{-2.8-1.1}^{+3.8+1.2} \text{ MeV}, \quad (3.10)$$

$$M_{\Sigma_b^-} = 5815.5_{-0.5}^{+0.6} \pm 1.7 \text{ MeV}, \quad \Gamma = 4.9_{-2.1}^{+3.1} \pm 1.1 \text{ MeV}, \quad (3.11)$$

$$M_{\Sigma_b^{*+}} = 5832.1 \pm 0.7_{-1.8}^{+1.7} \text{ MeV}, \quad \Gamma = 11.5_{-2.2-1.5}^{+2.7+1.0} \text{ MeV}, \quad (3.12)$$

$$M_{\Sigma_b^{*-}} = 5835.1_{-1.8}^{+1.7} \pm 0.6 \text{ MeV}, \quad \Gamma = 7.5_{-1.8-1.4}^{+2.2+0.9} \text{ MeV}. \quad (3.13)$$

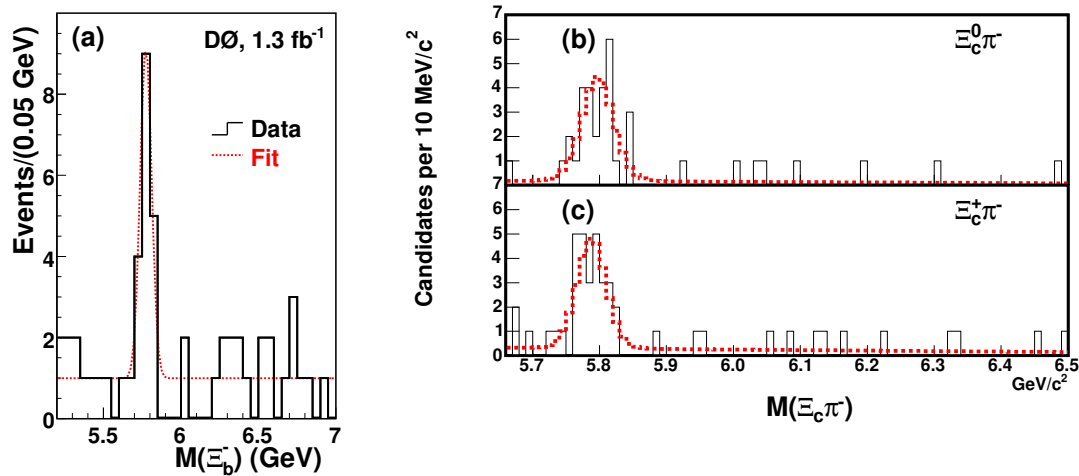
Moreover, the authors report on the first-time extraction of the isospin mass splittings within the $I = 1$ triplets, with

$$M_{\Sigma_b^+} - M_{\Sigma_b^-} = -4.2_{-1.0}^{+1.1} \pm 0.1 \text{ MeV}, \quad (3.14)$$

$$M_{\Sigma_b^{*+}} - M_{\Sigma_b^{*-}} = -3.0_{-0.9}^{+1.0} \pm 0.1 \text{ MeV}. \quad (3.15)$$

The observed widths are in good agreement with theoretical expectations and the isospin splittings agree with the predictions of [86].

Figure 10. (Colour online) Left: First-time observation of the Ξ_b^- baryon at DØ. Picture from [46]. Right: The discovery of the Ξ_b^0 heavy baryon at CDF [63]. Both the invariant $\Xi_b^- \rightarrow \Xi_c^0 \pi^-$ mass distribution in (b) and the $\Xi_b^0 \rightarrow \Xi_c^+ \pi^-$ mass distribution in (c) show evidence for a signal around 5.8 GeV. The dashed lines show the projection of the likelihood fits used to extract the masses and yields. Picture from [63].

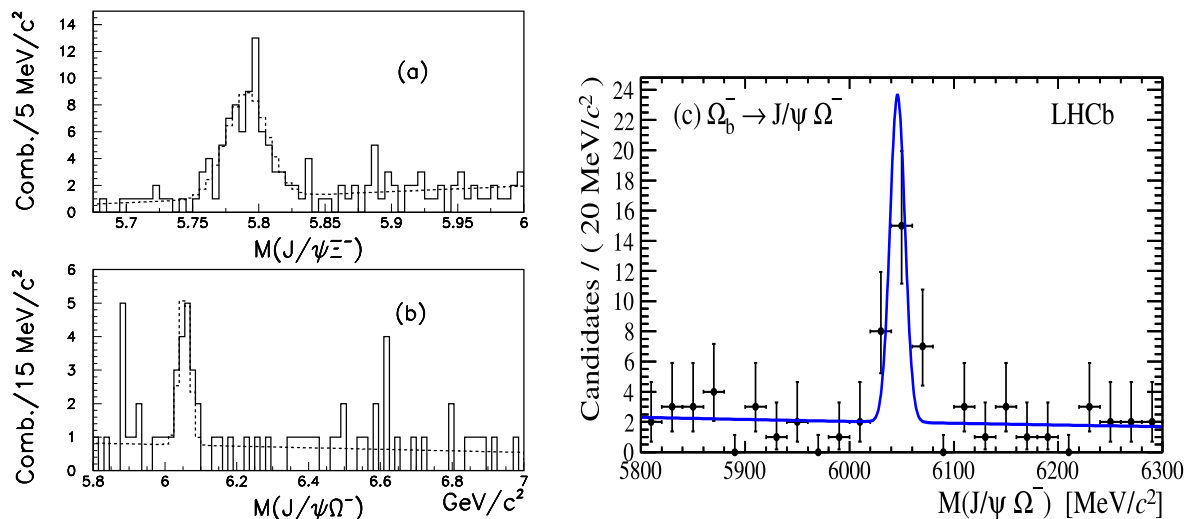


3.4.3. The Ξ_b States The first direct observation of a Ξ_b baryon was reported in 2007 by the DØ collaboration at Fermilab in $p\bar{p}$ collisions at $\sqrt{s} = 1.96$ TeV [46] and later confirmed by CDF [57, 60, 63]. Earlier experiments at the CERN LEP e^+e^- collider had only observed indirect evidence of the Ξ_b^- baryon based on an excess of same-sign $\Xi^- l^-$ events in jets [85, 87, 88]. The left side of Figure 10 shows the $M(\Xi_b^-)$ distribution of the Ξ_b^- candidates from the original DØ analysis. The dotted curve represents an unbinned likelihood fit to the model of a constant background plus a Gaussian signal. The fit yields 15.2 ± 4.4 (stat) $_{-0.4}^{+1.9}$ (syst) signal events with a significance of 5.5σ . A higher-statistics CDF analysis observed 66_{-9}^{+14} candidates in $\Xi_b^- \rightarrow J/\psi \Xi^-$ decays [60]. The mass was found to be 5790.9 ± 2.6 (stat) ± 0.8 (syst) MeV. Figure 11 (a) shows the $J/\psi \Xi^-$ mass distribution from CDF. The most precise mass measurement of the Ξ_b^- was recently reported by LHCb to be 5795.8 ± 0.9 (stat) ± 0.4 (syst) MeV [12].

The observation of the Ξ_b^0 has almost completed the discovery of the ground-state baryons with beauty content. The $\Sigma_b^{(*)0}$ states remain hitherto unobserved. In 2011, CDF reported a signal of $25.3_{-5.4}^{+5.6}$ candidates through the decay chain $\Xi_b^0 \rightarrow \Xi_c^+ \pi^-$, where $\Xi_c^+ \rightarrow \Xi^- \pi^+ \pi^+$, using data from $p\bar{p}$ collisions at $\sqrt{s} = 1.96$ TeV [63]. Figure 10 (c) shows a clear signal at about 5.8 GeV in the invariant $\Xi_c^+ \pi^-$ mass distribution. Reconstructed from a similar decay sequence involving five final-state tracks and four decay vertices, Figure 10 (b) shows the signal for the Ξ_b^- in the invariant $\Xi_c^0 \pi^-$ mass distribution. The masses and yields of the signals were obtained in unbinned likelihood fits (dashed line in the figure). For the Ξ_b^0 , a mass of $5787.8 \pm 5.0_{\text{stat.}} \pm 1.3_{\text{sys.}}$ MeV was determined.

The most recent discovery of a baryon resonance with beauty-strange content has been reported from the LHC. In 2012, the CMS collaboration has reported on the

Figure 11. (Colour online) Observation of the Ω_b^- baryon. Left: The invariant mass distributions of (a) $J/\psi \Xi^-$ and (b) $J/\psi \Omega^-$ candidates from CDF showing the Ξ_b^- and the Ω_b^- , respectively. The projections of the unbinned mass fit are indicated by the dashed lines. Picture from [60]. Right: Invariant mass distribution of $\Omega_b^- \rightarrow J/\psi \Omega^-$ candidates from LHCb. Picture from [12].



observation of an excited Ξ_b^0 state, most likely Ξ_b^{*0} with $J^P = \frac{3}{2}^+$ [14]. The signal of about 20 events was observed in the difference between the mass of the $\Xi_b^- \pi^+$ system and the sum of the masses of the Ξ_b^- and π^+ , with a significance exceeding 5 standard deviations. Given the charged-pion and Ξ_b^- masses from the 2010 edition of the RPP [2], the resulting mass of the new resonance is 5945.0 ± 0.7 (stat.) ± 0.3 (syst.) ± 2.7 (PDG) MeV, where the last uncertainty reflects the accuracy of the PDG Ξ_b^- mass [2]. The new excited Ξ_b^{*0} state was observed in its strong decay into $\Xi_b^- \pi^+$. The signal yield of the Ξ_b^- was determined to be 108 ± 14 events, exceeding the earlier best CDF result by almost a factor of two. This shows again the big potential of the LHC as a machine for the discovery of new hadron resonances in the future.

3.4.4. The Ω_b States The doubly-strange Ω_b^- baryon (quark content ssb), was just recently discovered at Fermilab. None of its quantum numbers has been measured, but it is almost certainly the $\frac{1}{2}^+$ ground state. First reported in 2008 by the DØ collaboration in $\Omega_b^- \rightarrow J/\psi \Omega^-$ decays [49], it was confirmed in 2009 by the CDF collaboration in the same decay using 4.2 fb^{-1} of data from $p\bar{p}$ collisions at $\sqrt{s} = 1.96 \text{ TeV}$. Figure 11 (b) shows the $J/\psi \Omega^-$ distribution from CDF [60]. The signal is observed at a mass of 6054.4 ± 6.8 (stat.) ± 0.9 (syst.) MeV, in disagreement with the initial mass from DØ, which was determined to be $6165 \pm 10 \pm 13 \text{ MeV}$.

The mass measurements of the Ω_b^- baryon is thus particularly interesting because the CDF and DØ results differ by more than 6σ . The LHCb collaboration has also studied the Ω_b^- using data corresponding to an integrated luminosity of 1.0 fb^{-1} of

pp collisions at a center-of-mass energy of $\sqrt{s} = 7$ TeV [12]. This corresponds to the full data sample collected in 2011. Figure 11 (right) shows the $J/\psi \Omega^-$ distribution from the LHCb analysis [12]. The mass of the Ω_b^- signal has been extracted by performing an unbinned extended maximum likelihood fit using a Gaussian function for the signal and an exponential function for the background. It has been determined to [12]

$$M_{\Omega_b^-} = 6046.0 \pm 2.2 \pm 0.5 \text{ MeV}, \quad (3.16)$$

which is in very good agreement with the earlier CDF result [60] and closer to most theoretical predictions for the Ω_b^- which vary in the range from 5940 to 6120 MeV.

4. Light-Quark Baryons

4.1. From Cross Sections to Baryon Parameters

In contrast with the heavy baryons discussed above, light baryons are not usually found as narrow, isolated peaks in mass distributions or cross section measurements. Indeed, examination of the total or elastic cross section for πN scattering shows only three or four structures. Somehow, the parameters of a number of excited nucleons and Deltas have been extracted from the measurements that have been made. How is this done? We illustrate the challenges by discussing the process $\pi N \rightarrow \pi N$.

The process $\pi N \rightarrow \pi N$ is described in terms of two complex amplitudes. These may be helicity amplitudes, transversity amplitudes, Chew-Goldberger-Low-Nambu (CGLN) amplitudes, or amplitudes defined in some other convention. The fact that these amplitudes are complex means that the process requires four real numbers at every kinematic point for its description. Information about baryon resonances that may be formed as intermediate states in the process is contained in the amplitudes. Thus, the task required is the extraction of the amplitudes from the observables, which are necessarily bilinear in the amplitudes.

The extraction of four real numbers at every kinematic point requires four observables, but since the relationships between the observables and the amplitudes are bilinear, there are necessarily ambiguities in the extracted amplitudes. Furthermore, in order to extract information on different isospin states (nucleons and Deltas), observables from different processes ($\pi^+ p \rightarrow \pi^+ p$, $\pi^- p \rightarrow \pi^- p$ and $\pi^- p \rightarrow \pi^0 n$) must be combined. In general, these different processes may have been measured in different experiments, with different detectors, having different systematic uncertainties.

Once amplitudes have been extracted, they are expanded in partial waves according to isospin, and the task of searching for resonance signatures begins. Here, one does not look for peaks or bumps, but the phase structure of the amplitudes is used to provide clues about resonant contributions. For a single, narrow, isolated resonance that couples to a single channel, the real part of the scattering amplitude vanishes on resonance, and the imaginary part will go through a maximum. On an Argand plot (real part of the amplitude vs. the imaginary part of the amplitude), the amplitude will describe a circle, or very nearly. When there are nearby resonances in the same channel, the behaviour of

the real and imaginary parts of the amplitude become significantly harder to interpret. The real part may no longer have a zero at the resonant mass, or the imaginary part may not go through a maximum. A weakly-coupled resonance may have very little effect on the amplitudes. If the data available do not provide good kinematic coverage, or one or more observables have not been measured, the extraction of resonance information becomes more challenging and more sensitive to model dependences and interpretation.

Just as it is well nigh impossible to identify resonances from total or differential cross sections alone, so, too, is it extremely difficult to identify resonance signatures from examining a single polarization observable. Such observables may give hints to underlying resonances, but it is unlikely that any sharp structures will be seen. Resonant effects turn on over an energy range that spans the width of the resonance, and this should be the case in any observable examined. Since these resonances are typically 100 to 300 MeV wide, any effect in a polarization observable can be expected to be gradual enough to be almost imperceptible.

For photoproduction processes, the number of independent amplitudes increases, and so does the number of observables that must be measured in order to extract these amplitudes with the least amount of ambiguity possible. The current status of photoproduction data in *any* channel is such that a full partial wave analysis (PWA) cannot be done, as an insufficient number of observables has been measured with sufficient precision. A few of the groups that extract baryon resonance parameters from experimental observables are carrying out *bona fide* partial wave analyses of the kind described above. However, many are constructing explicit models of the process, and using these models to obtain information. Whatever method is being used, not enough data yet exist to constrain these extractions. Hence, different groups make different claims about which resonances, old and new, are important in which region and for which process. It must be understood that a claim of a new resonance really means that ‘inclusion of such a state improves the fit to the data available’. For the analysts who do not see evidence for such a resonance, this really means that ‘inclusion of such a resonance, at the very best, does not significantly improve our fit to the data available’.

In the following sections, we discuss many ‘observations’ of resonances by various groups. We emphasize that these ‘observations’ really mean extractions, which means that inclusion of the resonance improved the fit to the available data.

4.2. The Known Baryons

In the 2012 edition of the RPP, the PDG lists 17 N^* resonances (including the proton and neutron) and 10 Δ resonances in its Summary Table [1] which have at least a 3-star assignment. This represents a significant change from the previous edition. Table 9 shows the Baryon Summary Table including recent changes. In the N^* sector, one new 3-star N^* resonance, $N(1875) \frac{3}{2}^-$, has been added and one further resonance, $N(1900) \frac{3}{2}^+$, has been upgraded to a 3-star state. Moreover, seven additional resonances

have been proposed and three removed. In the Δ sector, one negative-parity resonance, $\Delta(1940)\frac{3}{2}^-$, has been upgraded to a slightly better established state, but the 2-star assignment indicates that the evidence for its existence is still poor. The list of hyperons remains unchanged from the 2010 edition.

Table 9. (Colour online) Baryon Summary Table for N^* and Δ resonances including recent changes from PDG 2010 [2] to PDG 2012 [1].

N^*	$J^P (L_{2I,2J})$	2010	2012	Δ	$J^P (L_{2I,2J})$	2010	2012
p	$1/2^+ (P_{11})$	****	****	$\Delta(1232)$	$3/2^+ (P_{33})$	****	****
n	$1/2^+ (P_{11})$	****	****	$\Delta(1600)$	$3/2^+ (P_{33})$	***	**
$N(1440)$	$1/2^+ (P_{11})$	****	****	$\Delta(1620)$	$1/2^- (S_{31})$	****	****
$N(1520)$	$3/2^- (D_{13})$	****	****	$\Delta(1700)$	$3/2^- (D_{33})$	****	****
$N(1535)$	$1/2^- (S_{11})$	****	****	$\Delta(1750)$	$1/2^+ (P_{31})$	*	*
$N(1650)$	$1/2^- (S_{11})$	****	****	$\Delta(1900)$	$1/2^- (S_{31})$	**	**
$N(1675)$	$5/2^- (D_{15})$	****	****	$\Delta(1905)$	$5/2^+ (F_{35})$	****	****
$N(1680)$	$5/2^+ (F_{15})$	****	****	$\Delta(1910)$	$1/2^+ (P_{31})$	****	****
$N(1685)$			*				
$N(1700)$	$3/2^- (D_{13})$	**	**	$\Delta(1920)$	$3/2^+ (P_{33})$	**	**
$N(1710)$	$1/2^+ (P_{11})$	**	**	$\Delta(1930)$	$5/2^- (D_{35})$	**	**
$N(1720)$	$3/2^+ (P_{13})$	****	****	$\Delta(1940)$	$3/2^- (D_{33})$	*	**
$N(1860)$	$5/2^+$		**				
$N(1875)$	$3/2^-$		***				
$N(1880)$	$1/2^+$		**				
$N(1895)$	$1/2^-$		**				
$N(1900)$	$3/2^+ (P_{13})$	**	***	$\Delta(1950)$	$7/2^+ (F_{37})$	****	****
$N(1990)$	$7/2^+ (F_{17})$	**	**	$\Delta(2000)$	$5/2^+ (F_{35})$	**	**
$N(2000)$	$5/2^+ (F_{15})$	**	**	$\Delta(2150)$	$1/2^- (S_{31})$	*	*
$N(2080)$	D_{13}	**		$\Delta(2200)$	$7/2^- (G_{37})$	*	*
$N(2090)$	S_{11}	*		$\Delta(2300)$	$9/2^+ (H_{39})$	**	**
$N(2040)$	$3/2^+$		*				
$N(2060)$	$5/2^-$		**				
$N(2100)$	$1/2^+ (P_{11})$	*	*	$\Delta(2350)$	$5/2^- (D_{35})$	*	*
$N(2120)$	$3/2^-$		**				
$N(2190)$	$7/2^- (G_{17})$	****	****	$\Delta(2390)$	$7/2^+ (F_{37})$	*	*
$N(2200)$	D_{15}	**		$\Delta(2400)$	$9/2^- (G_{39})$	**	**
$N(2220)$	$9/2^+ (H_{19})$	****	****	$\Delta(2420)$	$11/2^+ (H_{3,11})$	****	****
$N(2250)$	$9/2^- (G_{19})$	****	****	$\Delta(2750)$	$13/2^- (I_{3,13})$	**	**
$N(2600)$	$11/2^- (I_{1,11})$	**	**	$\Delta(2950)$	$15/2^+ (K_{3,15})$	**	**
$N(2700)$	$13/2^+ (K_{1,13})$	**	**				

4.3. Experimental Methods and Major Experiments

Light-flavour baryon resonances can be studied using a large variety of different production mechanisms. Most laboratories employ fixed-target experiments and different kinds of either hadronic or electromagnetic beams to induce a reaction. Prominent examples are pion, electron, and photon beams, but kaon and proton beams have also been used.

Baryons can be produced directly in formation (as opposed to production) experiments without a recoil particle, so that they may be identified in the cross section, e.g. in the reaction $\pi^+p \rightarrow \Delta^{++} \rightarrow p\pi^+$. All peaks in Figure 12 can be assigned to short-lived states, although the broad resonances strongly overlap. This method allows access only to states with strangeness $S \leq 1$ owing to the nature of the available particle beams. A more general method is the production of baryons in production experiments. A prominent example is the photoproduction of hyperons, e.g. $\gamma p \rightarrow KY^*$, where the hyperon is produced with a strange partner, or the production of Ξ resonances in the decay of excited Σ or Λ states, e.g. $Y^* \rightarrow K\Xi$. An alternative approach is the production of excited nucleons in the decays of heavy mesons like the J/ψ and the $\psi(2S)$.

In this section, we discuss the different production mechanisms and associated observables which can be determined experimentally. A brief survey of major experiments will be given. As has been pointed out in Section 4.1, PWA are recognized as the most powerful tools for the purpose of extracting resonance contributions. For this reason, we will briefly review some approaches in the last part of this section.

4.3.1. Baryon Production using Hadronic Probes Most of the information about non-strange baryon resonances listed by the PDG has been extracted from PWA of πN elastic scattering data in the reaction, $\pi N \rightarrow \pi N$, and charge exchange data, e.g. in the reaction $\pi^-p \rightarrow n\pi^0$. The total reaction rate for elastic πN scattering is given as [89]

$$\rho_f I = I_0 \left[1 + \vec{\Lambda}_i \cdot \vec{P} + \vec{\sigma} \cdot \vec{P}' + \Lambda_i^\alpha \sigma^{\beta'} O_{\alpha\beta'} \right], \quad (4.1)$$

where \vec{P} represents the polarization asymmetry that arises if the target nucleon is polarized, $\rho_f = \frac{1}{2}(1 + \vec{\sigma} \cdot \vec{P}')$ is the density matrix of the recoiling nucleon, and $O_{\alpha\beta'}$ represent the double-polarization observables if the Cartesian α component of the target polarization is known and the Cartesian β' component of the recoil polarization is measured. The primes indicate that the recoil observables, defined in terms of helicity amplitudes, are measured with respect to the set of axes x', y', z' , in which the z' -axis is parallel to the momentum of the recoil nucleon. If the observables are defined in terms of transversity amplitudes, the x', y', z' axes are the same as the x, y, z axes. $\vec{\Lambda}_i$ is the polarization of the initial nucleon. The 16 quantities in (Equation (4.1)) are not all independent, and many of them vanish. For instance, since the strong interaction conserves parity, the observables P_x, P_z, P'_x and P'_z must vanish for the process $\pi N \rightarrow \pi N$. In fact, for this process, there are only four linearly-independent

non-vanishing observables. A number of relationships among the observables reduce to a single relationship

$$P_y^2 + O_{xx'}^2 + O_{xz'}^2 = 1. \quad (4.2)$$

A summary of the relevant formulas including those for the reaction $\pi N \rightarrow \pi\pi N$ and the derivation of (Equation (4.2)) are given in [89]. The observables in (Equation (4.2)) can also be expressed in terms of the observables, P , R , and A , more often found in the literature

$$R = O_{xx'} \cos \theta - O_{xz'} \sin \theta, \quad (4.3)$$

$$A = O_{xx'} \sin \theta + O_{xz'} \cos \theta, \quad \text{and} \quad (4.4)$$

$$P^2 + A^2 + R^2 = 1, \quad (4.5)$$

where $P = P_y$ is the (target or recoil) polarization of the proton perpendicular to the reaction plane, and R and A are the components of the proton polarization transfer along its direction of flight and perpendicular to its direction of flight, respectively. The measurement of the two spin-rotation parameters, R and A , provides experimental information on the relative phase of the transverse scattering amplitude and is required to unambiguously extract the πN elastic scattering amplitude. Note that the same observables can be measured in any process $PB \rightarrow P'B'$, where P and P' are pseudoscalar mesons, and B and B' are spin- $\frac{1}{2}$ baryons.

The first experiments using strongly-interacting beams were performed between 1957 and 1979 with most of the largest resonance-region experiments done at the Nimrod accelerator at Rutherford Laboratory. They focused mostly on the πN system and the production of non-strange baryon resonances. Later πN experiments extracted cross sections with much smaller statistical and systematic uncertainties and also measured polarization observables. We refer to the Durham Reaction Database [90] and the Data Analysis Center at George-Washington University [91] for the full experimental database. The most recent πN elastic and charge-exchange results published after 2000 come from experiments at the Brookhaven National Laboratory (BNL) [92], the Tri-University Meson Facility (TRIUMF) [93], and the Paul Scherrer Institute (PSI) [94, 95], for instance. The polarization parameter, P , and the spin-rotation parameter, A , were published recently by the ITEP-PNPI collaboration based on experiments at the Institute for Theoretical and Experimental Physics (ITEP) [96, 97]. Earlier recoil polarization data were accumulated in the 1980s at Los Alamos, e.g. [98, 99]. A description of the experimental setups can be found in the references given.

In addition to πN elastic scattering, the Crystal Ball collaboration studied inelastic pion and kaon nucleon scattering in experiments at BNL. At the center of the experimental setup was the Crystal Ball (CB) multiphoton spectrometer, which consisted of 672 optically isolated NaI(Tl) crystals covering 93% of the 4π solid angle. The typical energy resolution for electromagnetic showers in the CB spectrometer was $\Delta E/E = 0.020/(E[\text{GeV}])^{0.36}$. The detector is described in more detail in [100]. The collaboration also performed important measurements of kaon-induced reactions.

Relevant results can be found in [100, 101, 102, 103, 104, 105, 106, 107, 108, 109, 110, 111, 112]. The Crystal Ball detector was later moved to MAMI where photoproduction experiments are currently being performed.

4.3.2. Baryons in Electromagnetically-Induced Reactions Many baryon resonances are produced abundantly in electromagnetically-induced reactions off the nucleon. While photoproduction experiments serve to establish the systematics of the spectrum, electron beams are ideal to measure resonance form factors and their corresponding Q^2 dependence. The latter provides information on the structure of excited nucleons and on the (effective) confining forces of the 3-quark system.

The electromagnetic transition from the nucleon ground state to any resonant excited state can be described in terms of photon helicity amplitudes, so that the transverse and longitudinal virtual photon cross sections at resonance can be written as

$$\sigma_T(\nu_R, Q^2) = \frac{2M}{\Gamma_R M_R} [|A_{\frac{1}{2}}|^2 + |A_{\frac{3}{2}}|^2], \quad (4.6)$$

$$\sigma_L(\nu_R, Q^2) = \frac{4M}{\Gamma_R M_R} [|S_{\frac{1}{2}}|^2], \quad (4.7)$$

where M_R and Γ_R are the invariant mass of the resonance and its decay width, respectively. The detailed analysis of the Q^2 dependence of the virtual photon cross sections from electron scattering data can be used to extract transition form factors for each of the nucleon resonances, see e.g. [10] for a recent review.

In processes such as $(e, e' \pi)$ and $(e, e' \eta)$, the initial and final nucleon can each have two possible spin states, and the photon has one longitudinal (L) and two transverse (T) helicity states. Parity considerations reduce these 12 initial matrix elements to six independent amplitudes, which can be expanded in multipoles, i.e. amplitudes ordered according to angular momentum. The detailed derivation of these expansions in so-called CGLN amplitudes has been discussed in [113]. The individual contributions to the differential cross section for electroproduction of a single pseudoscalar meson off the nucleon, $d\sigma_i/d\Omega$ ($i = T, L, TL, TT, TT, TL', TT'$), are usually parametrised in terms of response functions, $R_i^{\beta\alpha}$, which depend on the independent kinematical variables. The additional indices, α and β , describe the target and recoil polarization of the final-state baryon, respectively. A nice summary and derivation of formulae relevant to electroproduction is given in [114]. A full determination of the six electroproduction amplitudes requires a suitable combination of polarization observables, such as the beam asymmetry (of the polarized photon) or the target asymmetry (of the polarized proton), and the polarization of the recoil nucleon. Recent results from electroproduction experiments come from MAMI and Jefferson Lab, for instance.

For real photons, the longitudinal component of the photon polarization vanishes. The photoproduction of single-pseudoscalar mesons off the nucleon is thus described by four complex helicity amplitudes: two for the spin states of the photon, two for the target nucleon, and two for the recoiling baryon; parity considerations reduce these eight amplitudes to four. Experimentally, 16 observables can be determined: the unpolarized

differential cross section, $d\sigma_0$, three single-spin observables, Σ (beam), T (target), P (recoil), and three sets of four asymmetries: beam-target (BT), beam-recoil (BR), and target-recoil (TR). It has been shown in [115] that angular distributions of at least eight carefully chosen observables at each energy are needed for both proton and neutron to determine the full scattering amplitude without ambiguities. The ambitious program of a complete experiment in photoproduction was first formulated by Barker *et al.* in 1975 [116]. The differential cross section for the three sets of asymmetries can be written (for BT, BR, and TR, respectively) (colour online)

$$\begin{aligned} \frac{d\sigma}{d\Omega} = \sigma_0 \{ & 1 - P_T \Sigma \cos 2\phi + P_x (-P_T H \sin 2\phi + P_\odot F) \\ & - P_y (-T + P_T P \cos 2\phi) \\ & - P_z (-P_T G \sin 2\phi + P_\odot E) \}, \end{aligned} \quad (4.8)$$

$$\begin{aligned} \frac{d\sigma}{d\Omega} = \sigma_0 \{ & 1 - P_T \Sigma \cos 2\phi + P_{x'} (-P_T O_{x'} \sin 2\phi - P_\odot C_{x'}) \\ & - P_{y'} (-P + P_T T \cos 2\phi) \\ & - P_{z'} (-P_T O_{z'} \sin 2\phi + P_\odot C_{z'}) \}, \end{aligned} \quad (4.9)$$

$$\begin{aligned} \frac{d\sigma}{d\Omega} = \sigma_0 \{ & 1 + P_{y'} P + P_x (P_{x'} T_{x'} + P_{z'} T_{z'}) \\ & + P_y (T + P_y \Sigma) \\ & - P_z (P_{x'} L_{x'} - P_{z'} L_{z'}) \}, \end{aligned} \quad (4.10)$$

where σ_0 denotes the unpolarized differential cross section, P_T and P_\odot denote the linear and circular degree of photon polarization, respectively, and ϕ is the angle between the photon polarization vector and the reaction plane. The target polarization vector is represented by (P_x, P_y, P_z) and the polarization observables are shown in blue. A total of 16 observables exist in photoproduction, whereas in electroproduction, four additional observables exist for the exchange of longitudinal photons and further 16 observables arise from longitudinal-transverse interference [114].

The polarization observables that can be extracted from experiments in single-pseudoscalar photoproduction are summarised in Table 10. Since some observables can be extracted from more than one experiment, this will allow multiple cross checks of measurements with different systematics. For example, the beam asymmetry, Σ , can be extracted in a single-polarization experiment with a linearly-polarized beam and an unpolarized target, but it can also be extracted in a double-polarization experiment with an unpolarized beam and a transversely-polarized target and measuring the recoil polarization $P_{y'}$.

Major Experimental Facilities Photo- and electroproduction experiments have been performed for decades at many different laboratories. However, high-statistics results and a large variety of single- and double-polarization observables have become available only recently.

Table 10. Polarization observables in single-pseudoscalar photoproduction using all combinations of beam, target, and recoil polarization. The observables without hats and tildes can be extracted directly. Moreover, observables with hats are single-polarization observables that can be extracted from double-polarization asymmetries and observables with tildes are double-polarization observables that can be extracted from triple-polarization asymmetries [117].

Beam		Target	Recoil	Target-Recoil									
		x y z	x' y' z'	x y z	x y z	x y z	x y z	x y z	x y z	x y z			
	σ_0	T	P	$T_{x'}$	$L_{x'}$	$\hat{\Sigma}$	$T_{z'}$	$L_{z'}$					
P_T	Σ	H \hat{P} G	$O_{x'}$ \hat{T} $O_{z'}$	$\tilde{L}_{z'}$	$\tilde{C}_{z'}$	$\tilde{T}_{z'}$	\tilde{E}	\tilde{F}	$\tilde{L}_{x'}$	$\tilde{C}_{x'}$	$\tilde{T}_{x'}$		
P_\odot		F E	$C_{x'}$ $C_{z'}$	$\tilde{O}_{z'}$	\tilde{G}	\tilde{H}	$\tilde{O}_{x'}$						

The CEBAF Large Acceptance Spectrometer (CLAS) at Jefferson Lab can be operated with electron beams and with energy-tagged photon beams. It utilizes information from a set of drift chambers in a toroidal magnetic field and time-of-flight information to detect and reconstruct charged particles. Each of the six drift-chamber sectors is instrumented as an independent spectrometer with 34 layers of tracking chambers allowing for the full reconstruction of the charged particle 3-momentum vectors. A detailed description of the spectrometer and its various detector components is given in [118]. Since CLAS has only a very limited photon-detection coverage, an undetected neutral particle is inferred through the overdetermined kinematics, making use of the good momentum and angle resolution of $\Delta p/p \approx 1\%$ and $\Delta\theta \approx 1\text{--}2^\circ$, respectively. Recent double-polarization measurements in photoproduction have been performed utilizing a frozen-spin butanol target for reactions off the proton and a polarized solid HD target for reactions off the neutron. Relevant results from electroproduction experiments are given in [119, 120, 121, 122, 123, 124, 125, 126, 127, 128, 129, 130, 131, 132] and results from photoproduction experiments can be found in [133, 134, 135, 136, 137, 138, 139, 140, 141, 142, 143, 144].

At ELSA, different experimental setups were used to extract cross section data and further polarization observables for several photo-induced reactions using tagged photons. In 2001, the CB-ELSA detector recorded events to analyze the reactions $\gamma p \rightarrow p\pi^0$ [145, 146], $\gamma p \rightarrow p\eta$ [147, 148], $\gamma p \rightarrow p\pi^0\pi^0$ [149], $\gamma p \rightarrow p\pi^0\eta$ [150, 151], and $\gamma p \rightarrow p\pi^0\omega$ [152]. The original experiment consisted of the Crystal Barrel (CB) calorimeter with its 1380 CsI(Tl) crystals covering 97.8% of 4π [153]. The CB

calorimeter had an excellent photon-detection efficiency and covered polar angles from 12° to 168° . Charged reaction products were detected in a three-layer scintillating fiber detector which surrounded the 5 cm long liquid hydrogen target. More information about the experiment can be found in [146].

The experimental setup was later modified and in a series of measurements in 2002/2003, utilized a combination of the CB calorimeter and the BaF₂ TAPS detector in the forward direction. The experiment covered almost the full 4π solid angle. The CB detector in its CBELSA/TAPS configuration consisted of 1290 CsI(Tl) crystals, which had a trapezoidal shape and were oriented toward the target, with a thickness of $16 X_R$, and covered the polar angles from 30° to 168° . TAPS consisted of 528 hexagonal BaF₂ crystals with a length of approximately $12 X_R$, and covered the polar angles from 5° to 30° . Both calorimeters covered the full azimuthal circle. TAPS was configured as a hexagonal wall and served as the forward endcap of the CB. Forward-going protons were detected by plastic scintillators (5 mm thick) located in front of each TAPS module; the other protons were detected by the three-layer scintillating fiber detector. Results of the CBELSA/TAPS setup on measurements off the proton can be found in [154, 155, 156, 157, 158, 159, 160, 161, 162, 163] and off the neutron in [164, 165, 166]. Results from a modified CBELSA/TAPS setup include a polarized frozen-spin butanol target [167].

The SAPHIR detector [168] was a multi-purpose magnetic spectrometer at ELSA with a large angular acceptance consisting of a tagging facility, drift chambers and a scintillator wall for triggering and time-of-flight measurements. The detector covered the full polar angular range from 0° to 180° , but the accepted solid angle was limited to approximately $0.6 \times 4\pi$ sr due to the magnet pole pieces. The photon flux was measured using the tagging system and a photon-veto counter downstream of the detector. Relevant results can be found in [169, 170, 171, 172, 173, 174].

At the recently upgraded Mainz Microtron (MAMI-C), an experimental setup utilizing a combination of the NaI(Tl) Crystal Ball and the BaF₂ TAPS multiphoton spectrometers has recorded high-quality data for several years. While the NaI(Tl) crystals are arranged in two hemispheres which cover 93 % of the 4π solid angle, TAPS subtends the full azimuthal range for polar angles from 1° to 20° . Since the TAPS calorimeter was installed 1.5 m downstream of the Crystal Ball center, the resolution of TAPS in the polar angle θ was better than 1° . For an electron beam energy of 1508 MeV, a tagger channel in this experiment has a width of about 2 MeV at 1402 MeV and about 4 MeV at 707 MeV (the η -production threshold). Relevant results from MAMI including the Crystal Ball experiment can be found in [175, 176, 177, 178, 179, 180, 181, 182, 183].

The GRAAL facility was located at the European Synchrotron Radiation Facility (ESRF) in Grenoble, France. For a detailed description of the facility, we refer to [184]. The tagged and polarized γ -ray beam was produced by Compton scattering of laser photons off the 6 GeV electrons circulating in the storage ring. The photon energy was provided by an internal tagging system consisting of silicon microstrips for the detection of the scattered electron and a set of plastic scintillators for Time-of-Flight

(ToF) measurements [185]. At larger angles, the photons from the decay of a neutral meson were detected in a BGO calorimeter made of 480 crystals. At forward angles, the photons could be detected in a lead-scintillator sandwich ToF wall, but the detector was not used in all analyses, thus limiting somewhat the forward acceptance. Results on cross section measurements were recently reported for $p\pi^0$ [184], $p\eta$ [185, 186], $p\omega$ [187], $p\pi^0\pi^0$ [188], and $n\pi^0\pi^0$ [189]. Results on beam asymmetries for a large variety of reactions can be found in [184, 187, 188, 189, 190, 191, 192, 193, 194, 195, 196].

At the SPring-8/LEPS facility, the γ beam was produced by backward-Compton scattering of laser photons off electrons with an energy of 8 GeV. The liquid hydrogen target had a length of 16.5 cm and data were accumulated with about 1.0×10^{12} photons at the target. Charged particles were detected by using the LEPS magnetic spectrometer with an angular coverage of about $\pm 20^\circ$ and $\pm 10^\circ$ in the horizontal and vertical directions, respectively. Relevant results are published in [197, 198, 199].

4.3.3. Baryon Production in the Decay of Heavy Mesons The decays of charmonium ($c\bar{c}$) mesons have proven to be a good laboratory in recent years for studying not only excited nucleon states, but also excited hyperons, such as Λ^* , Σ^* , and Ξ^* states. The production of excited baryons in J/ψ decays has a particular advantage since it serves as an isospin filter. The πN system in decays such as $J/\psi \rightarrow \bar{N}N\pi$ is limited to isospin $\frac{1}{2}$. Excited Δ states are thus excluded, but all excited nucleons which are accessible in photo- and electroproduction experiments can also be studied in charmonium decays. Table 11 shows a selection of branching ratios of heavy mesons into a baryon, an anti-baryon and mesons. In addition to the J/ψ , the $\psi(2S)$ can be used to study excited baryons. Further heavy mesons, e.g. the $\psi(3770)$ and B mesons, have been observed to decay into $p\bar{p} +$ mesons, but the branching ratios are small and the available statistics not yet sufficient to allow partial wave analyses.

Table 11. Selected branching ratios of heavy mesons for decays into a baryon, an anti-baryon, and mesons (Particle Data Group [1]).

	J/ψ	$\psi(2S)$	$\psi(3770)$	B^0
$p\bar{p}\pi^0$	$(1.19 \pm 0.08) \times 10^{-3}$	$(1.50 \pm 0.08) \times 10^{-4}$	$< 1.2 \times 10^{-3}$	$< 2.5 \times 10^{-4}$
$p\bar{p}\pi^+\pi^-$	$(6.0 \pm 0.5) \times 10^{-3}$	$(6.0 \pm 0.4) \times 10^{-4}$	$< 5.8 \times 10^{-4}$	
$p\bar{p}\eta$	$(2.00 \pm 0.12) \times 10^{-3}$	$(5.7 \pm 0.6) \times 10^{-5}$	$< 5.4 \times 10^{-4}$	
$p\bar{p}\omega$	$(1.10 \pm 0.15) \times 10^{-3}$	$(6.9 \pm 2.1) \times 10^{-5}$	$< 2.9 \times 10^{-4}$	
$p\bar{n}\pi^-$	$(2.12 \pm 0.09) \times 10^{-3}$	$(2.48 \pm 0.17) \times 10^{-4}$		
$\Lambda\bar{\Lambda}\pi^0$	$< 6.4 \times 10^{-5}$	$< 1.2 \times 10^{-4}$		
$\Lambda\bar{\Lambda}\eta$	$(2.6 \pm 0.7) \times 10^{-4}$	$< 4.9 \times 10^{-5}$		
$pK^-\bar{\Lambda}$	$(8.9 \pm 1.6) \times 10^{-4}$			
$pK^-\bar{\Sigma}^0$	$(2.9 \pm 0.8) \times 10^{-4}$			

Excited nucleon states in J/ψ and $\psi(2S)$ decays have mostly been studied at the BEIJING Spectrometer (BES). The upgraded BESIII spectrometer is a general purpose solenoidal detector at the Beijing Electron Positron Collider II operating in the energy range 2-4.6 GeV with a reported peak luminosity of $6 \times 10^{32} \text{ cm}^{-2} \text{ s}^{-1}$ at a beam energy of 1.88 GeV [200]. Charged particles are observed in a small-cell, helium-based drift chamber with a momentum resolution of 0.5% at $p = 1 \text{ GeV}$. An electromagnetic CsI(Tl) calorimeter allows the detection and reconstruction of photons with an energy resolution of 2.5% in the barrel and 5% in the endcaps. Additional particle identification is based on a Time-of-Flight (ToF) system which provides a 2σ K/π separation for momenta up to about 1 GeV. The BESIII detector is described in more details in [201]. Results relevant to this review are given in [202, 203, 204, 205, 206, 207, 208, 209, 210, 211].

The reaction $\psi(2S) \rightarrow p\bar{p}\pi^0$ was also studied by the Mark-II collaboration [212] and more recently at CLEO [29]. The CLEO detector has been discussed in Section 3.2. The decay of the $\psi(2S)$ provides a larger phase space than the decay of the J/ψ , which limits the N^* search in the $p\bar{p}\pi^0$ channel to states with $M_{N^*} \approx 2.1 \text{ GeV}$.

4.4. Partial-Wave Analyses

The recently accumulated high-statistics data sets of electromagnetically-induced meson production reactions provide an unprecedented opportunity to obtain a better understanding of the properties of excited baryons. Owing to the broad and overlapping nature of these resonances, amplitude or partial-wave analyses need to be performed to extract N^* parameters from the data. While such approaches have been well developed in the Δ region, the situation is very complicated at higher energies. Many open channels need to be considered and any reliable extraction of resonance properties must be based on a coupled-channel approach. Several groups have significantly contributed to our understanding of baryon resonances, but a comprehensive PWA based on a larger database of observables has been performed only at very few institutions. These approaches are briefly discussed in this section.

PWA formalisms have been developed at several places using different techniques to extract nucleon resonance parameters. A detailed discussion of the theoretical approaches goes beyond the scope of this review, but a few general remarks are appropriate. In most coupled-channel analyses, instead of using partial wave amplitudes, the database of scattering observables, such as differential and total cross sections as well as polarization observables, is fitted directly. Masses and widths of resonances can be determined from Breit-Wigner parametrizations, but more than one possible Breit-Wigner pole parametrization exists. The K -matrix formalism is used for overlapping resonances in the same partial wave and provides an elegant way of ensuring that the amplitudes preserve unitarity. Based on properties of the trace of the T -matrix and the associated K -matrix, Ceci *et al.* [213] proposed an alternative method for extracting resonance parameters from a multi-channel fit to scattering data, without relying on

Breit-Wigner parametrizations. However, a recent study did not find a simple connection between T -matrix poles and the associated K -matrix poles [214]. The authors also note that K -matrix poles are not generally independent of background contributions. The PDG [1] typically gives the T -matrix poles in the particle listings.

4.4.1. SAID and MAID The SAID (Scattering Analysis Interactive Dial-in) group maintains an extensive database of (elastic) πN (including πd), KN , and NN scattering data as well as of data on the electromagnetic production of a single pseudoscalar meson [215]. In addition to the data, the SAID website also provides access to partial-wave amplitudes extracted, and to predictions of a large variety of energy-dependent observables. The most recent solution for π photoproduction including the full SAID database for single π production is discussed in [216]. Baryon masses and widths are determined from a Breit-Wigner parametrization of the resonance contributions using πN scattering data. The helicity amplitudes $A_{1/2}$ and $A_{3/2}$ are extracted based on the masses, widths, and πN branching fractions determined in earlier analyses of πN elastic scattering data [217]. Progress was reported on the extraction of photo-decay couplings, but no new resonances have been proposed. The most recent solution for η photoproduction was discussed in [180].

The MAID partial wave analysis group maintains a similar website, which gives predictions for multipoles, amplitudes, cross sections, and polarization observables for photo- and electroproduction in the energy range from the pion threshold up to $W = 2$ GeV [218]. A recent comprehensive study of the world data of pion photo- and electroproduction was reported in [219] using the unitary isobar model MAID2007. In addition to resonance properties, the longitudinal and transverse helicity amplitudes of nucleon resonance excitations for all the 4-star resonances below $W = 2$ GeV were presented. The group has developed similar models for η and η' production. The most recent solution for η photoproduction was discussed in [180]. Amplitudes for K photoproduction in a multipole approach were presented in [220].

Neither MAID nor SAID treats the important $\pi\pi$ production channels explicitly and their results need to be re-examined. Nevertheless, the databases and model predictions represent an invaluable tool for the field.

4.4.2. The Excited Baryon Analysis Center at Jefferson Lab The Excited Baryon Analysis Center (EBAC) at Jefferson Lab was established in 2006 with the goal of performing a dynamical coupled-channels analysis of the world πN and $\gamma^* N$ scattering data in order to determine meson-baryon partial-wave amplitudes and to extract N^* parameters from these amplitudes. The developed dynamical coupled-channel (DCC) reaction model is based on an energy-independent Hamiltonian formulation [221] and satisfies the essential two- and three-body unitarity conditions. Since the bare N^* states are defined as the eigenstates of the Hamiltonian in which the couplings to the meson-baryon continuum states are turned off, the extracted bare states can be related to the hadron states from constituent quark models and those from Dyson-Schwinger

approaches (static hadron models). Within the EBAC model, the bare N^* states become resonance states through the reaction processes. Thus, the model explicitly allows one to distinguish between the couplings of the bare N^* states from the meson-cloud (meson-baryon dressing) effects. This important and distinct feature will be discussed further in Section 5.3. A brief overview of EBAC results is given in [222].

First results from the DCC model were reported on the pion-induced reactions $\pi N \rightarrow \pi N$ [223], $\pi N \rightarrow \eta N$ [224], and $\pi N \rightarrow \pi\pi N$ [225]. The application of the model was also discussed for the analysis of π photoproduction [226] as well as electroproduction [227], which included the channels γ^*N , πN , ηN , and $\pi\pi N$. A simultaneous analysis of both single- and double-pion photoproduction is published in [228]. The authors note that the analysis of the single-pion production reactions alone is not enough to determine the amplitudes associated with the electromagnetic interactions. Both channels are required for the extraction of reliable information on N^* states below $W = 2$ GeV.

Several other groups have developed and used dynamical reaction models. We list here the approaches mentioned in the minireview on N^* and Δ resonances from the latest edition of the RPP: Argonne-Osaka [229], Bonn-Jülich [230, 231], Dubna-Mainz-Taipch [232], and Valencia [233].

4.4.3. The Gießen Coupled-Channel Analysis The group at the university in Gießen, Germany, has studied π - and γ -induced reactions for the final states γN , πN , $\pi\pi N$, ηN , and ωN within a coupled-channel phenomenological Lagrangian approach in the energy region from the pion threshold up to 2 GeV. In the model, the Bethe-Salpeter equation is solved in the K -matrix approximation in order to obtain the multi-channel scattering T -matrix. More details on the model are discussed in [234, 235, 236], for instance. Updates of the PWA have been reported regularly for several meson-production channels, e.g. more recently for ωN [237], $K\Lambda$ [238], $K\Sigma$ [239], and ηN [240].

4.4.4. The Bonn-Gatchina Partial-Wave Analysis Among all PWA groups, the Bonn-Gatchina group uses the largest experimental database in their multichannel approach including results from multiparticle final states like $p\pi^0\pi^0$ and $p\pi^0\eta$. To retain all correlations among the five independent kinematic variables for the latter reactions, these data are included in event-based likelihood fits. The analysis uses a K -matrix parametrization deriving the background terms from phenomenology rather than from a chiral Lagrangian as in the above Gießen model. The PWA method is described in more details in [241, 242] and the main findings from the different analyses are discussed in [243, 244, 245] for a large variety of reactions. The group also maintains a website which provides the Bonn-Gatchina πN partial wave amplitudes and photoproduction multipoles, as well as predictions for many yet to be determined observables [246].

The Bonn-Gatchina group has reported regularly on systematic searches for new baryon resonances. The latest summary of their results is presented in [247] including a list of all data used in the analysis. The group has proposed several new states and

strongly inspired the recent modifications in the RPP [1].

5. Recent Results in the Spectroscopy of Light-Quark Baryons

5.1. Pion-Nucleon Scattering Experiments

The most prominent signal in the $N\pi$ total cross section is that of the $\Delta(1232)$ which can be seen in Figure 12 at $p_{\pi^\pm} \approx 300$ MeV. The higher-mass structures consist of more than one resonance, and using a simple Breit-Wigner formula which describes a resonance enhancement with spin J and mass M in the total cross section for meson-nucleon scattering [5]

$$\Delta\sigma = 4\pi \left(\frac{\hbar}{p_{\text{c.m.}}} \right)^2 \left(J + \frac{1}{2} \right) x / (1 + \epsilon^2) \quad (5.1)$$

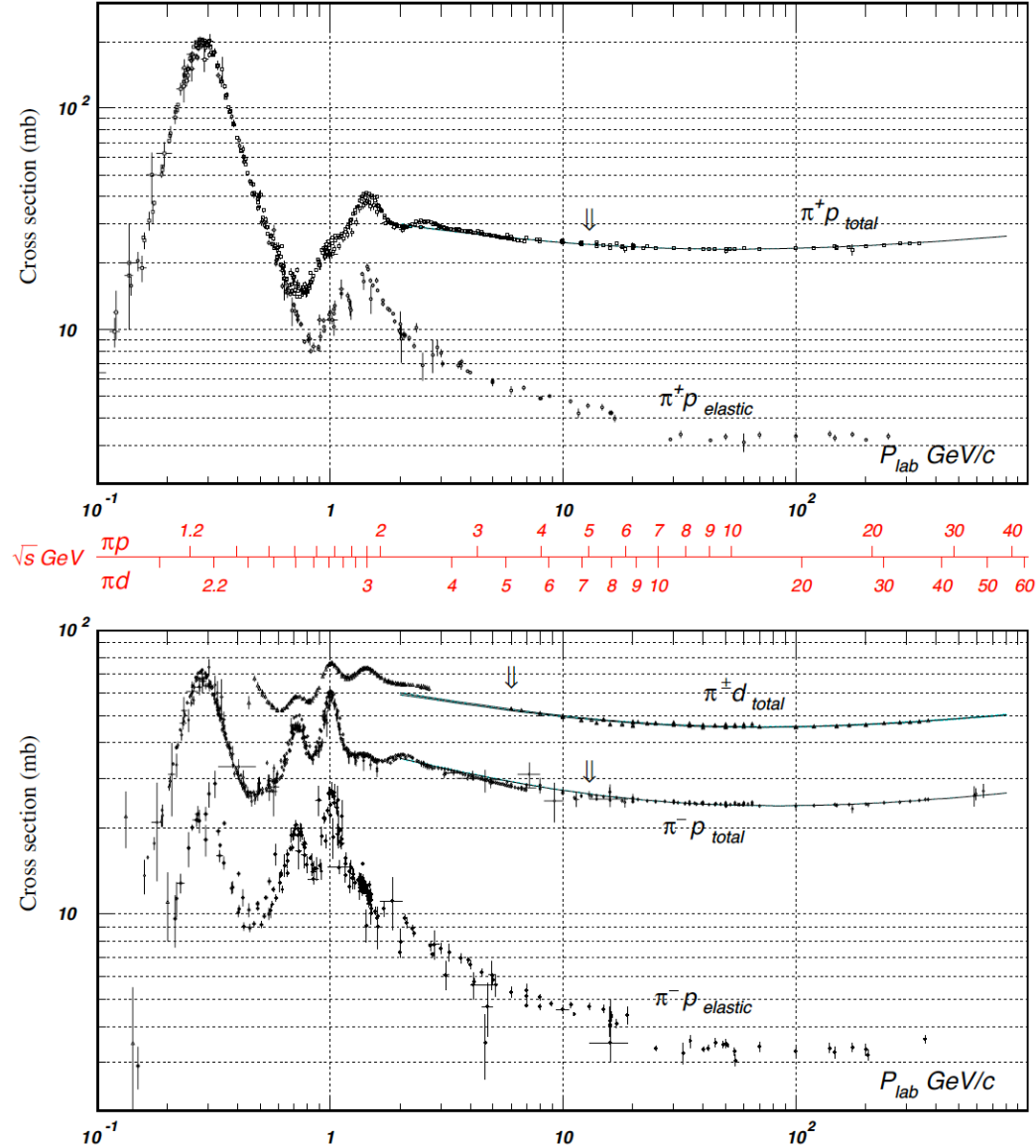
does not yield reliable information on resonance properties. Here, $\epsilon = 2(M - E_{\text{c.m.}})/\Gamma_{\text{tot}}$ and $x = \Gamma_{\text{el}}/\Gamma_{\text{tot}}$ denotes the resonance elasticity, which decreases strongly with mass. For this reason, the total cross section becomes almost featureless, as can be seen in Figure 12. An increasing number of inelastic channels becomes accessible with increasing resonance mass. The structures seen in the graph have been named first, second, third, etc. resonance region.

A large amount of data including polarization observables has been accumulated over the decades on the elastic πN channel and on the charge-exchange reaction, $\pi^- p \rightarrow n\pi^0$ (Section 4.3.1). Much fewer statistics are available for many other π -induced reactions. After 1980, studies of several inelastic channels were performed by the Crystal Ball collaboration at BNL in reactions such as $\pi^- p \rightarrow \eta n$ [101, 110], $\pi^- p \rightarrow \pi^0\pi^0 n$ [105, 107], and $\pi^- p \rightarrow \pi^0\pi^0\pi^0 n$ [102]. A review of the experimental situation on $\pi^- p \rightarrow \eta n$ before the recent BNL measurements is given in [248]. In 2009, the EPECUR collaboration started data-taking at the ITEP proton synchrotron with the goal of searching for narrow states in the second and third resonance regions via πp elastic scattering and $K\Lambda$ production. The first high-statistics results on the differential cross section for $\pi^- p$ elastic scattering have been published for the mass range (1650 - 1735) MeV with an excellent resolution of about 1 MeV [249].

As discussed in Section 4.1, all information on the N^* and Δ states listed by the PDG was determined from PWAs of πN total, elastic, and charge-exchange scattering data. Usually listed as the most comprehensive are the πN analyses performed by the Karlsruhe-Helsinki [250], the Carnegie-Mellon-Berkeley [251], and the George Washington [217] groups. The first two analyses used only data from the experiments performed before 1980, whereas the latter analysis represents the most recent study of πN scattering data (published in 2006). It includes not only an extended database with the most recent polarization data, but also data from inelastic channels like $\pi N \rightarrow \eta N$, needed for a better description of the πN S -wave.

All 4-star resonances were confirmed in the most recent analysis [217]. Surprisingly, however, all but two 3-star resonances and several with a fewer-star assignment

Figure 12. (Colour online) Total and elastic cross sections for $\pi^\pm p$ and $\pi^\pm d$ (total only) collisions from <http://pdg.lbl.gov/current/xsect/>. (Courtesy of the COMPAS Group, IHEP, Protvino, August 2005)



were either not observed or observed with different properties. For example, the $N(2000) F_{15}$ nucleon state was found, but with a mass closer to 1800 MeV. In the latest edition of the RPP [1], a further 2-star state with $J = \frac{5}{2}$, $N(1860) \frac{5}{2}^+$, has been added (Table 9). No evidence was found for the two 3-star states, $N(1700) \frac{3}{2}^-$ and $N(1710) \frac{1}{2}^+$. However, a new structure was observed in the $H_{1,11}$ wave with a mass around 2200 MeV. In the Δ sector, only a single P_{31} state was found with a pole position more in line with the (*) $\Delta(1750) \frac{1}{2}^+$ than with the (****) $\Delta(1910) \frac{1}{2}^+$. Below 2 GeV, three additional states, (**) $\Delta(1900) \frac{1}{2}^-$, (***) $\Delta(1920) \frac{3}{2}^+$, and (*) $\Delta(1940) \frac{3}{2}^-$, were absent.

As a step toward performing a complete coupled-channels analysis of the world database on the πN , $\gamma^* \rightarrow \pi N$, ηN , $\pi\pi N$ channels, EBAC has reported first results on the study of the $\pi N \rightarrow \pi N$ [223] and $\pi N \rightarrow \pi\pi N$ reactions [225]. The group observes all well-established 4-star resonances below 2 GeV. However, several of the resonances first announced in the late 1970s and listed by the PDG are also absent in the EBAC results. No evidence is found for the 3-star state, $N(1700) \frac{3}{2}^-$, consistent with the findings of the George-Washington group [217]. Moreover, only one $\Delta \frac{1}{2}^+$ state is reported with a mass consistent with the PDG $\Delta(1910) \frac{1}{2}^+$ state.

The differential cross section for the reaction $\pi^- p \rightarrow \eta n$ was measured recently by the Crystal Ball collaboration over the full angular range at seven incident π^- beam momenta from threshold to $p_{\pi^-} = 747$ MeV [110]. The angular distributions of this reaction are reported to be S -wave dominated. The total cross section was obtained by fully integrating over the differential cross sections and shows a rapid rise at threshold, as expected for S -wave-dominated production. A coupled-channel analysis of η production by the Gießen group shows that the main effects at $\sqrt{s} < 2$ GeV come from the three resonances, $N(1535) \frac{1}{2}^-$, $N(1650) \frac{1}{2}^-$, and $N(1710) \frac{1}{2}^+$ [240]. The well-established higher-spin resonance, $N(1520) \frac{3}{2}^-$, is required to reproduce the correct shape of the cross section, but the second $\frac{3}{2}^-$ state, $N(1900)$, is not consistent with the 3-star state, $N(1700) \frac{3}{2}^-$, currently listed by the PDG [1]. Results of the EBAC group confirm the dominance of the $N(1535) \frac{1}{2}^-$ resonance in the reaction $\pi^- p \rightarrow n\eta$ [224]. The authors also discuss the non-negligible roles of the two states, $N(1440) \frac{1}{2}^+$ and $N(1720) \frac{3}{2}^+$. It is worth noting though that the scarce experimental situation for most of the π -induced reactions does not provide enough information to reliably constrain resonance parameters.

An analysis of the reaction $\pi^- p \rightarrow n\pi^0\pi^0$ reveals no evidence for the strong production of a low-mass scalar meson, but double-pion production appears to become dominated by sequential π^0 decays through the $\Delta(1232)$ resonance as the beam momentum increases [105, 107]. The results are consistent with a recent PWA which observed large contributions from $N(1440) \frac{1}{2}^+$ interfering with $N(1535) \frac{1}{2}^-$ and $N(1520) \frac{3}{2}^-$ [252]. We will discuss resonance contributions in double-pion production in more details in Section 5.4.5.

5.2. Kaon-Nucleon Scattering Experiments

The observation of the relatively long-lived Σ baryon which can be produced by the strong interaction in $\pi^- p \rightarrow K^+\Sigma^-$, but decays only weakly via $\Sigma^- \rightarrow n\pi^-$ inspired the introduction of a new quantum number: Strangeness, S . The Σ hyperon with mass $M_{\Sigma^-} = (1197.449 \pm 0.030)$ MeV could also decay via strong interaction, but the decay into $\Lambda\pi^-$ is kinematically forbidden because $M_{\Lambda} = (1115.683 \pm 0.006)$ MeV. The “strangeness” scheme was confirmed by the subsequent discovery of a large number of strange particles. The nucleon isospin doublet has strangeness $S = 0$, the isospin singlet Λ and triplet Σ have strangeness $S = -1$, and the isospin doublet Ξ has strangeness

$S = -2$. The new strangeness quantum number suggested an internal SU(3) symmetry of the hadron spectrum and the simple quark model of the nucleon was generalized to the flavour SU(3) group by adding the strange quark, s , with strangeness $S = -1$. By 1964, “flavour SU(3)” based on the three lightest flavours of quark was established as a new symmetry group which naturally fits the hadrons with similar properties into its multiplet representations.

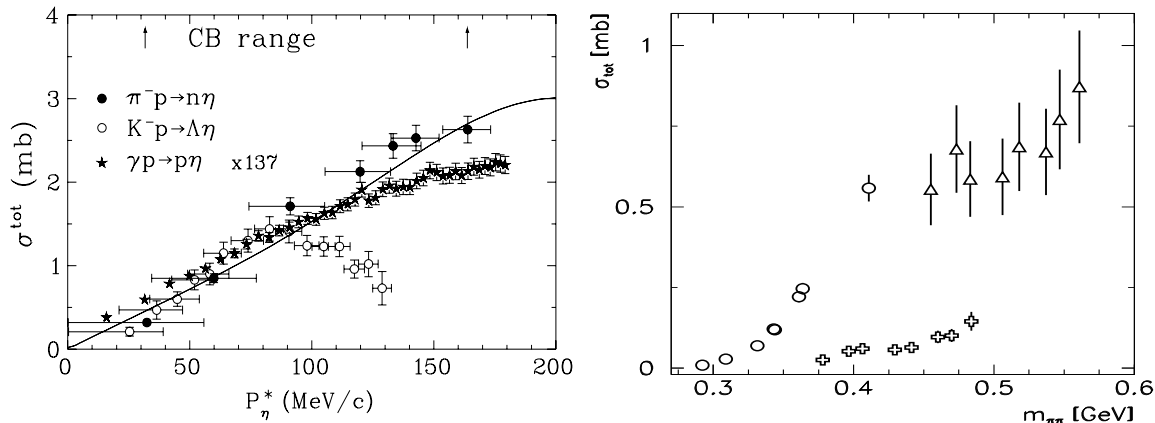
The “strange” $\Lambda^{(*)}$ and $\Sigma^{(*)}$ resonances can of course be more easily produced and studied in K -induced reactions, rather than in reactions with a non-strange beam particle. The most recent measurements were presented by the Crystal Ball collaboration using the low-momentum K^- beam at BNL’s Alternating Gradient Synchrotron (AGS) on the reactions $K^- p \rightarrow \eta\Lambda$ [100], $K^- p \rightarrow \pi^0\Lambda$ [111], $K^- p \rightarrow \pi^0\pi^0\Lambda$ [108], $K^- p \rightarrow \pi^0\pi^0\pi^0\Lambda$ [103], $K^- p \rightarrow \pi^0\Sigma^0$ [104, 111], $K^- p \rightarrow \pi^0\pi^0\Sigma^0$ [109], and $K^- p \rightarrow \bar{K}^0 n$ [111]. At SLAC, the Large Aperture Superconducting Solenoid (LASS) spectrometer performed the last such experiments using an intense kaon beam of 11 GeV/ c . Evidence was reported for an Ω^* resonance with a mass of 2474 ± 12 MeV and a width of 72 ± 33 MeV [253].

The threshold region in the reaction $K^- p \rightarrow \eta\Lambda$ is dominated by formation of the intermediate $(***) \Lambda(1670) \frac{1}{2}^-$ state, which was discovered in 1965 at BNL as a peak in the same reaction [254]. A unitary, multi-channel analysis [255] determined the mass and width of the resonance to be (1673 ± 2) MeV and (23 ± 6) MeV, respectively, which are in excellent agreement with quark-model predictions [256]. Isospin-1 states can be observed in the reaction $K^- p \rightarrow \pi^0\Lambda$ [104, 111]. It was found that the resonance, $(***) \Sigma(1385) \frac{3}{2}^+$ contributes, but no evidence is observed for any of the remaining Σ states below 1600 MeV listed by the PDG. In particular, contributions from the state, $(*) \Sigma(1580) \frac{3}{2}^-$, were shown to be inconsistent with the observed angular distributions [104]. A recent effective Lagrangian approach [257], which includes the data on $K^- p \rightarrow \pi^0\Lambda$ from the Crystal Ball experiment [111], supports the existence of $(***) \Sigma(1660) \frac{1}{2}^+$ but finds no evidence for $(**) \Sigma(1620) \frac{1}{2}^-$.

Production of two π^0 mesons in the reaction $K^- p \rightarrow \pi^0\pi^0\Lambda$ was reported in [108] to proceed dominantly via $\Lambda^* \rightarrow \pi^0\Sigma^0(1385) \rightarrow \pi^0\pi^0\Lambda$. Contributions from the scalar meson, $f_0(600)$, were found to be insignificant (a broad uniform $\pi\pi$ band for the $f_0(600)$ is absent in the Dalitz plot) and no other Σ^* intermediate state was observed. The isospin-related reaction $K^- p \rightarrow \pi^0\pi^0\Sigma^0$ was found to be dominated by the decay chain $\Sigma^* \rightarrow \pi^0\Lambda(1405) \rightarrow \pi^0\pi^0\Sigma^0$ with increasing contributions from the $\Lambda(1520)$ toward the highest beam momentum of 750 MeV at which data were obtained [109]. The authors determine a total cross section for $K^- p \rightarrow \pi^0\pi^0\Sigma^0$, which gradually rises from about 35 to 180 μb . Such behaviour is consistent with dominant contributions from either $\Sigma(1660) \frac{1}{2}^+$ or $\Sigma(1670) \frac{3}{2}^-$ [109], a 3-star and a 4-star state, respectively.

In the limit of massless quarks, the flavour-blindness of the QCD gluon interactions would result in a perfect SU(3)-flavour symmetry. Neglecting additional Coulomb forces, the states corresponding to the $J = \frac{1}{2}$ ground-state octet would be degenerate and, so would the states of the $J = \frac{3}{2}$ ground-state decuplet. For the octet (Figure 2 (b)), the

Figure 13. Total cross sections. Left: Results for single- η production: $\pi^- p \rightarrow n\eta$ [110], $K^- p \rightarrow \Lambda\eta$ [100], $\gamma p \rightarrow p\eta$ [175]. The solid line represents the SAID-FA02 solution [258]. Picture taken from [110]. Right: Results for $\pi^0\pi^0$ production compared at incident beam momenta such that the reactions have the same $m_{\max}(\pi^0\pi^0)$: $\pi^- p \rightarrow \pi^0\pi^0 n$ (\circ), $K^- p \rightarrow \pi^0\pi^0 \Lambda$ (\triangle), $K p \rightarrow \pi^0\pi^0 \Sigma^0$ (crosses). Picture from [259].



mass differences between the single-strange resonances and the nucleon are

$$M_{\Lambda} - M_N = 177 \text{ MeV}, \quad M_{\Sigma} - M_N = 254 \text{ MeV}, \quad (5.2)$$

and similarly, the mass difference for the double-strange Ξ to the Λ is

$$M_{\Xi} - M_{\Lambda} = 203 \text{ MeV}. \quad (5.3)$$

The mass differences are ≈ 200 MeV and are much smaller than the resonance masses themselves. The corresponding mass splittings in the decuplet (Figure 2 (a)) are similar, having the values

$$M_{\Sigma(1385)} - M_{\Delta} = 153 \text{ MeV}, \quad (5.4)$$

$$M_{\Xi(1530)} - M_{\Sigma(1385)} = 145 \text{ MeV}, \quad (5.5)$$

$$M_{\Omega^-} - M_{\Xi(1385)} = 142 \text{ MeV}. \quad (5.6)$$

In reality, SU(3)-flavour symmetry is broken by the finite mass of the strange quark. Although the multiplets exhibit an excellent isospin symmetry because $m_u \simeq m_d \simeq 0$, the states containing strange quarks have masses which correspond approximately to integral multiples of m_s . The mass difference between the quarks is still much smaller than Λ_{QCD} and therefore, an approximate SU(3)-flavour symmetry can be observed in the baryon spectrum.

It is now generally accepted that the previously mentioned $\Lambda(1670) \frac{1}{2}^-$ is the partner of the $N(1535) \frac{1}{2}^-$ in the $S = \frac{1}{2}$ octet of the $(\mathbf{70}, 1_1^-)$ supermultiplet that contains the lowest-lying baryon excitations with negative parity. Both resonances show a sizable branching fraction for decays into η and the corresponding baryon ground state. Interestingly, the shapes of the cross sections of the two reactions $K^- p \rightarrow \Lambda\eta$ and $\pi^- p \rightarrow \eta n$ exhibit a remarkable similarity in the threshold region (Figure 13, left) – which may be an example of SU(3)-flavour symmetry. The threshold of the reaction

$\gamma p \rightarrow p\eta$ is also dominated by the $N(1535) \frac{1}{2}^-$ resonance, but flavour symmetry does not apply in electromagnetic processes. However, η production at threshold via γp and $\pi^- p$ agree fairly well once the photoproduction cross section is multiplied by a factor of 137, i.e. η photoproduction is about α times η production in $\pi^- p$ reactions.

The authors of [259] suggest that there are relationships among the processes

$$\pi^- p \rightarrow \eta n \quad \pi^- p \rightarrow N^* \rightarrow \pi^0 \Delta(1232) \ 3/2^+ \rightarrow \pi^0 \pi^0 n, \quad (5.7)$$

$$K^- p \rightarrow \Lambda \eta \quad K^- p \rightarrow \Lambda^* \rightarrow \pi^0 \Sigma^0(1385) \ 3/2^+ \rightarrow \pi^0 \pi^0 \Lambda, \quad (5.8)$$

$$K^- p \rightarrow \Sigma^* \rightarrow \pi^0 \Lambda(1405) \ 1/2^- \rightarrow \pi^0 \pi^0 \Sigma^0, \quad (5.9)$$

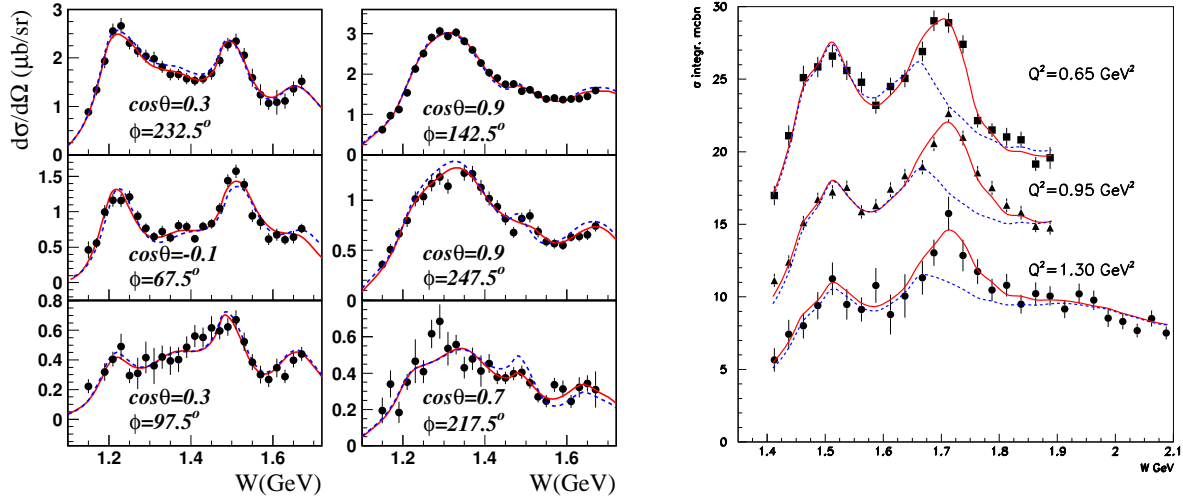
$$\gamma p \rightarrow \eta p \quad \gamma p \rightarrow N^* \rightarrow \pi^0 \Delta(1232) \ 3/2^+ \rightarrow \pi^0 \pi^0 n. \quad (5.10)$$

They argue that the first two $\pi^0 \pi^0$ reactions have the same SU(3)-flavour structure, similar to single- η production. The two resonances, $\Delta(1232)$ and $\Sigma(1385)^0$, are members of the same ground-state decuplet. The two K^- -induced reactions, however, differ in the flavour structure of their dominant intermediate states and thus, the cross sections should be quite different. Figure 13 (right) shows the $\pi^0 \pi^0$ cross section data plotted versus $m_{\max}(\pi^0 \pi^0)$ rather than beam momentum. The total cross section for $K^- p \rightarrow \pi^0 \pi^0 \Sigma^0$ is about a factor of five smaller than the total cross section for $K^- p \rightarrow \pi^0 \pi^0 \Lambda$. This big difference indicates that the $\pi^0 \pi^0$ production in $K^- p$ reactions occurs likely via sequential baryon decays with very different flavour structure. They go on to argue that if the SU(2) and SU(3) Clebsch-Gordan coefficients are ignored, and these reactions proceed through the same mechanism, then their cross sections should be comparable. The mechanism they assume is that of $f_0(600)$ production in the intermediate state. The total cross section for $\pi^- p \rightarrow \pi^0 \pi^0 n$ is similar to the total cross section for $K^- p \rightarrow \pi^0 \pi^0 \Lambda$. However, this similarity may be accidental, as the argument provided is not very rigorous.

The concept of flavour-symmetry may provide some guidance, but its application is certainly limited. The symmetry is broken by the strange-light quark mass difference and corrections in quark models can be substantial. The PDG lists four Σ states in the mass range 1300-1600 MeV: ($*$ $*$ $*$ $*$) $\Sigma(1385) \frac{3}{2}^+$, ($*$) $\Sigma(1480)$, ($**$) $\Sigma(1560)$, and ($*$) $\Sigma(1580) \frac{3}{2}^-$. Without doubt, the $\Sigma(1385) \frac{3}{2}^+$ is a member of the ground-state decuplet. Only two Λ states are listed in the same mass range: ($*$ $*$ $*$ $*$) $\Lambda(1405) \frac{1}{2}^-$ and ($*$ $*$ $*$ $*$) $\Lambda(1520) \frac{3}{2}^-$. For the first-excitation band, ($\mathbf{70}, 1_1^-$), it has been well accepted that the two Λ states are the members of the ${}^2\mathbf{1}$ -plet (Equation (2.5)). All Λ octet states then have masses close to or above 1700 MeV. In the framework of SU(3)-flavour symmetry, the low masses of the remaining Σ states rule them out as possible partners and raise doubts about their existence. Similar arguments have been made about the $\Sigma(1580) \frac{3}{2}^-$ state by the Crystal Ball collaboration [104]. All three of the Σ states mentioned have also been omitted from the recent classification by Klempt and Richard [4].

The spectroscopy of Λ and Σ resonances remains at a standstill due to the lack of suitable K beams. A minireview in the latest version of the RPP [1] refers to the note in

Figure 14. (Colour online) Left: CLAS differential cross sections for $\gamma^*p \rightarrow n\pi^+$ [127]. Upper, middle, and lower rows are for $Q^2 = 1.72, 2.44,$ and 3.48 GeV^2 , respectively. The solid (dashed) curves denote results using a fixed- t dispersion relations (effective Lagrangian) approach [261]. Right: Data on fully integrated $p\pi^+\pi^-$ electroproduction cross sections from CLAS [121]. The dashed curves represent a description within the framework of the reaction model in [264] considering only conventional N^* states, the solid curves include an additional $(1720) \frac{3}{2}^+$ candidate. Pictures from [117].



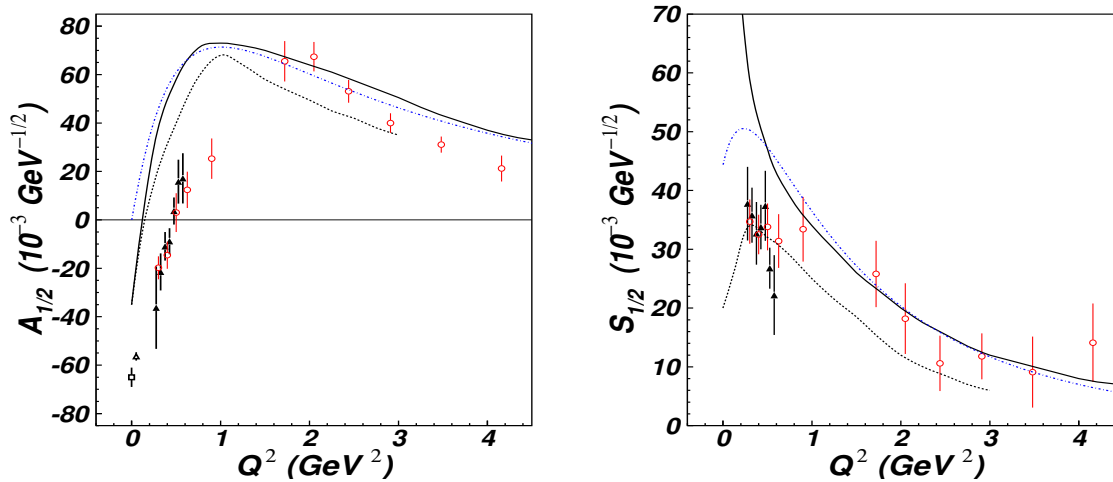
the 1990 edition. A few measurements on branching fractions have been added. Recent classifications of the hyperon spectrum can be found in [1, 4, 260].

5.3. Electroproduction Experiments

An important component of the N^* program is the probing of resonance transitions at different distance scales in order to study the structure of excited nucleons as well as the (effective) confining forces of the three-quark system. Electron beams are the ideal tool to study such resonance form factors. A variety of measurements of single-pion electroproduction on a proton target have been performed in recent years. Electroproduction of π mesons in the threshold region was studied at MAMI at very low values of Q^2 [177] and for $0.16 < Q^2 < 6 \text{ GeV}^2$ at Jefferson Lab using the CLAS spectrometer. The experimental data include differential cross sections for the reactions $\gamma^*p \rightarrow p\pi^0$ [120, 125] and $\gamma^*p \rightarrow n\pi^+$ [124, 127, 131], beam [122, 123, 127] and target [128] asymmetries using longitudinal polarization, and beam-target asymmetries [128]. Differential cross sections from CLAS were also published for the reactions $\gamma^*p \rightarrow p\pi^+\pi^-$ [121, 129] and $\gamma^*p \rightarrow p\eta$ [119, 126].

Figure 14 (left) shows examples of the cross section data on $\gamma^*p \rightarrow n\pi^+$ for different polar and azimuthal angles [127]. The upper, middle, and lower rows correspond to $Q^2 = 1.72, 2.44,$ and 3.48 GeV^2 , respectively. The curves denote descriptions of the data using two different approaches. The solid curve [261] is based on fixed- t dispersion relations (DR), an approach which was developed in the 1950s for pion-

Figure 15. (Colour online) Helicity amplitudes for the $\gamma^*p \rightarrow N(1440)\frac{1}{2}^+$ transition in comparison with quark-model predictions. The photocouplings ($Q^2 = 0$) are taken from the RPP [2] (open square) and an analysis of $\gamma p \rightarrow n\pi^+$ [139] (open triangle). The other data points are from a CLAS analysis of $p\pi^+\pi^-$ [129] (black triangles) and $N\pi$ electroproduction data [261] (circles). The solid and dashed curves are predictions of light-front relativistic quark models [268, 269] considering the $N(1440)\frac{1}{2}^+$ a radial excitation of the $3q$ ground state. Results of a covariant valence quark spectator diquark model [270] are shown by the dashed dotted line. Pictures from [132].



and electroproduction on nucleons [113, 262]. Recent extensions of the model into kinematical regions covered by the new data, e.g. [261], allowed a more reliable extraction of the amplitudes for the important $\gamma^*p \rightarrow \Delta(1232)\frac{3}{2}^+$ transition. The dashed curve [261] is based on an effective Lagrangian approach – Unitary Isobar Model (UIM), which goes back to the late 1990s [263].

Important results of this analysis [261] include a better understanding of the amplitudes for the $\Delta(1232)\frac{3}{2}^+$ indicating the importance of a meson-cloud contribution to quantitatively explain the magnetic dipole strength [221, 265, 266], as well as the electric and scalar quadrupole transitions. Recent lattice QCD calculations also identified contributions from the pion-cloud important for the $\gamma^*p \rightarrow \Delta(1232)\frac{3}{2}^+$ transition [267]. Furthermore, the helicity amplitudes for the electroexcitation of the low-mass resonances $\Delta(1232)\frac{3}{2}^+$, $N(1440)\frac{1}{2}^+$, $N(1520)\frac{3}{2}^-$, and $N(1535)\frac{1}{2}^-$ were extracted in [261]. More recently, very consistent results on the electrocouplings of the $N(1440)\frac{1}{2}^+$ and the $N(1520)\frac{3}{2}^-$ resonances have become available from the independent analysis of the single- and double-pion channel [132] within the framework of the phenomenological reaction model in [264]. As an example, Figure 15 shows the helicity amplitudes $A_{\frac{1}{2}}$ (left) and $S_{\frac{1}{2}}$ (right) for the $N(1440)\frac{1}{2}^+$ “Roper” resonance. These data provide strong evidence for the state to be a predominantly radial excitation of a 3-quark ground state. In particular, the non-zero $S_{\frac{1}{2}}$ amplitude rules out an interpretation of the resonance as a gluonic baryon excitation, which was predicted in [271, 272], for instance. In contrast, descriptions by light-front relativistic quark models considering

the state a radial excitation of the $3q$ ground state, e.g. [268, 269], are in reasonable agreement with the data at large values of Q^2 (short distances). Stronger contributions from the meson-baryon cloud can explain the discrepancies below $Q^2 < 1 \text{ GeV}^2$ (large distances) [261].

For the $N(1520) \frac{3}{2}^-$ resonance, the results show a rapid helicity switch from the dominant $A_{\frac{3}{2}}$ amplitude at $Q^2 = 0 \text{ GeV}^2$ (photon point) to $A_{\frac{1}{2}}$ at $Q^2 > 1 \text{ GeV}^2$, which confirms predictions of constituent quark models. A better understanding of the $N(1535) \frac{1}{2}^-$ resonance remains a challenge, though. Quark models cannot describe correctly the sign of the $S_{\frac{1}{2}}$ amplitude below $Q^2 < 3 \text{ GeV}^2$ and also have difficulties in describing the substantial $N(1535) \frac{1}{2}^-$ coupling to the $N\eta$ channel. This may again be indicative of large meson-cloud contributions or of representations of this state different from a $3q$ excitation. Alternative interpretations range from a quasi-bound meson-baryon molecule [273] to a dynamically-generated resonance coming from the interaction of the octet of pseudoscalar mesons with the ground-state octet of baryons [274, 275].

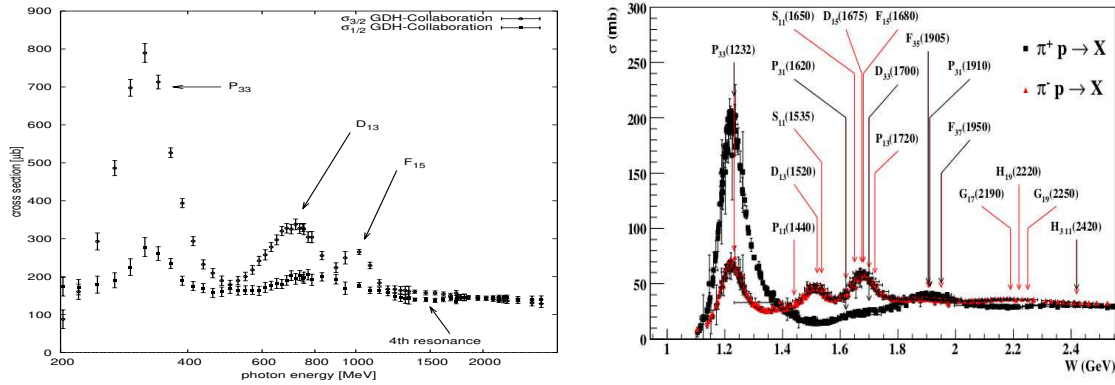
A new resonance, $(1720) \frac{3}{2}^+$, was proposed on the basis of recent CLAS data on $\gamma^*p \rightarrow p\pi^+\pi^-$ [121]. Figure 14 (right) shows the fully integrated cross sections at three different Q^2 values. The data are well described by the (red) solid curve, which is based on calculations within the framework of the reaction model in [264]. The difference between the solid and dashed (blue) curves represents the signal from the proposed new state.

5.4. Photoproduction Experiments

Most of the information on light-flavour baryon resonances reported by the PDG is still based on πN scattering experiments, but the plethora of results coming from the recent photoproduction experiments will likely have a big influence on the particle listings. Before we discuss the wealth of information obtained from individual reactions, it is worth discussing the total photoabsorption cross section in comparison with the total πN cross section.

The left side of Figure 16 shows the separate helicity contributions to the total photoabsorption cross section measured by the GDH collaboration [276]. The right side of Figure 16 shows the corresponding cross sections for π^+p and π^-p reactions. The total π^-p cross section exhibits many more structures since only Δ^{++} resonances can contribute to the total π^+p cross section owing to the conservation of electric charge. The overall shapes of the total γp and πp cross sections are similar and the four resonance regions are clearly observed in both reactions. The large peak at threshold in all distributions originates from the production of the $\Delta(1232) \frac{3}{2}^+$ resonance. In the total photoabsorption cross section, most of the resonance strength in the first three resonance regions comes clearly from the helicity $\frac{3}{2}$, which indicates that resonances with $J \geq \frac{3}{2}$ provide the dominant contributions. The situation appears to be different for the fourth resonance region around $W \approx 1920 \text{ MeV}$ where the π^+p cross section shows a broad structure and the π^-p cross section is featureless.

Figure 16. (Colour online) The total cross sections for γp and πp reactions. Left: Total photoabsorption cross sections, $\sigma_{\frac{3}{2}}$ and $\sigma_{\frac{1}{2}}$ measured by the GDH collaboration. Picture from [276] (and data references therein). Right: Total cross section for pion-induced reactions; courtesy M. Williams, Ph.D. thesis, Carnegie-Mellon university.



The photoproduction cross section clearly depends on the helicity of the proton and photon and therefore, the helicity difference defined as

$$E = \frac{\sigma_{\frac{3}{2}} - \sigma_{\frac{1}{2}}}{\sigma_{\frac{3}{2}} + \sigma_{\frac{1}{2}}} \quad (5.11)$$

is a very important quantity, not only for the total cross section, but also for individual meson-production channels (Equation (4.8)). At long distance scales in the confinement regime, the integrated total helicity-difference cross section can be related to the static properties of the nucleon. One such sum rule was derived by Gerasimov, Drell, and Hearn (GDH) [277, 278] in the mid-1960s and provides an elegant connection between the nucleon structure functions obtained in high-energy lepton-scattering experiments and the anomalous magnetic moment, κ , and the nucleon mass, m . At $Q^2 = 0$ (for real photons), the GDH integral is given as

$$\int_{\nu_{\text{th}}}^{\infty} \frac{d\nu}{\nu} [\sigma_{\frac{3}{2}}(\nu) - \sigma_{\frac{1}{2}}(\nu)] = \frac{2\pi^2\alpha}{m^2} \kappa^2, \quad (5.12)$$

where $\nu = E_\gamma$ is the incident photon energy in the lab frame and ν_{th} is the photoabsorption threshold. Consequently, it provides a bridge between perturbative and non-perturbative QCD.

The GDH sum rule was confirmed experimentally by the GDH collaboration in measurements from a proton target at MAMI [279, 280, 281] and ELSA [282]. The uncertainties for the neutron measurements are larger, though. A nice review on the Gerasimov-Drell-Hearn sum rule is given in [276]. Including some extrapolation to high energies, the experimental value of the GDH integral for the proton was determined to be $212 \pm 6_{\text{stat.}} \pm 16_{\text{syst.}} \mu\text{b}$ [276], which agrees with the prediction of $205 \mu\text{b}$.

The total photo-absorption cross section in Figure 16 clearly exhibits features that suggest resonance production, but such inclusive measurements do not allow a detailed investigation of the closely-spaced baryon resonances contributing to the

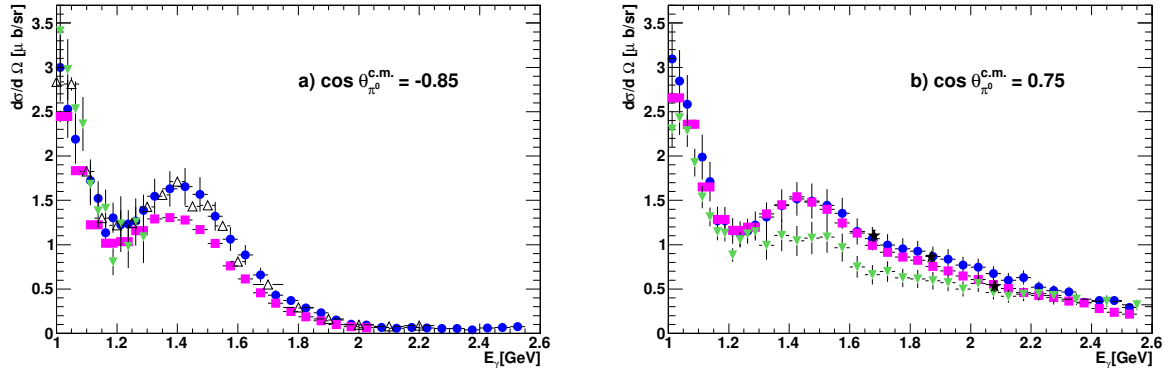
different resonance regions. The dominant decay of any excited nucleon state is via the emission of mesons in the strong interaction, e.g. $N^* \rightarrow N\pi$, $N\eta$, $N\omega$, $N\pi\pi$, KY , etc. Electromagnetic decays via photon emission have typical branching ratios below the 1% level and are usually difficult to identify in the presence of large background contributions to the final states. Although meson production has been studied mostly in pion-induced reactions, many nucleon resonances have been predicted to couple only very weakly to the πN channel. This has inspired new programs in baryon spectroscopy where the focus has shifted to studying resonances using electromagnetic probes.

In the following sections, recent photoproduction results obtained in a large variety of meson-production channels are presented. The current focus at the laboratories worldwide is on the so-called complete experiments which involve the determination of all 16 spin-dependent observables in single- and double-polarization experiments, discussed in Section 4.3.2. While only eight well-chosen observables are needed in the mathematical problem to extract the scattering amplitude without ambiguities, an experimental approach will require a significantly larger number of observables because of unavoidable experimental uncertainties. Observables for complete experiments will also come from different facilities which use detectors optimized for different reactions and kinematical regions. Many cross section results are not statistically limited anymore, but the various theoretical approaches to better understand the underlying production mechanisms face large systematic discrepancies among results from different experiments. In some cases, a combined analysis of the available data is even impossible at the moment.

5.4.1. Photoproduction of a Single π Meson The single-meson reactions $\gamma p \rightarrow p\pi^0$ and $\gamma p \rightarrow n\pi^+$ are among the best studied photoproduction channels, but a comprehensive study of polarization observables has only begun recently. For the full database of differential cross section results, we refer to the GWU Data Analysis Center [91]. A good summary of references on π^0 production is also given in [146]. The most recent cross section results for π^0 production, which cover a large angular and energy range, come from JLab [136] and ELSA [162]. The latter data cover in particular the very forward and backward angles of the π^0 in the c.m. system, which are sensitive to higher-spin resonances. Very precise differential cross sections for $\gamma p \rightarrow n\pi^+$ were measured at CLAS for energies from 0.725 to 2.875 GeV [139].

The overall agreement of the available π^0 cross section results is very good, but some discrepancies have been observed and need to be resolved in order to reliably extract resonance properties. As an example, Figure 17 shows some of the available data for a large energy range from 1.0 to 2.6 GeV for fixed angles of $\cos\theta_{\text{c.m.}} = -0.85$ (left) and $\cos\theta_{\text{c.m.}} = 0.75$ (right). At the backward angle, most of the experiments show a very consistent behaviour. However, the CLAS (g1c) data (■) are clearly lower. At the forward angle, the CB-ELSA data (▼) are somewhat lower than the other data sets. An overall large normalization problem is generally not observed for π^0 production and we conclude that the photon flux normalization appears to be reasonably well understood,

Figure 17. (Colour online) Differential cross sections for the reaction $\gamma p \rightarrow p\pi^0$ for $E_\gamma \in [1.0, 2.6]$ GeV at two different polar angles of the π^0 in the c.m. system: $\theta \approx 148^\circ$ (left) and $\theta \approx 41^\circ$ (right). Data are from CLAS \blacksquare [136], CB-ELSA \blacktriangledown [145, 146], CBELSA/TAPS \bullet [162], Becks *et al.* \triangle [283], and Brefeld *et al.* \star [284]. Statistical and systematic errors have been added in quadrature.

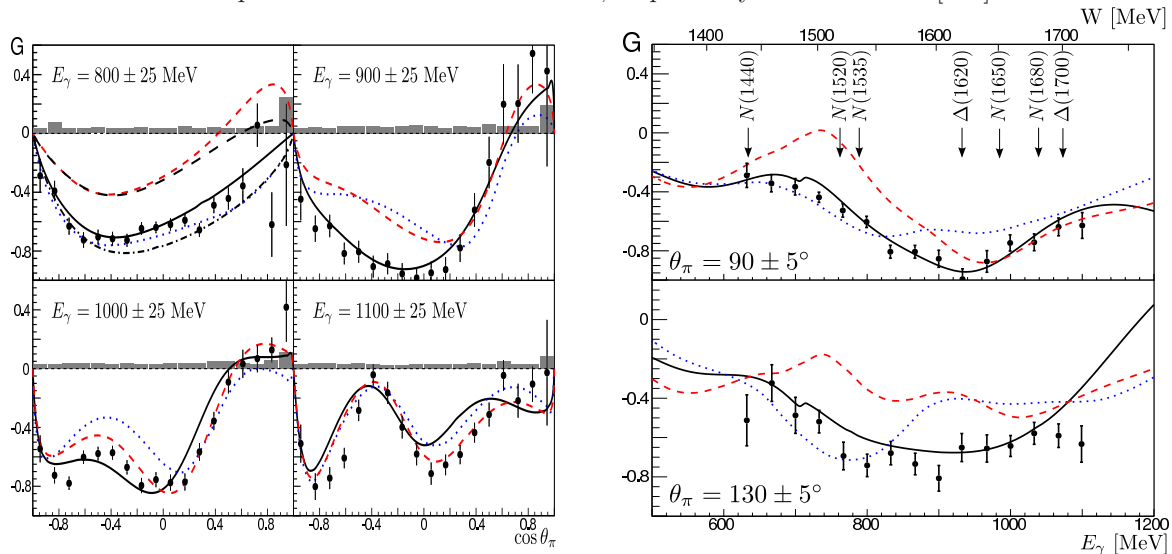


but likely some detector acceptance effects are not correctly accounted for.

Some data on target and proton recoil polarization are available in the reaction databases [90, 91] in addition to a few data on double-polarization. The best studied polarization observable is the beam asymmetry, Σ , which has been recently measured for $\vec{\gamma}p \rightarrow p\pi^0$ at GRAAL [184] in the energy range from 550 to 1500 MeV, at MAMI at low energies in the Δ resonance region [176], and at ELSA [158, 161]. High-statistics data are expected from CLAS in the very near future. GRAAL also reported measurements for $\vec{\gamma}p \rightarrow n\pi^+$ [190] as well as $\vec{\gamma}n \rightarrow n\pi^0$ [196] and found that the asymmetries from the quasi-free proton and the quasi-free neutron were equal up to 0.82 GeV, but substantially different at higher energies. The beam asymmetry, Σ , arises from a linearly-polarized photon beam and addresses the non-spin-flip terms in the transition current (e.g. convection currents and double spin-flip contributions), whereas spin-flip contributions are projected out by a circularly-polarized photon beam. At low photon energies, between the production threshold and the Δ region, the π^0 beam asymmetry is important in addition to the differential cross section to measure the S -wave amplitude, E_{0+} ($l_\pi = 0$), and the P -wave amplitudes, M_{1+} , M_{1-} , and E_{1+} ($l_\pi = 1$) separately [176]. In the second resonance region, detailed analysis of the data in π photoproduction yields clear signals for the $N(1520) \frac{3}{2}^-$ and $N(1535) \frac{1}{2}^-$ states. The unpolarized cross section and the Σ observable are somewhat less sensitive to the $N(1440) \frac{1}{2}^+$ resonance. Additional observables are needed to understand the reaction at higher energies.

New high-statistics data on (single- and double-) polarization observables for $\gamma p \rightarrow p\pi^0$, e.g. the E , P , H , T observables (Equation (4.8)), have been presented at recent conferences. Surprisingly, big discrepancies have been observed in single- π photoproduction, even at lower energies, between the latest predictions and the new polarization data. In 2012, CBELSA/TAPS reported on the first ever measurement of the double-polarization observable, G , for the photon energy range from 620 to

Figure 18. (Colour online) Recent results for the double-polarization observable G from CBELSA/TAPS [167] for the reaction $\gamma p \rightarrow p\pi^0$ as a function of $\cos\theta_\pi$ (left) and as a function of energy for two selected $\cos\theta_\pi$ bins (right). Systematic errors are shown as gray bars. The curves represent predictions from the SAID (red, dashed) [216], MAID (blue, dotted) [263], and Bonn-Gatchina (black, solid) [247] PWAs. The black, long-dashed and dashed-dotted lines denote Bonn-Gatchina with the E_{0+} and E_{2-} amplitudes from SAID and MAID, respectively. Pictures from [167].



1120 MeV and the full solid angle [167]. The G observable describes the correlation between the photon polarization plane and the scattering plane for protons polarized along the direction of the incoming photon. Figure 18 shows the observable for fixed energies (left) and fixed angles (right). The deviations of the current model predictions from the data are clearly observed even for photon energies below 1 GeV. In particular, SAID shows large deviations for the two shown angles. It has been discussed [167] that the discrepancies among the models arise from the two multipoles, E_{0+} and E_{2-} , which receive significant contributions from the $\frac{1}{2}^-$ resonances, $N(1535)$, $\Delta(1620)$, $N(1650)$, and the $\frac{3}{2}^-$ resonances, $N(1520)$, $\Delta(1700)$, respectively.

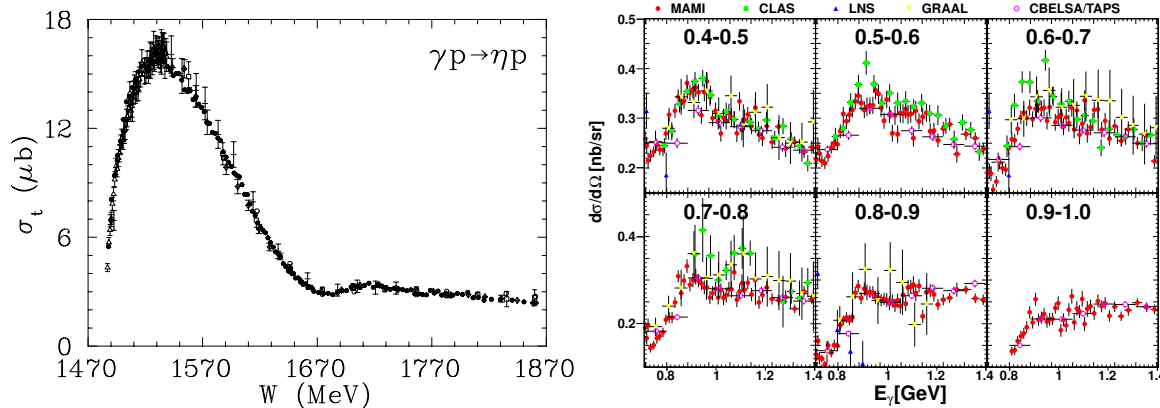
Several new resonances which are also observed to decay into πN have been proposed in the latest edition of the RPP. While most of the new entries have been inspired by recent results of the Bonn-Gatchina PWA group [247], some (or all) of them were already reported earlier by other groups, e.g. by Manley *et al.* [285]. However, most of the new states have not been observed in the recent analysis of πN data by Arndt *et al.* [217] including the $N(1700) \frac{3}{2}^-$ resonance. The new states including more recent references are listed in Table 12.

5.4.2. Photoproduction of Single η and η' Mesons The total cross section for the reaction $\gamma p \rightarrow p\eta$ is shown in Figure 19 (left). It exhibits a step rise at the reaction threshold of $E_{\text{th}} \approx 706$ MeV, reaches a maximum of about $16 \mu\text{b}$ very close to the threshold, and is dominated by the broad peak around $W \approx 1540$ MeV. Apart from a

Table 12. Summary of newly proposed resonances observed in πN . We list all the resonances for the partial waves with at least a 2-star assignment by the PDG (without the nucleon ground state). New states are given in red.

J^P	Resonance Region			
$1/2^+$	$N(1440)$	$N(1710)$	$N(1880)$ [247, 285]	
$1/2^-$	$N(1535)$	$N(1650)$	$N(1895)$ [247, 285]	
$3/2^-$	$N(1520)$	$N(1700)$	$N(1875)$ [247, 285]	$N(2120)$ [247]
$5/2^+$		$N(1680)$	$N(1860)$ [217, 247, 285]	$N(2000)$
$5/2^-$		$N(1675)$		$N(2060)$ [247]

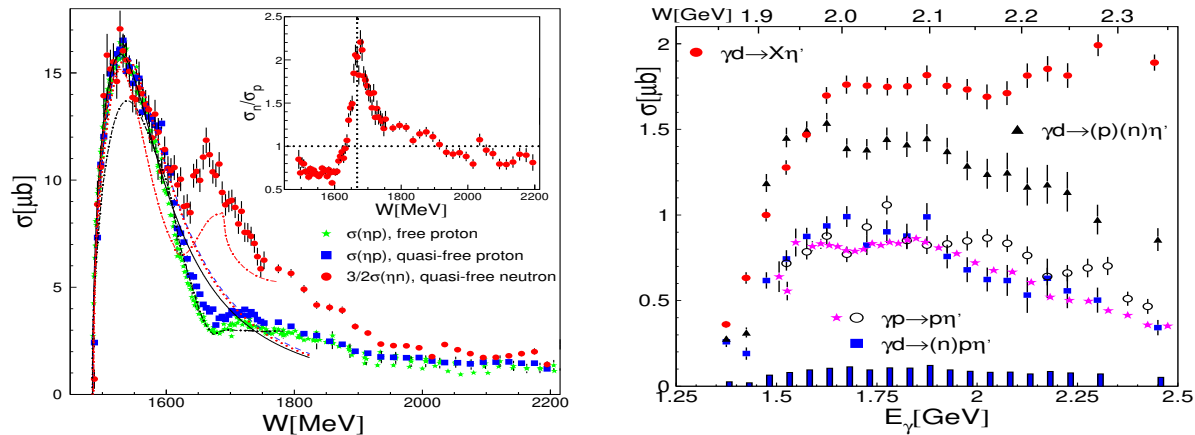
Figure 19. (Colour online) Cross sections for the reaction $\gamma p \rightarrow p\eta$. Left: Total cross section. Picture from [180]. Right: Differential cross sections for $E_\gamma \in [0.8, 1.4]$ GeV and different angle bins in the forward direction. Data are taken from CLAS g11a \blacksquare [142], CBELSA/TAPS \circ [160], MAMI \bullet [180], and GRAAL \blacktriangledown [185]. The error bars comprise statistical and systematic errors added in quadrature.



small dip at $W = 1680$ MeV, the total cross section for this reaction shows no further structures.

The latest data come from MAMI with unprecedented statistical quality, but are limited in energy to 1.4 GeV [180]. In recent years, the differential cross section has also been measured at CLAS [142], at ELSA using the CB-ELSA [147, 148] and CBELSA/TAPS [160] setups, and at GRAAL [185]. Overall, great experimental progress can be reported for η photoproduction. In addition to the improved statistical quality, the differential cross section covers the full angular range for energies below $E_\gamma = 2.5$ GeV. As an example, Figure 19 (right) shows results for $E_\gamma \in [0.7, 1.4]$ GeV and $0.4 < \cos \theta_{c.m.}^\eta < 1.0$. However, a fairly large normalization discrepancy of almost 60% at higher energies (above 2 GeV) between the results from ELSA and CLAS render a combined analysis of all available data sets currently almost impossible. The effect of this discrepancy on PWA results was discussed in [286], for instance. The authors point out that all recent experimental results on differential cross sections are in good

Figure 20. (Colour online) Left: Total cross sections for η photoproduction as a function of the final-state invariant mass, W ; for γd reactions, no cut on the spectator momentum was applied. The n cross section was scaled up 3/2 to match the p results. The insert shows the ratio of quasi-free neutron to proton data. Data and picture from [166]. Right: Total cross sections for η' photoproduction. Data and picture from [165]. Other data are free proton results from [160] (open circles) and [142] (magenta stars). With kind permission of The European Physical Journal (EPJ).



agreement with each other, except for the recent CLAS data. In the analysis, overall consistency can be achieved by introducing an energy-dependent renormalization factor for the CLAS data [286]. The situation is unsatisfactory and needs to be resolved soon. It is worth mentioning that results from LEPS [199] and older results from the Daresbury facility [287] are in excellent agreement with CBELSA/TAPS at energies above 2 GeV.

Precise measurements of polarization observables in η photoproduction are currently only available for the beam asymmetry, Σ . Very few older data can be found in the reaction databases, e.g. [91]. In 2007, results on Σ were reported from CBELSA/TAPS [154] and GRAAL [185]. GRAAL also reported the beam asymmetry for the photoproduction reaction off the neutron [195]. Many other observables including double-polarization observables from ELSA and CLAS have been presented at recent conferences and will be available soon, e.g. [288].

A striking observation has been made recently in the reaction $\gamma n \rightarrow n\eta$ [164, 166, 370, 371] where a narrow peak at $W \approx 1660$ MeV is observed, absent in the reaction $\gamma p \rightarrow p\eta$. The peak position coincides with the dip observed in the cross section off the proton. Figure 20 (left) shows total cross sections for η photoproduction as a function of the final state invariant mass [166]. The quasi-free neutron cross section was scaled by a factor of 3/2 to match the broad peak at the threshold. The inset shows the ratio of quasi-free neutron to proton data and the narrow peak is clearly visible. The observation has given rise to speculations about a narrow resonance, but no direct evidence that supports this conjecture exists. Alternative explanations range from an interference effect in the $\frac{1}{2}^-$ -waves [289] to coupled channel effects related to the $N(1650)\frac{1}{2}^-$ and the $N(1710)\frac{1}{2}^+$ resonances [290] or a cusp effect from the $K\Sigma$ and $K\Lambda$ rescattering

channels [291]. The PDG lists the state as $N(1685)$ with a 1-star assignment and unknown quantum numbers. Polarization observables should shed more light on the nature of this structure.

There is no doubt about the dominant contribution of the $N(1535)\frac{1}{2}^-$ state to η photoproduction at threshold. Other $\frac{1}{2}^-$ resonances also couple strongly to the $p\eta$ channel. The dip in the total cross section off the proton is likely due to destructive interference between the contributions from $N(1535)\frac{1}{2}^-$ and $N(1650)\frac{1}{2}^-$ [240]. The large positive values of the η beam asymmetry in this mass range have been interpreted as being due to $N(1520)\frac{3}{2}^-$, although the effect of this resonance on the differential cross section is small, see e.g. the discussion in [7]. More recently, the $N(1710)\frac{1}{2}^+$ [240, 247] and $N(1720)\frac{3}{2}^+$ [217, 247] resonances have been found to play an important role in η production. Indications for contributions from additional $\frac{1}{2}^+$ and $\frac{3}{2}^-$ resonances are very weak. Further evidence for resonances in η production comes from the Bonn-Gatchina group [247]. They observe the new resonances listed by the PDG, $N(1895)\frac{1}{2}^-$ and $N(2060)\frac{5}{2}^-$, as well as the known $N(1900)\frac{3}{2}^+$ and $N(2000)\frac{5}{2}^+$ decaying to $p\eta$ in their multichannel analysis.

We briefly mention results for η' production, which has been measured with a fair amount of statistics at CBELSA/TAPS [160]. High-statistics results on the reaction $\gamma p \rightarrow p\eta'$ are available from CLAS, e.g. [142]. Moreover, $\gamma n \rightarrow n\eta'$ has been studied recently at CBELSA/TAPS and the total cross section found to be very small [165]. Figure 20 (right) shows the corresponding total quasi-free proton cross section from the same analysis. The data are in good agreement with the results for the free proton, which indicates that nuclear effects have no significant impact. The total cross section off the proton reaches a maximum of about $1 \mu\text{b}$ in the photon energy range 1.8-1.9 MeV ($E_{\text{th}} \approx 1448 \text{ MeV}$) and then slowly declines without any structures.

A recent combined analysis of η' production in photon- and hadron-induced reactions by Huang *et al.* [292], based on an effective Lagrangian approach, finds the importance of three high-mass resonances which the authors tentatively identify with (**) $N(1895)\frac{1}{2}^-$, (*) $N(2100)\frac{1}{2}^+$, and (*) $N(2040)\frac{3}{2}^+$. Additional contributions from the sub-threshold resonance, $N(1720)\frac{3}{2}^+$, are required for a good fit in their analysis. The authors stress that the normalization discrepancy between the results from CLAS [142] and CBELSA/TAPS [160], similar to the discrepancy observed in η photoproduction, has an impact on the extracted resonance parameters but do not favour one data set over the other.

5.4.3. Photoproduction of K Mesons Production of open strangeness, particularly in the $\gamma p \rightarrow K^+Y$ ($Y = \Sigma^0, \Lambda$) channels, has received much attention recently since a true complete experiment appears feasible. None of the current experimental facilities employs a recoil polarimeter, but the parity-violating weak decay of the hyperon (self-analyzing particle) still provides access to the polarization of the recoiling baryon.

The differential cross sections for the reactions $\gamma p \rightarrow K^+\Lambda$ and $\gamma p \rightarrow K^+\Sigma^0$ were measured with good statistics at JLab using the CLAS detector, e.g. [133, 143, 144], at

ELSA using the SAPHIR detector [170], at GRAAL [192], and, in the forward region, at LEPS [198]. The reactions $\gamma p \rightarrow K^0 \Sigma^+$ and $\gamma p \rightarrow K^{*0} \Sigma^+$ were studied at CLAS [135], CBELSA/TAPS [155, 157, 163], and SAPHIR [173]. Recent measurements of the beam-recoil observables, $C_{x,z}$ at CLAS [134] and $O_{x,z}$ at GRAAL [193], in $\gamma p \rightarrow K^+ Y$ mark an important step toward complete experiments for these reactions. Despite the use of an unpolarized target at GRAAL, values for the target asymmetry T could also be extracted for energies below 1.5 GeV [193].

The observables, $C_{x,z}$, describe the spin transfer from the circularly-polarized photon to the recoiling hyperon along and perpendicular to the beam axis in the c.m. system, respectively. Most remarkable, the CLAS collaboration reported that the total Λ polarization vector, $R_\Lambda = \sqrt{P^2 + C_x^2 + C_z^2}$, is consistent with unity and that the results also suggest $C_z \simeq C_x + 1$ over a large range of W values and K^+ angles [134]. This observation implies that the Λ hyperons produced in the reaction $\vec{\gamma} p \rightarrow K^+ \vec{\Lambda}$ using circularly-polarized photons are almost 100% spin polarized, which is not required by the reaction kinematics. Figure 21 (left) shows the CLAS results for C_z [134]. None of the models shown in the figure reproduces the experimental results well. The phenomenon is still not properly understood. The right side of Figure 21 shows results from GRAAL for the observables, O_z [193]. The authors of [134] used a number of inequalities and the two equations

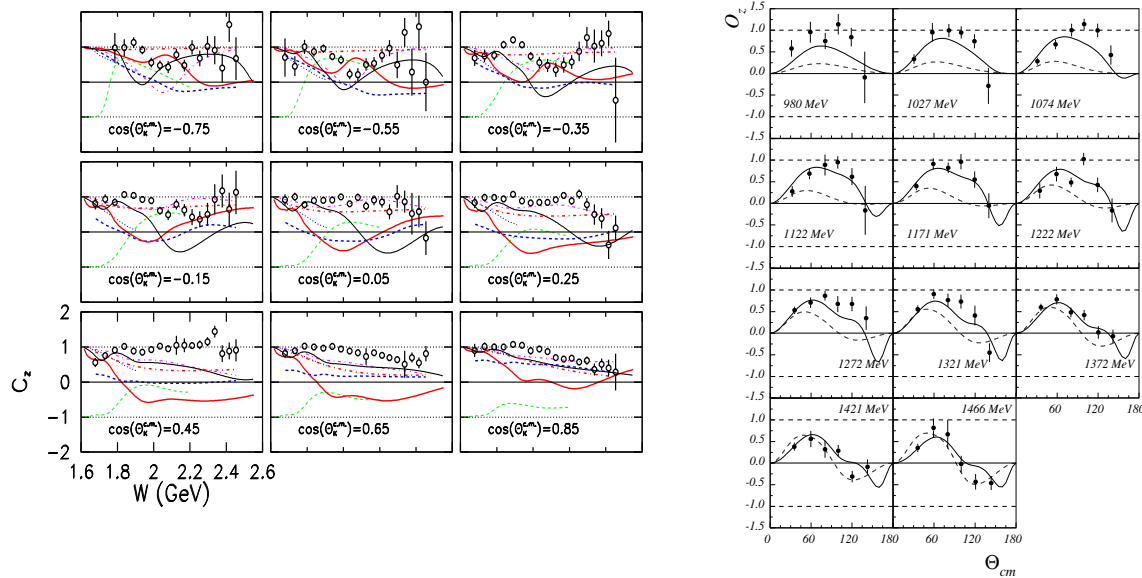
$$C_x^2 + C_z^2 + O_x^2 + O_z^2 = 1 + T^2 + P^2 + \Sigma^2 \quad (5.13)$$

$$C_z O_x - C_x O_z = T - P \Sigma \quad (5.14)$$

to show the overall consistency of the CLAS and GRAAL results. In principle, one additional double-polarization observable (either beam-target or target recoil) would be sufficient in the energy range below 1.5 GeV to extract the helicity amplitudes for $K^+ \Lambda$ photoproduction (see also the discussion in Section 4.3.2). The large polarization transfer in $K^+ \Lambda$ production was confirmed in CLAS electroproduction experiments, $\vec{e} p \rightarrow e' K^+ \vec{\Lambda}$, which span a wide range of momentum transfer Q^2 from 0.7 to 5.4 GeV² [130]. The Λ polarization was found to be largest along the direction of the virtual photon. The authors of [130] also discuss the reaction dynamics in the framework of a partonic model. It appears to be important to shed light on the relevance of the quark-gluon dynamics when the $s\bar{s}$ pair is created in a domain thought to be dominated by meson/baryon degrees of freedom. The Σ^0 hyperon differs substantially from the simple behaviour of the Λ hyperon.

A full discussion of the relevant nucleon resonance contributions in hyperon photoproduction goes beyond the scope of this review. We only give a short summary in this section. Since the Λ hyperon is an isoscalar, only intermediate $I = \frac{1}{2}$ nucleon resonances can couple to $K^+ \Lambda$ and the reaction serves thus as an isospin filter. The Σ^0 hyperon is an isovector, which allows it to couple to both $I = \frac{1}{2} N^*$ and $I = \frac{3}{2} \Delta$ states. The total cross section for $K^+ Y$ ($Y = \Lambda, \Sigma^0$) reaches about 2.5 μb and a structure around 1900 MeV is observed in both reactions. However, its interpretation in terms of s -channel baryon resonances has been highly controversial. The latest double-

Figure 21. (Colour online) Beam-recoil observables in the reaction $\gamma p \rightarrow K^+\Lambda$. Left: The observable C_z from CLAS using circularly-polarized photons. The data and picture are from [134]. We refer to [134] for a full description of the curves denoting a large variety of different models. Right: The observable O_z from GRAAL using linearly-polarized photons. The data and picture are from [193]. The curves denote the Bonn-Gatchina (solid line) and Ghent RPR (Regge-plus-resonance) isobar [293] (dashed line) models. With kind permission of The European Physical Journal (EPJ).



polarization observables have revealed indications for baryon resonances and additional observables will further our understanding of this peak structure. The cross section for $K^+\Sigma^0$ photoproduction is about a factor of four bigger than for $K^0\Sigma^+$, partly owing to forbidden background contributions from K exchange in the latter reaction.

Strong contributions from the new resonances listed by the PDG are observed in the Bonn-Gatchina multichannel approach [247]. The $N(1880)\frac{1}{2}^+$ state was first proposed on the basis of data on $\gamma p \rightarrow \Sigma^+K_S$ [155], but was also seen earlier in an analysis of $\pi N \rightarrow \pi N$ and $\pi N \rightarrow \pi\pi N$ [285]. Overall evidence for the existence of the $N(1895)\frac{1}{2}^-$ resonance appears to be stronger. It was recently observed in $K^+\Lambda$ and $K^+\Sigma^0$ production [247], but also found earlier in several analyses of $\pi N \rightarrow \pi N$ data [1]. The latest analysis of the SAID group [217] finds no indication for this resonance, though. Evidence for $N(1875)\frac{3}{2}^-$ was claimed in [294] based on $\gamma p \rightarrow K^+\Lambda$ from SAPHIR [170]. It was confirmed in several more recent multichannel analyses, e.g. [234, 247]. The recently published beam-recoil observables provide important evidence for the existence of the $N(1900)\frac{3}{2}^+$ state and inspired an upgrade of the resonance's star assignment from two to three. The right side of Figure 21 shows two curves in addition to the GRAAL data on the O_z observable denoting the Bonn-Gatchina solution (solid line) and a description within the Ghent RPR (Regge-plus-resonance) isobar model (dashed line) [293]. Both models require the $N(1900)\frac{3}{2}^+$ to describe the data at the highest energies. Initial evidence for this resonance in the Bonn-Gatchina model came from the CLAS data on the $C_{x,z}$ observables [295].

5.4.4. Photoproduction of Vector Mesons The vector mesons, ρ , ω , and ϕ , carry spin-parity quantum numbers $J^{PC} = 1^{--}$ and thus have the same quantum numbers as the photon. For this reason, when a photon probes a nucleon, one should expect vector mesons to play an important role in the spectrum of intermediate hadronic states. The total cross sections for photoproduction of these three mesons reach about $24 \mu\text{b}$, $8.5 \mu\text{b}$, and $0.2 \mu\text{b}$, respectively. The total ω cross section exhibits a pronounced peak structure at about $E_\gamma = 1.3 \text{ GeV}$ in addition to a broader peak similar in shape to that seen in ρ and ϕ production. The differential cross sections show an exponential fall-off at small values of the squared recoil momentum, t . Further strong contributions that cannot be explained by t -channel pion (kaon) exchange are observed at larger values of t .

In contrast to pseudoscalar mesons, vector-meson decays give rise to additional observables. The decays provide a measure of their spin-density matrices, which is equivalent to determining the intensity, polarization, and tensor polarization of these vector mesons. Without polarization observables, a more detailed analysis of resonance contributions as well as the study of the relative strength of the diffractive production and π^0 exchange is impossible. At CLAS, a determination of a large variety of such observables in ω production including spin-density matrix elements (SDMEs) has become feasible and has consequently received renewed interest in recent years. The full decay angular distributions were initially discussed in [296] for decays into pseudoscalar mesons and more recently also for the radiative decay of the ω meson into $\pi^0\gamma$ [297].

Differential cross sections for ρ and ϕ production were reported by SAPHIR [171, 174], LEPS [197] and CLAS [298]. Production of ω mesons was studied at SAPHIR [172], GRAAL [187], and recently, with large statistics, at CLAS [140] for energies from threshold to $W = 2.4 \text{ GeV}$. The experimental situation for polarization observables is still scarce. Data on the ω beam asymmetry, Σ , come from CBELSA/TAPS [156] and high-statistics results on the SDMEs, ρ_{00}^0 , ρ_{10}^0 , ρ_{1-1}^0 , using an unpolarized photon beam from CLAS [141]. The first measurements of ω double-polarization observables from the CLAS-FROST program were presented recently at conferences [299].

At lower energies, $W < 2 \text{ GeV}$, an earlier analysis included the beam asymmetries measured by the GRAAL collaboration and reported significant sensitivity to $N(1720) \frac{3}{2}^+$ and the off-shell states $N(1520) \frac{3}{2}^-$ and $N(1680) \frac{5}{2}^+$ in the energy ranges $E_\gamma \in [1.108, 1.218] \text{ GeV}$ and $E_\gamma \in [1.327, 1.423] \text{ GeV}$ [191]. A PWA of the Bonn-Gatchina group included the SAPHIR and GRAAL data and also found the $\frac{3}{2}^+$ wave as the dominant contribution, which was identified with the $N(1720) \frac{3}{2}^+$. The CLAS PWA found strong contributions from a $\frac{3}{2}^-$ wave at threshold, but did not include other data in the analysis. The Gießen group studied ω production within a coupled-channel effective Lagrangian approach in the energy range from the pion threshold up to 2 GeV and included data on π - and γ -induced reactions available at that time for the final states γN , πN , $2\pi N$, ηN , and ωN [237]. The analysis indicates that the initial resonance peak around 1700 MeV is primarily a result of the two sub-threshold resonances, $N(1675) \frac{5}{2}^-$ and $N(1680) \frac{5}{2}^+$. The latter hardly influences the reaction $\pi N \rightarrow \omega N$, but is significant in ω photoproduction due to its large $A_{\frac{3}{2}}$ helicity amplitude.

At higher energies, the $\gamma p \rightarrow p\omega$ differential cross section is dominated by t -channel exchange, but resonance production is still observed. At energies above $W = 2$ GeV, a PWA based on the CLAS unpolarized cross section alone [140] required contributions from at least two spin- $\frac{5}{2}$ resonances and from a heavier spin- $\frac{7}{2}$ resonance to correctly describe the cross section and the corresponding phase motion. The higher-spin state was identified as the $N(2190) \frac{7}{2}^-$ resonance listed as a 4-star state in the RPP [1]. The first-time observation of this resonance in photoproduction was later confirmed in $\gamma p \rightarrow p\pi^0$ [162]. The two $\frac{5}{2}$ -states were identified as the well-known $N(1680) \frac{5}{2}^+$ and the $N(2000) \frac{5}{2}^+$. The latter is a 2-star resonance that was also observed in the latest SAID analysis [217].

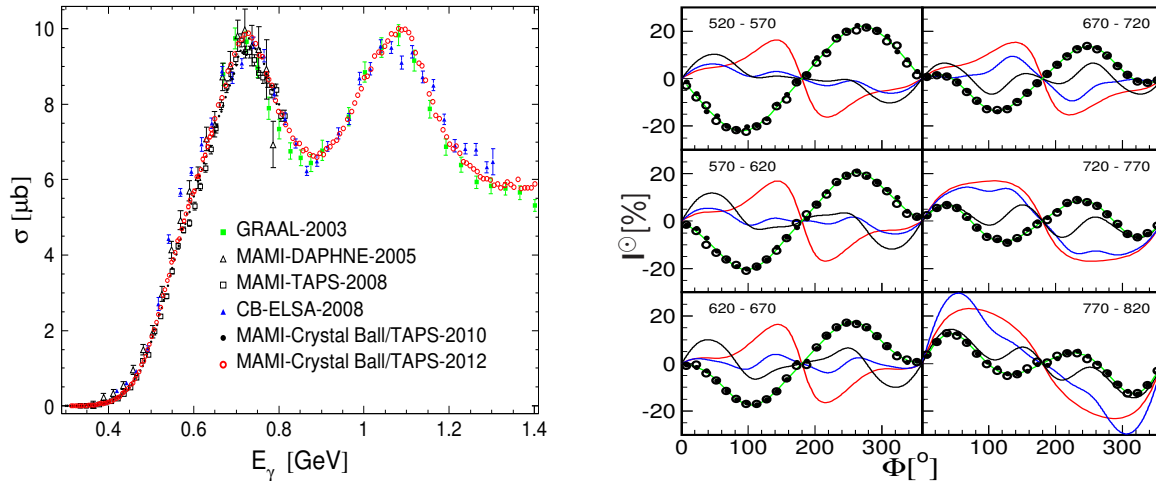
5.4.5. Photoproduction of Multi-Meson Final States The photoproduction of two mesons, in particular the production of two pions, plays an increasing role toward higher energies. Above $E_\gamma = 2$ GeV, the double-pion cross section is the biggest contributor to the total photoabsorption cross section. The two-pion cross section exhibits a double-peak structure, which is most pronounced in the reaction $\gamma p \rightarrow p\pi^0\pi^0$. The total cross section for this reaction is shown in Figure 22 (left). The first peak is in the second resonance region around $W \approx 1500$ GeV, the second peak around $W \approx 1700$ GeV. For the $p\pi^0\pi^0$ final state, it reaches a maximum of about $10 \mu\text{b}$ in the first peak, which is about a factor of eight smaller than the strength in the $p\pi^+\pi^-$ cross section. A complete description of the production of two pseudoscalar mesons requires five independent kinematic variables. Since the reaction plane and the decay plane spanned by the final state particles form an angle, the reaction does not proceed *in plane* as the production of a single meson does. The differential cross section is thus five-fold differential and using a polarized beam and an unpolarized target, can be written as

$$\frac{d\sigma}{dx_i} = \left(\frac{d\sigma}{dx_i} \right)_{\text{unpol.}} (1 + \delta_\odot I^\odot + \delta_l (I^s \sin 2\beta + I^c \cos 2\beta)), \quad (5.15)$$

where δ_\odot and δ_l denote the degrees of circular and linear polarization, β the angle between the reaction plane and the direction of the linear beam polarization vector, and I^\odot , I^s , I^c are the circular and linear polarization observables. A full theoretical discussion of the 64 possible polarization observables is given in [89].

The photoproduction cross sections of two neutral pions in the reaction $\gamma p \rightarrow p\pi^0\pi^0$ have been studied at ELSA [149], at GRAAL [188], and very recently at MAMI with a fine energy binning from threshold up to 0.8 GeV [182] and 1.4 GeV [183]. We refer to the references in [183] for the large variety of earlier MAMI results obtained with the DAPHNE and TAPS detectors. In [182], results are also discussed for the reaction $\gamma p \rightarrow n\pi^+\pi^0$. The reaction $\gamma n \rightarrow n\pi^0\pi^0$ was studied at GRAAL [189]. The photoproduction of two charged pions was studied at SAPHIR [174] and, at higher energies ($E_\gamma > 3$ GeV) with a focus on meson spectroscopy, at CLAS [137, 138]. Polarization results are scarce. At low energies ($E_\gamma < 820$ MeV), the beam-helicity asymmetry, I^\odot , has been recently measured at MAMI [179] for the reactions $\vec{\gamma}p \rightarrow p\pi^+\pi^-$, $n\pi^+\pi^0$, and $p\pi^0\pi^0$. Earlier, the helicity difference, P_z^\odot , was determined by the GDH collaboration at MAMI for

Figure 22. (Colour online) Left: Total cross section for the reaction $\gamma p \rightarrow p\pi^0\pi^0$ as a function of the incident-photon energy. Picture from [183]. Right: Beam-helicity asymmetry, I^\odot , for $\vec{\gamma}p \rightarrow n\pi^+\pi^0$ from MAMI [179]. The different curves denote model descriptions from [300] (red) and [301] (blue, black). Picture from [179].

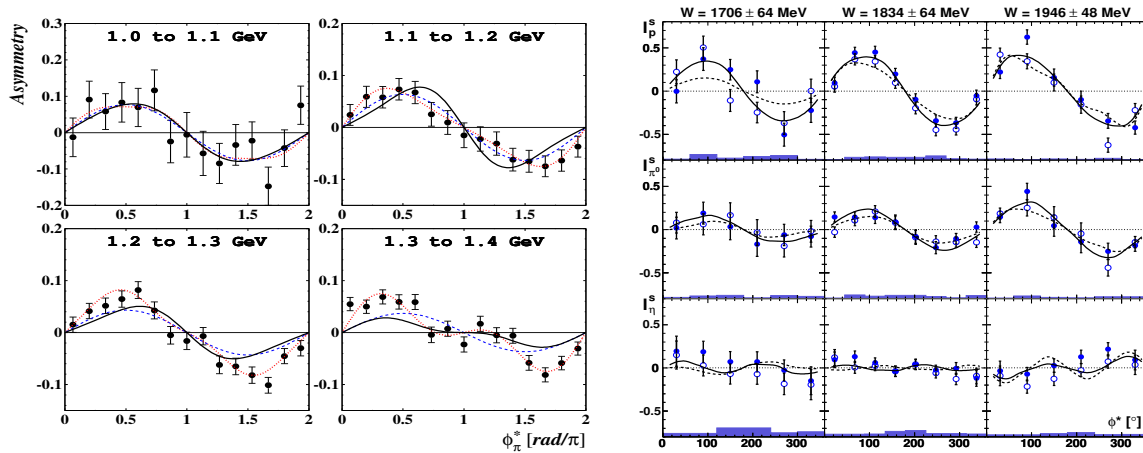


$p\pi^+\pi^-$ [178]. CLAS published data on I^\odot in $p\pi^+\pi^-$ for the $1.4 < W < 2.4$ GeV range and some data on the linear beam asymmetry, Σ , are available from GRAAL [188].

Double-pion photoproduction allows the study of sequential decays of nucleon resonances via intermediate excited states, but also the investigation of direct decays into $N\rho$ and $N\sigma$. However, large background contributions, in particular in the reaction $\gamma p \rightarrow p\pi^+\pi^-$, render an analysis challenging. Resonance contributions are more pronounced in $\pi^0\pi^0$ [149, 183, 188], but contributions from $N\rho$ intermediate states are excluded. Even at low energies, in and below the second resonance region, double-pion production is still poorly understood. While the unpolarized cross sections are fairly well described, models disagree substantially on the description of the available polarization data. As an example, Figure 22 (right) shows the unprecedented quality of the data for the beam-helicity observable, I^\odot , in $\vec{\gamma}p \rightarrow n\pi^+\pi^0$, but also the discrepancies between the models discussed in [300, 301].

It is widely believed that double-pion production is dominated by intermediate production of a $\Delta\pi$ state. In the second resonance region, the $N(1520) \frac{3}{2}^-$ state plays an important role in $\gamma p \rightarrow p\pi^0\pi^0$. A large contribution from the $J = \frac{3}{2}$ wave (as a reflection of the $J^P = \frac{3}{2}^+$ fraction of $\pi^+\pi^- \rightarrow \pi^0\pi^0$ rescattering) appears also crucial at energies below the second resonance region [183]. In [252], the same low-energy behaviour and the large peak around $E_\gamma = 700$ MeV (Figure 22, left) is explained by interference of the $N(1520) \frac{3}{2}^-$ and $\Delta(1700) \frac{3}{2}^- \rightarrow (\Delta\pi)_{L=0}$ resonances. However, the strong contribution of the $\Delta(1700) \frac{3}{2}^-$ state is in conflict with the model results discussed in the GRAAL publication [188] and the Valencia model, e.g. [302]. The $N(1720) \frac{3}{2}^+$ was found in [149] to decay strongly into $\Delta\pi$, not reported by the PDG at that time. A similar discrepancy in the width was observed in $\pi^+\pi^-$ electroproduction data from JLab but interpreted as a second (rather narrow) $N \frac{3}{2}^+$ resonance, e.g. [121]. At higher energies, the Bonn-

Figure 23. (Colour online) Beam asymmetries in $\bar{\gamma}p \rightarrow p\pi^0\eta$. Left: The observable I^\odot measured at MAMI [181]. The dotted curve denotes a Fourier expansion, the remaining curves represent predictions of a full isobar model with six resonances (solid line) and with only the $\Delta \frac{3}{2}^-$ amplitude (dashed line) [303]. Data and picture from [181]. Right: The observable I^s from CBELSA/TAPS [159]. The rows (top to bottom) show the proton, π^0 , and η as recoiling particle in the c.m. system, respectively (open circles: $-I^s(2\pi - \phi^*)$). The curves denote the Bonn-Gatchina fit for the full solution (solid line) and without the $\frac{3}{2}^-$ wave. Data and picture from [159].



Gatchina group observes a strong coupling of the (newly-listed) $N(1875) \frac{3}{2}^-$ state to $N\sigma$ [247]. In conclusion, double-pion production is far from understood and the full spectrum of polarization observables is likely required for progress in this exciting field.

The reaction $\gamma p \rightarrow p\pi^0\eta$ was measured at GRAAL [194], MAMI [181], and ELSA [150, 151, 159]. The published results include cross section measurements and the first-time extraction of the beam asymmetries using circularly- (Figure 23, left) and linearly-polarized photons (Figure 23, right). The total unpolarized cross section rises rapidly from the reaction threshold at $E_\gamma \approx 930$ MeV to a maximum of about $3.5 \mu\text{b}$ at 1500 MeV and then slowly declines without any structures. Most of the reaction rate proceeds via the $\Delta\eta$ intermediate state, which serves as an isospin filter for Δ^* resonances. Other dominant contributions include the $pa_0(980)$ and $N(1535) \frac{1}{2}^- \pi^0$ intermediate states.

Several analyses have observed strong contributions from the $\Delta \frac{3}{2}$ wave to $p\pi^0\eta$. This is not surprising. The $\Delta(1232)$ and the η have $J^P = \frac{3}{2}^+$ and $J^P = 0^-$, respectively, and can thus form the total spin-parity state $J = \frac{3}{2}^-$ with orbital angular momentum $L = 0$. Little doubt exists about the importance of the $(***) \Delta(1700) \frac{3}{2}^-$ resonance in this reaction [247, 303, 304], but contributions from the higher-mass $\Delta(1940) \frac{3}{2}^-$ resonance seem to be confirmed. Figure 23 (left) shows a description of the beam asymmetry, I^\odot , using the model in [303] for the full solution (solid line), and for the $\Delta \frac{3}{2}^-$ amplitude (dashed line) only. Figure 23 (right) shows a description of the beam asymmetry, I^s , using the Bonn-Gatchina framework [247]. The full solution is again given by the solid line, whereas the dashed line denotes the full solution without

the $\Delta \frac{3}{2}^-$, which demonstrates the importance of this contribution. Both models also include the positive-parity $\Delta \frac{3}{2}^+$ waves, $\Delta(1600)$ and $\Delta(1920)$. Weaker contributions are also observed from the higher-spin resonance, $\Delta(1905) \frac{5}{2}^+$, and from a corresponding negative-parity state above $W = 2$ GeV [159]. However, the experimental situation clearly becomes worse at these higher energies. It is also important to emphasize that despite the observation of the $\Delta(1700) \frac{3}{2}^-$ state in the reaction $\gamma p \rightarrow p\pi^0\eta$, no agreement on the nature of this resonance has been reached. Interpretations range from a dynamically-generated resonance [304] to a regular $3q$ quark model state.

The reaction $\gamma p \rightarrow p\pi^0\omega$ gives access to the $\Delta\omega$ system, which also serves as an isospin filter for Δ^* resonances. The reaction is very interesting and promises a rich source of baryon production. Similar to the $p\pi^0\eta$ final state, first results indicate that $\gamma p \rightarrow p\pi^0\omega$ proceeds dominantly via $\Delta\omega$. Since the ω has $J^P = 1^-$, $\Delta \frac{3}{2}$ and $\Delta \frac{5}{2}$ states should strongly contribute. The current experimental situation is weak, though. Cross sections based on about 2000 events from CB-ELSA were published in 2007 [152], but a higher-statistics data set from CBELSA/TAPS with almost an order of magnitude more events has been presented at conferences [305] and will be available soon. Signatures of the reaction $\gamma p \rightarrow \Delta\rho$ have been observed in CLAS data at high photon energies [306].

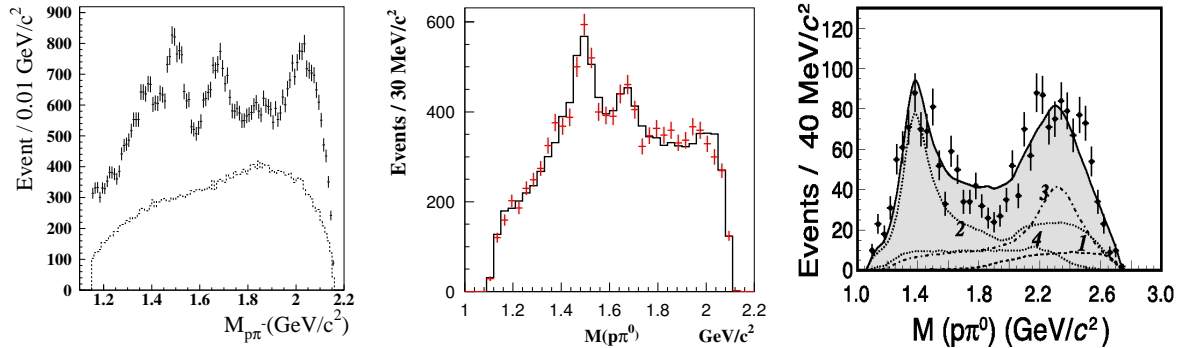
5.5. Observation of Baryons in J/ψ Decays

An alternative approach to studying nucleon resonances in induced reactions from a nucleon target is the investigation of baryons which are observed in J/ψ and ψ' decays into a baryon, an antibaryon, and an additional meson. In reactions such as $\psi' \rightarrow p\bar{p}\pi^0$, N^* resonances coupling to $p\pi^0$ or $\bar{p}\pi^0$ can be studied. In these decays, contributions of the Δ resonance are excluded owing to isospin conservation, which greatly facilitates this type of analysis. Excited hyperons, such as Λ^* , Σ^* , and Ξ^* , can also be studied. First measurements of J/ψ and $\psi(2S)$ decays into $\Lambda\bar{\Lambda}\pi^0$ and $\Lambda\bar{\Lambda}\eta$ were published by the BES collaboration [206], and more recently even branching fractions for the decay $J/\psi \rightarrow \Lambda\bar{\Lambda}\pi^+\pi^-$ [211].

N^* production was studied at BES in the reactions $J/\psi \rightarrow p\bar{p}\pi^0$ [208], $J/\psi \rightarrow p\bar{p}\eta$ [202], and $J/\psi \rightarrow p\bar{n}\pi^-$ [203]. In 2005, the decays $\psi' \rightarrow p\bar{p}\pi^0$ and $\psi' \rightarrow p\bar{p}\eta$ were presented in [204], but first results of a PWA were reported just recently in [209, 210]. Branching fractions were also published for $J/\psi \rightarrow p\bar{p}\omega$ [207], $\psi' \rightarrow p\bar{n}\pi^-$ [205], and $\psi' \rightarrow \bar{p}n\pi^+$ [205], but the statistics are not sufficient to perform a PWA. Even double-pion production was observed in the reactions $\psi' \rightarrow \bar{p}n\pi^0\pi^+$ [205]. Moreover, BES has studied the interesting J/ψ and ψ' decays into $B_8\bar{B}_8$ ($p\bar{p}$, $n\bar{n}$, $\Lambda\bar{\Lambda}$, $\Sigma^0\bar{\Sigma}^0$, $\Xi^-\bar{\Xi}^+$) [307, 308, 309, 310, 311] and $\psi' \rightarrow B_{10}\bar{B}_{10}$ ($\Delta^{++}\bar{\Delta}^{--}$, $\Sigma^+(1385)\bar{\Sigma}^-(1385)$, $\Xi^0(1530)\bar{\Xi}^0(1530)$, $\Omega^-\bar{\Omega}^+$) [307]. Studying excited hyperons in such decays remains thus a strong possibility. CLEO has recently presented PWA results for the reactions $\psi' \rightarrow p\bar{p}\pi^0$ and $\psi' \rightarrow p\bar{p}\eta$ [29].

An early PWA of the $J/\psi \rightarrow p\pi^-\bar{n}$ channel at BES, based on about 5.5×10^4 events, observed four peaks [203], which the authors identify with the first direct observation

Figure 24. (Colour online) Left: Invariant $p\pi^-$ distribution for $J/\psi \rightarrow p\pi^-\bar{n}$ from BES [203]; the phasespace Monte Carlo distribution is shown as a dotted line. Middle: Invariant $p\pi^0$ mass spectrum for $J/\psi \rightarrow p\bar{p}\pi^0$ from BES [208]. The data are represented by crosses and the histogram denotes the fit. Pictures from [203, 208]. Right: Invariant $p\pi^0$ spectrum for $\psi' \rightarrow p\bar{p}\pi^0$ from CLEO [29]. The solid line denotes the sum of the Monte Carlo distributions labeled in the figure for $N^*(1440)$ (1), $N^*(2300)$ (2), and two additional $p\bar{p}$ states (3,4). Picture from [29].



of the $N^*(1440)$ peak, the well-known second and third resonance regions, and a new N^* state with a mass around 2030 MeV. The invariant $p\pi^-$ mass distribution is shown in Figure 24 (left). A more recent PWA of the $J/\psi \rightarrow p\bar{p}\pi^0$ channel based on about 11,000 events confirms the resonance above 2 GeV and determines a mass and width of $2040^{+3}_{-4} \pm 25$ MeV and $230^{+8}_{-8} \pm 52$ MeV, respectively [208]. The analysis used the relativistic covariant tensor amplitude formalism described in [312, 313]. The observed invariant $p\pi^0$ mass distribution is shown in Figure 24 (middle). Since $L = 1$ is suppressed in the fits, the spin-parity of the N^* state is limited to $\frac{1}{2}^+$ and $\frac{3}{2}^+$, which may explain the strong peak in the mass spectrum (Figure 24 (left)). The analysis favours a $\frac{3}{2}^+$ assignment. Baryon production in πN and γN reactions allows all N^* quantum numbers including contributions from their Δ partners.

The CLEO collaboration reported results on the analysis of the $\psi(2S) \rightarrow p\bar{p}\pi^0$ channel [29] and observed two clear enhancements in the $p\pi^0$ mass around 1400 and 2300 MeV (Figure 24 (right)). Without considering interferences between resonances, the spectrum was described by two N^* ($N(1440)$ and $N(2300)$) and two further $p\bar{p}$ resonances (the solid curve in the figure denotes the sum of corresponding Monte Carlo distributions). Mass and width of the $N^*(2300)$ were determined to be 2300 ± 25 MeV and 300 ± 30 MeV, respectively. Very recently, the BES collaboration announced the observation of two new N^* resonances in $\psi(2S) \rightarrow p\bar{p}\pi^0$ [210] based on a $\psi(2S)$ data set, which is about four times larger than the CLEO statistics. The earlier reported $N^*(2300)$ is confirmed by BES with mass and width of $2300^{+40+109}_{-30-0}$ MeV and $340^{+30+110}_{-30-58}$ MeV, respectively, consistent with the CLEO results. A $J^P = \frac{1}{2}^+$ assignment for this state is preferred in the analysis. The second new state has been reported with a mass of 2570^{+19+34}_{-30-0} MeV, a width of 250^{+14+69}_{-24-21} MeV, and a J^P assignment of $\frac{5}{2}^-$. A total of seven intermediate N^* states has been observed to contribute significantly in

Table 13. Summary of all nucleon resonances which have been observed by the BES collaboration in charmonium $c\bar{c}$ decays.

N^*	2012 [1]	Reference
$N(1440) 1/2^+$	****	$J/\psi \rightarrow p\bar{p}\pi^0$, $p\pi^-\bar{n} + c.c.$ [203, 208], $\psi(2S) \rightarrow p\bar{p}\pi^0$ [210]
$N(1520) 3/2^-$	****	J/ψ & $\psi(2S) \rightarrow p\bar{p}\pi^0$ [208, 210]
$N(1535) 1/2^-$	****	J/ψ & $\psi(2S) \rightarrow p\bar{p}\pi^0$ [208, 210], $J/\psi \rightarrow p\bar{p}\eta$ [202]
$N(1650) 1/2^-$	****	J/ψ & $\psi(2S) \rightarrow p\bar{p}\pi^0$ [208, 210], $J/\psi \rightarrow p\bar{p}\eta$ [202]
$N(1710) 1/2^+$	***	$J/\psi \rightarrow p\bar{p}\pi^0$ [208]
$N(1720) 3/2^+$	****	$\psi(2S) \rightarrow p\bar{p}\pi^0$ [210]
$N(2065) 3/2^+$	*	$J/\psi \rightarrow p\pi^-\bar{n} + c.c.$ [203], $J/\psi \rightarrow p\bar{p}\pi^0$ [208]
$N(2300) 1/2^+$		$\psi(2S) \rightarrow p\bar{p}\pi^0$ [210] (also observed by CLEO [29])
$N(2570) 5/2^-$		$\psi(2S) \rightarrow p\bar{p}\pi^0$ [210]

the $\psi(2S)$ decay, but the authors do not claim evidence for the $N(2065)$ state previously observed by BES in J/ψ decays [208] or any further resonance in the 1900 MeV mass region. A summary of all nucleon resonances observed in charmonium decays is given in Table 13.

6. Models and Phenomenology

To get a better understanding of baryon structure, dynamics must be added to the symmetry schemes outlined in the early sections of this article. Theoretical studies of baryons are just about as old as the entire field of particle physics, and the literature is vast. Any attempt at summarizing this quantity of material in a few pages is futile: there are review articles on specific approaches that are longer than the space allowed for this entire review. Ruthless selectivity has to be exercised in choosing those approaches discussed, and even for those, only a very brief synopsis can be given.

The overarching goals of baryon spectroscopy are to understand the relevant degrees of freedom in a baryon, and how the strong interaction in the non-perturbative regime gives rise to the states we observe. Different hypotheses regarding the relevant degrees of freedom, symmetries and dynamics lead to different spectra, and comparison with experiment will serve to validate or repudiate one set of assumptions or another. Unfortunately, no models can yet be completely eliminated.

Perhaps the most prevalent approach for attempting to understand the internal structure and dynamics of a baryon is through some kind of quark model. More recently, the lattice has been brought to bear with increasing success, and the large N_c limit of QCD has also been used. Relativistic bound state equations have also been applied to the study of baryon spectra and properties, as have holographic models. In the next few subsections, the salient points of some of these approaches are discussed. Later in the manuscript, the numerical predictions for the masses of baryons are shown and

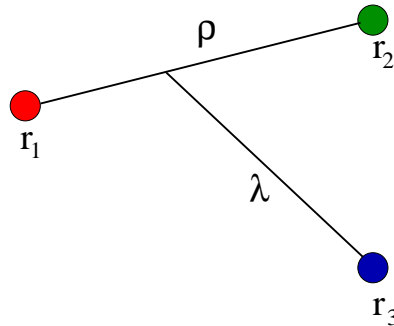
compared among the approaches discussed, as well as with the masses extracted from experiments.

6.1. Quark Models

6.1.1. Non- and Semi-Relativistic Models The constituent quark model provides perhaps the simplest, most intuitive insight into the structure of a baryon. Originally constructed as a classification scheme that predates QCD, to explain the regularities among the new particles being discovered in the 1960s, this model has been through a number of incarnations, with varying degrees of sophistication and refinement, as well as varying degrees of success. The main appeal of such models is that they provide a simple framework within which a vast array of phenomenology may be integrated and understood.

In its simplest version the quark model posits that a baryon consists of three valence quarks, as depicted in Figure 25. All of the nonperturbative dynamics of the gluons being exchanged between pairs of quarks are assumed to be mimicked by a potential that at least provides the expected confinement when the separation between the quarks is large. The baryon spectrum is thus obtained by solving the wave equation for three particles moving in a potential. As far as possible, the symmetries discussed are built into the model.

Figure 25. Quark model depiction of a baryon.



The full wave function of the baryon is written as

$$\psi = \psi_{\text{colour}}\psi_{\text{spin}}\psi_{\text{space}}\psi_{\text{flavour}}. \quad (6.1)$$

Since baryons are colour singlets, ψ_{colour} is antisymmetric under exchange of any pair of quarks. The product $\psi_{\text{spin}}\psi_{\text{space}}\psi_{\text{flavour}}$ must therefore be symmetric under exchange of any pair of identical quarks. For baryons constructed of only u , d and s quarks, the flavour part of the wave function, ψ_{flavour} , is constructed in accordance with the representations discussed in Section 2.1.

The spins of the quarks are coupled to either spin $\frac{3}{2}$ with a totally symmetric wave function, or spin $\frac{1}{2}$ with mixed symmetry in the wave function. The maximally stretched

spin wave functions are

$$\begin{aligned} \left| \frac{3}{2}, \frac{3}{2} \right\rangle_S &= |\uparrow\uparrow\uparrow\rangle, \\ \left| \frac{1}{2}, \frac{1}{2} \right\rangle_\lambda &= -\frac{1}{\sqrt{6}} |\uparrow\downarrow\uparrow + \downarrow\uparrow\uparrow - 2\uparrow\uparrow\downarrow\rangle, \\ \left| \frac{1}{2}, \frac{1}{2} \right\rangle_\rho &= \frac{1}{\sqrt{2}} |\uparrow\downarrow\uparrow - \downarrow\uparrow\uparrow\rangle, \end{aligned} \quad (6.2)$$

where the subscripts indicate fully symmetric (S), symmetric under exchange of the first two quarks (λ) or antisymmetric under exchange of the first two quarks (ρ).

The spatial part of the wave function is obtained by solving a Hamiltonian equation that treats the baryon as consisting of three valence quarks that interact through a potential that includes spin-independent confining terms, as well as any number of spin-dependent contributions. The dynamics of the quarks in the baryon are described in terms of the Jacobi coordinates, $\vec{\rho}$, $\vec{\lambda}$ and \vec{R} which are related to the quark positions by

$$\begin{aligned} \vec{\rho} &= \frac{1}{\sqrt{2}} (\vec{r}_1 - \vec{r}_2), \\ \vec{\lambda} &= \sqrt{\frac{2}{3}} \left(\frac{m_1 \vec{r}_1 + m_2 \vec{r}_2}{m_1 + m_2} - \vec{r}_3 \right), \\ \vec{R} &= \frac{1}{M} (m_1 \vec{r}_1 + m_2 \vec{r}_2 + m_3 \vec{r}_3), \end{aligned} \quad (6.3)$$

where

$$M = m_1 + m_2 + m_3. \quad (6.4)$$

Here $\vec{\rho}$ is proportional to the separation between quarks 1 and 2, and λ is proportional to the separation between quark 3 and the centre of mass of quarks 1 and 2. The choice of normalization of the coordinates is arbitrary. This particular choice leads to

$$\vec{\lambda} = \frac{1}{\sqrt{6}} (\vec{r}_1 + \vec{r}_2 - 2\vec{r}_3) \quad (6.5)$$

when all quarks have the same mass.

In the nonrelativistic version of the quark model, the kinetic part of the Hamiltonian is

$$T = \sum_{i=1}^3 \left(\frac{p_i^2}{2m_i} + m_i \right). \quad (6.6)$$

This can be rewritten in terms of p_ρ , p_λ and p_R , the momenta conjugate to the Jacobi coordinates defined above. This part of the Hamiltonian then becomes

$$T = -\frac{\nabla_\rho^2}{2m_\rho} - \frac{\nabla_\lambda^2}{2m_\lambda} - \frac{\nabla_R^2}{2M} + M, \quad (6.7)$$

where $m_\rho = \frac{2m_1 m_2}{m_1 + m_2}$ and $m_\lambda = \frac{2}{3} \frac{m_3(m_1 + m_2)}{m_1 + m_2 + m_3}$. The spatial part of the wave function is then written as a sum of separable components, namely

$$\psi_{\text{space}} = \sum \psi_\rho(\vec{\rho}) \psi_\lambda(\vec{\lambda}), \quad (6.8)$$

and the dependence on the centre-of-mass coordinate R is trivial. In some models, the kinetic energy term is treated relativistically, and is written

$$K_i = \sqrt{m_i^2 + p_i^2}. \quad (6.9)$$

Such versions of the model are referred to as ‘semi-relativistic’, since the kinetic energies of the quarks in the baryon are treated relativistically, but the model lacks Lorentz covariance.

In this picture of a baryon, each Jacobi coordinate may be independently excited, either radially, orbitally, or both. The total orbital angular momentum of the baryon is

$$\vec{L} = \vec{\ell}_\rho + \vec{\ell}_\lambda, \quad (6.10)$$

and the total angular momentum is

$$\vec{J} = \vec{L} + \vec{S}, \quad (6.11)$$

where \vec{S} is the total spin of the quarks. The parity, P , of the baryon constructed in this way is

$$P = (-1)^{\ell_\rho + \ell_\lambda}. \quad (6.12)$$

A variety of forms for the potentials have been used in the literature. Many models treat the inter-quark potential as arising from exchange of gluons. In such models, the spin-independent confining potentials are approximated by linear and Coulomb forms,

$$V_{\text{conf}}^{ij} = \left(\frac{br_{ij}}{2} - \frac{2\alpha_{\text{Coul}}}{3r_{ij}} \right), \quad (6.13)$$

but other forms, including logarithmic forms, have been used. In such models, the spin-dependent parts of the potential take the forms

$$H_{\text{hyp}}^{ij} = \sum_{i < j=1}^3 \left[V_{\text{contact}}(\mathbf{r}_{ij}) \frac{1}{m_i m_j} + V_{\text{tensor}}(\mathbf{r}_{ij}) \frac{1}{m_i m_j} \left(\frac{3\mathbf{S}_i \cdot \mathbf{r}_{ij} \mathbf{S}_j \cdot \mathbf{r}_{ij}}{r_{ij}^2} - \mathbf{S}_i \cdot \mathbf{S}_j \right) \right] \quad (6.14)$$

where the functions $V_{\text{contact}}(\mathbf{r}_{ij})$ and $V_{\text{tensor}}(\mathbf{r}_{ij})$ are scalar functions of the separation r_{ij} . These functions vary from model to model. For instance, many authors use a Dirac delta function for $V_{\text{contact}}(\mathbf{r}_{ij})$, while others use a functional form that is not quite so singular at the origin. In addition, there are spin-orbit interactions, which usually have a small effect on the spectrum.

In models like this, as in most models of baryons, the baryons of the ground state octet and decuplet sit in the $(\mathbf{56}, 0_0^+)$ of Table 2, while excited states belong to some of the other multiplets shown in the same table. If all spin-dependent interactions are neglected, the states of the ground-state octet are degenerate with their flavour analogs in the decuplet. The contact hyperfine interaction removes this degeneracy, making the nucleon lighter and the Δ heavier, for instance. The tensor and spin-orbit interactions induce mixings with the other supermultiplets of Table 2, leading to components of the nucleon and Δ wave functions having non-zero orbital angular momentum, for

instance. The spin-orbit interaction also removes degeneracies between states with the same non-zero total orbital angular momentum and spin, but having different total angular momentum. One example of this is the $\Lambda(1405) \frac{1}{2}^-$ and the $\Lambda(1520) \frac{3}{2}^-$.

Results from one model of this kind, that of [76], are shown in the fourth columns of Tables 14 to 18, for baryons consisting of u , d and s quarks. It can be seen from these tables that this model, and others of similar ilk, provide a moderately successful description of both light and heavy baryon spectra, but they have a few notable shortcomings. One example is that it is customary to identify the lightest excited $\frac{1}{2}^+$ nucleon, $N(1440) \frac{1}{2}^+$, as the first radial excitation of the nucleon. With potentials motivated by gluon exchange, most models fail to get this state as light as it is.

A number of authors have treated the inter-quark potential as arising from exchange of mesons, starting with pseudoscalar mesons as Goldstone bosons, but expanding the list of exchanged particles to include vector and scalar mesons. A significant part of the motivation in such models is the failure of gluon-exchange models to reproduce the relatively light mass of the $N(1440) \frac{1}{2}^+$. In one such model [260], the interaction potential takes the form

$$\begin{aligned} V(ij)_{\text{conf}} &= V(ij)^{ps} + V(ij)^v + V(ij)^s \\ &= \sum_{a=1}^3 [V_\pi(ij) + V_\rho(ij)] \lambda_i^a \lambda_j^a + \sum_{a=4}^7 [V_K(ij) + V_{K^*}(ij)] \lambda_i^a \lambda_j^a \\ &\quad + [V_\eta(ij) + V_{\omega_8}(ij)] \lambda_i^8 \lambda_j^8 + \frac{2}{3} [V_{\eta'}(ij) + V_{\omega_1}(ij)] + V_\sigma(ij). \end{aligned} \quad (6.15)$$

Exchange of mesons in the pseudoscalar nonet provides spin-spin and tensor forces, the vectors provide central, spin-spin, tensor and spin-orbit forces, and the scalar singlet leads to central and spin-orbit forces.

Results from this model (reference [260]) are shown in column five of Tables 14 to 18. Although the mass of the radially excited nucleon is improved, the description of the spectra of baryons is not significantly better than that obtained with gluon-exchange forces.

One feature apparent in the results of columns four and five of these tables is the prediction of many more states than have been observed (this is less apparent for the results shown in column five: that model predicts about the same number of states as the model whose results are shown in column four, but the results are not published). This is the so-called missing or undiscovered baryon problem, one that is key to understanding the effective degrees of freedom in a baryon. A number of authors have suggested that the primary reason for the mismatch between the numbers of predicted and observed states is that models such as those discussed have the wrong degrees of freedom. Instead of being a system of three quarks, in which any of the three can be excited, the baryon should be treated as a quark-diquark system, with excitations in the diquark frozen out, or occurring at significantly higher energies. With fewer excitations possible, the

Table 14. Predictions for excited nucleons from a number of theoretical treatments. The first column shows the J^P of the state, while the second shows the PDG designation, including the star rating. Column three shows the PDG Breit-Wigner mass range. Numbers with no parentheses are PDG averages. Numbers in this column in parentheses show the range of measurements reported, with no average given by the PDG. Hyphens in columns two and three indicate that there is no experimental state that matches model states shown in the later columns. Column four shows the numbers from a relativized quark model (QM) with one-gluon-exchange (OGE) forces, that of Capstick and Isgur [76]. The numbers in column five come from a model in which the inter-quark interactions arise from meson exchanges (GBE) [260]. Column six shows the results from a diquark model [315]. Column seven shows the results obtained in the relativistic quark model (RQM) of Löring *et al.* [317, 318, 319]. The numbers in column eight are obtained in the large N_c treatment [320, 321, 322, 323, 324, 325, 326, 327, 328], and the numbers in column nine are the results of the lattice simulations of Edwards *et al.* [329, 330, 331]. For the diquark model (column six), a hyphen indicates that such a state cannot exist in the model. For other models, a blank line indicates that the model does predict such a state, but the prediction has not been published.

J^P	State	PDG Mass Range	QM OGE	QM GBE	Di-quark	RQM	Large N_c	Lattice
$\frac{1}{2}^+$	938(****)	938	960	939	939	939		1196±11
	1440(****)	1420-1470	1540	1459	1513	1518	1450	2187±45
	1710(***)	1680-1740	1770	1776	1768	1729	1712	2255±28
	1880(**)	(1835-1915)	1880		1893	1950		2351±37
	2100(*)	(2030-2200)	1975		—	1996	1983	2244±28
	—	—	2065		—	2009		2544±51*
$\frac{3}{2}^+$	1720(****)	1700-1750	1795		1768	1688	1674	2146±16
	1900(***)	(1862-1975)	1870		1808	1809	1885	2314±20
	2040(*)	2031-2065	1910		—	1936		2334±22
	—	—	1950		—	1969		2401±17
$\frac{5}{2}^+$	1680(****)	1680-1690	1770		1808	1723	1689	2143±17
	1860(**)	1820-1960	1980		—	1934		2352±22
	2000(**)	1950-2150	1995		—	1959	1850	2415±18
	—	—	1995		—	2120		2943±68*
$\frac{7}{2}^+$	1990(**)	(1920-2155)	2000		—	1989	1872	2481±20
	—	—	1995		—	2190		2900±57
	—	—			—	2365	2240	
$\frac{9}{2}^+$	2220(****)	2200-2300	2345			2221	2245	
$\frac{13}{2}^+$	2700(**)	(2570-3100)	2820			2616		
$\frac{1}{2}^-$	1535(****)	1525-1545	1460	1519	1527	1435	1541	1707±21
	1650(****)	1645-1670	1535	1647	1671	1660	1660	1860±27
	1895(**)	(1860-2260)	1945 2030		1882	1901 1918		2357±113
$\frac{3}{2}^-$	1520(****)	1515-1525	1495	1519	1527	1476	1532	1811±22
	1700(****)	1650-1750	1625	1647	1671	1606	1699	1889±21
	1875(****)	1820-1920	1960		1882	1926		2513±54
	2120(**)	(1980-2210)	2055 2095			1959 2070		2673±20
$\frac{5}{2}^-$	1675(****)	1670-1680	1630	1647	1671	1655	1671	1987±17
	2060(**)	(1900-2260)	2080 2095			1970 2104		2486±24
$\frac{7}{2}^-$	2190(****)	2100-2200	2090			2015		2635±22
$\frac{9}{2}^-$	2250(****)	2200-2350	2215			2212		
$\frac{11}{2}^-$	2600(****)	2550-2750	2600			2425 2600		

Table 15. Predictions for excited Δ baryons from a number of theoretical approaches. The key is as in Table 14.

J^P	State	PDG Mass Range	QM OGE	QM GBE	Di-quark	RQM	Large N_c	Lattice
$\frac{1}{2}^+$	1750 ^(*)	(1700-1780)	1835		1858	1866	1746	2193±34
	1910 ^(****)	1860-1910	1875		1952	1906	1897	2343±20
$\frac{3}{2}^+$	1232 ^(****)	1230-1234	1230	1240	1233	1260		1505±13
	1600 ^(***)	1500-1700	1795	1718	1602	1810	1625	2300±28
	1920 ^(***)	1900-1970	1915		1952	1871	1906	2380±40
	—	—	1985		—	1950		2436±57
$\frac{5}{2}^+$	1905 ^(****)	1855-1910	1910		1952	1897	1921	2334±18
	2000 ^(**)	(1600-2325)	1990		—	1985	1756	2422±17
					—		2368	2672±56
$\frac{7}{2}^+$	1950 ^(****)	1915-1950	1940		1952	1956	1942	2320±34
	2390 ^(*)	(2250-2485)	2370			2339	2372	
$\frac{9}{2}^+$	2300 ^(**)	(2240-2550)	2420			2393	2378	
$\frac{11}{2}^+$	2420 ^(****)	2300-2500	2450			2442	2385	
$\frac{15}{2}^+$	2950 ^(**)	(2750-3090)	2920			2824		
$\frac{1}{2}^-$	1620 ^(****)	1600-1660	1555	1642	1554	1654	1645	1897±18
	1900 ^(**)	1840-1920	2035		1986	2100		2572±53
	2150 ^(*)	(2050-2250)	2140			2141		2656±30
$\frac{3}{2}^-$	1700 ^(****)	1670-1750	1620	1642	1554	1628	1720	1945±19
	1940 ^(**)	1940-2060	2080			2089		2751±24
			2145		1986	2156		
		2155			2170			
$\frac{5}{2}^-$	1930 ^(***)	1900-2000	2155		2005	2170		2748±21
	2350 ^(*)	(2160-2525)	2165			2187		
$\frac{7}{2}^-$	2200 ^(*)	(2120-2360)	2230			2181		2677±26
$\frac{9}{2}^-$	2400 ^(**)	(2100-2780)	2295			2280		
$\frac{13}{2}^-$	2750 ^(**)	(2550-2870)	2750			2685		

numbers of predicted and observed states are closer to each other. Such models still predict as-yet undiscovered states, but they are far fewer.

Before exploring one of these diquark models further, we point out that there is an alternative explanation that has been proposed for the number of missing states. This is the suggestion, first made by Koniuk and Isgur [256], and later confirmed by Capstick and Roberts [314], that the missing states couple weakly to the channel that has been used predominantly for production of excited baryons, namely the $N\pi$ channel. This suggestion has provided the motivation for a significant part of the baryon spectroscopy

program at many labs around the world.

In diquark models, the wave function is no longer symmetrized for all three quarks, but only for the two quarks in the diquark. In SU(6), the diquark representations are

$$\mathbf{6} \otimes \mathbf{6} = \mathbf{21} \oplus \mathbf{15}, \quad (6.16)$$

and the symmetry of the wave function of the diquark requires it to be the $\mathbf{21}$, since the color wave function is antisymmetric. Thus the baryon multiplets possible are [332]

$$\mathbf{6} \otimes \mathbf{21} = \mathbf{56} \oplus \mathbf{70}. \quad (6.17)$$

In this variant, there is no $\mathbf{20}$ of baryons, and only one of the $\mathbf{70}$ multiplets exists. Since this multiplet has mixed-symmetry, it means that many states in the diquark model do not belong to irreducible representations of SU(6).

In the diquark model of Ferretti *et al.* [315], the mass operator for N^* and Δ resonances is chosen to be

$$M = E_0 + \sqrt{q^2 + m_1^2} + \sqrt{q^2 + m_2^2} + M_{\text{dir}}(r) + M_{\text{cont}}(r) + M_{\text{ex}}(r) \quad (6.18)$$

where E_0 is a constant, m_1 is the mass of the diquark, m_2 is the mass of the quark, r is their separation and q is the magnitude of the momentum conjugate to r . In this operator,

$$V_{\text{dir}}(r) = -\frac{\tau}{r} (1 - e^{-\mu r}) + \beta r, \quad (6.19)$$

is the so-called direct term and

$$V_{\text{ex}}(r) = (-1)^{l+1} e^{-\sigma r} [A_S \vec{s}_1 \cdot \vec{s}_2 + A_I \vec{t}_1 \cdot \vec{t}_2 + A_{SI} (\vec{s}_1 \cdot \vec{s}_2) (\vec{t}_1 \cdot \vec{t}_2)] \quad (6.20)$$

is the crucial exchange term first proposed by Lichtenberg [332]. \vec{s}_i and \vec{t}_i are spin and isospin operators, respectively. V_{cont} is the contact term. There is no spin-orbit or tensor interaction in this model. This exchange term was introduced by Lichtenberg as a way to ensure that the $(\mathbf{70}, 1_1^-)$ would emerge to be lighter than the $(\mathbf{70}, 0^+)$ supermultiplet.

The results obtained in the model of Ferretti *et al.* [315] are shown in column six of Tables 14 and 15. In this column, a ‘—’ indicates that such a state cannot exist in the diquark model, whereas a blank indicates that such a state could exist (from a higher oscillator band, for instance), but a prediction has not been made. Comparison of these results with those of columns five and four shows clearly that the diquark model predicts fewer states, as expected, and that there is a very good correspondance between the states predicted and those observed. There are a number of states that have been observed, but which do not exist in the diquark model. However, in all cases, evidence for such states is weak at present.

Extension of this kind of model to baryons containing at least one heavy quark is relatively straightforward, as it simply requires changing the masses of the quarks. If anything, such models, especially the non-relativistic versions, might be expected to work better when at least one of the quarks in the baryon is heavy. In addition, the

Table 16. Predictions for excited Λ baryons from a number of theoretical approaches. Columns one, two and three have the same meaning as in Tables 14 and 15. For column headings for columns four, five, six and seven have the same meaning and the same sources as columns four, five, seven and eight, respectively, of Tables 14 and 15.

J^P	State	PDG Mass Range	QM OGE	QM GBE	RQM	Large N_c	Lattice
$\frac{1}{2}^+$	1116 ^(****)	1114-1116	1115	1136	1108		1279±11
	1600 ^(***)	1560-1700	1680	1625	1677	1630	2170±29
	1810 ^(***)	1750-1850	1830	1799	1747	1742	2195±27
	—	—	1910		1898		2198±32
$\frac{3}{2}^+$	1890 ^(****)	1850-1910	1900		1823	1876	2225±15
	—	—	1960		1952		2287±36
	—	—	1995		2045		2318±36
	—	—	2050		2087		2367±14
$\frac{5}{2}^+$	1820 ^(****)	1815-1825	1890		1834	1816	2228±12
	2110 ^(***)	2090-2140	2035		1999	2104	2390±18
	—	—	2115		2078		2419±15
$\frac{7}{2}^+$	2020 ^(*)	(2000-2130)	2120		2130	2125	2545±14
	—	—	2447		2331	2350	3033±24
$\frac{9}{2}^+$	2350 ^(***)	2340-2370	2423		2340	2355	
	—	—	2518		2479		
$\frac{1}{2}^-$	1405 ^(****)	1404-1406	1550	1556	1524	1407	1709±17
	1670 ^(****)	1660-1680	1615	1682	1630	1667	1776±16
	1800 ^(***)	1720-1850	1675	1778	1816	1806	1847±20
$\frac{3}{2}^-$	1520 ^(****)	1518-1521	1545	1556	1508	1520	1816±12
	1690 ^(****)	1685-1695	1645	1682	1662	1676	1905±13
	—	—	1770		1775	1864	1936±17
	2325 ^(*)	(2305-2375)	2290		1987		2626±31
$\frac{5}{2}^-$	1830 ^(****)	1810-1830	1775	1778	1828	1836	2059±11
	—	—	2180		2080		2571±19
$\frac{7}{2}^-$	2100 ^(****)	2090-2110	2150		2090		2694±16

symmetries expected from effective theories like the heavy quark effective theory may either be used to constrain the model *a priori*, or to check the predictions of the model *a posteriori*. Results from extensions of such quark models to heavy baryons are shown in columns four [333] and five [76] of Tables 19 and 20, as well as column four [333] of Tables 21 and 22. The model of Roberts and Pervin [333] has also been extended to make predictions for the masses and properties of baryons containing two and three heavy quarks. In addition, there are a few subclasses of models that warrant a few words of discussion.

Table 17. Predictions for excited Σ baryons from a number of theoretical approaches. The sources of the numbers are the same as in Table 16.

J^P	State	PDG Mass Range	QM OGE	QM GBE	RQM	Large N_c	Lattice
$\frac{1}{2}^+$	1193 ^(****)	1190-1197	1190	1180	1190		1308 \pm 7
	1660 ^(***)	1630-1690	1720	1616	1760	1660	2270 \pm 14
	1770 ^(*)	(1730-1790)	1915	1911	1947	1776	2251 \pm 24
	1880 ^(**)	(1800-2035)	1970		2009	1810	2258 \pm 16
	—	—	2005		2052	2068	2326 \pm 22
$\frac{3}{2}^+$	1385 ^(****)	1382-1388	1370	1389	1411		1579 \pm 9
	1840 ^(*)	(1725-2125)	1920	1865	1896	1790	2243 \pm 14
	2080 ^(**)	(2040-2120)	1970		1961	2061	2317 \pm 16
	—	—	2010		2011		2366 \pm 13
$\frac{5}{2}^+$	1915 ^(****)	1900-1935	1955		1956	1920	2228 \pm 14
	2070 ^(*)	(2025-2080)	2030		2027	2051	2367 \pm 13
					2071	2478	2437 \pm 14
$\frac{7}{2}^+$	2030 ^(****)	2025-2040	2060		2070	2036	2427 \pm 24
	—	—	2390		2161	2350	2546 \pm 15
	—	—				2482	3021 \pm 25
$\frac{9}{2}^+$						2355	
	—	—	2390			2488	
$\frac{11}{2}^+$						2495	
	—	—	2390				
$\frac{1}{2}^-$	1620 ^(**)	(1600-1645)	1630	1677	1628	1637	1780 \pm 16
	1750 ^(***)	1730-1800	1675	1736	1771	1755	1837 \pm 20
	2000 ^(*)	(1755-2040)	2110	1759	1798		1951 \pm 14
	—	—	1695		2111	1784	2545 \pm 49
$\frac{3}{2}^-$	1580 ^(*)	(1578-1587)	1655	1677	1669		1903 \pm 15
	1670 ^(****)	1665-1685	1750	1736	1771	1667	1948 \pm 14
	—	—	1755	1759	2139	1769	1956 \pm 18
	1940 ^(***)	1900-1950	2120		1798	1847	2667 \pm 25
$\frac{5}{2}^-$	1775 ^(****)	1770-1780	1755	1736	1770	1784	2057 \pm 12
	—	—	2205		2174		2521 \pm 24
$\frac{7}{2}^-$	2100 ^(*)	(2040-2150)	2245		2236		2720 \pm 15

The fundamental tenet of the heavy quark effective theory (HQET) is that a single heavy quark in a hadron acts as a static source of colour. Consequently, the dynamics of the light quarks in the presence of this static colour source are independent of the flavour, spin and other properties of the heavy quark. In the context of quark models, this suggests a departure from the Jacobi coordinates used earlier, in favour of a set of

Table 18. Predictions for Ξ and Ω baryons in a number of theoretical approaches. The sources of the numbers are the same as in Table 16.

Flavor	J^P	State	PDG Mass Range	QM OGE	QM GBE	RQM	Large N_c	Lattice
Ξ	$\frac{1}{2}^+$	1318 ^(****)	1314-1322	1305	1348	1310		1351±9
		—	—	1840	1805	1876	1825	2281±17
	$\frac{3}{2}^+$	1530 ^(****)	1530-1532	1505	1528	1539		1635±8
		—	—	2045		1988	1955	2262±18
	$\frac{5}{2}^+$	—	—	2045		2013	1997	2296±13
		—	—	2165		2141	2181	2428±14
	$\frac{1}{2}^-$	1690 ^(***)	1680-1700	1755		1770	1779	1845±17
		—	—	1810		1922	1927	1875±15
	$\frac{3}{2}^-$	1820 ^(***)	1818-1828	1785	1792	1780	1815	1973±12
		—	—	1880		1870	1980	1998±17
	$\frac{5}{2}^-$	—	—	1900	1881	1955	1974	2127±11
	Ω	$\frac{1}{2}^+$	—	—	2220		2232	
				2255		2256		2449±18
$\frac{3}{2}^+$		1672 ^(****)	1671-1673	1635		1636		1692±7
		—	—	2165		2177	2120	2419±18
$\frac{5}{2}^+$				2280		2253		2486±13
$\frac{1}{2}^-$				1950		1992	2061	2011±23
		—	—	2410		2456		2764±19
$\frac{3}{2}^-$				2000		1976	2100	2104±14
		—	—	2440		2446		2771±27
$\frac{5}{2}^-$				2490		2528		2807±19

coordinates that highlight the special role of the heavy quark. With the heavy quark chosen as quark three, Albertus and collaborators [334] define the set of coordinates

$$\vec{\rho}_1 = \vec{r}_1 - \vec{r}_3, \quad \vec{\rho}_2 = \vec{r}_2 - \vec{r}_3. \quad (6.21)$$

In terms of these, the nonrelativistic kinetic energy of the quarks becomes

$$T = -\frac{\nabla_{\rho_1}^2}{2\mu_1} - \frac{\nabla_{\rho_2}^2}{2\mu_2} - \frac{\nabla_R^2}{2M} - \frac{\nabla_{\rho_1} \cdot \nabla_{\rho_2}}{m_3} + M, \quad (6.22)$$

where $\nabla_{\rho_i} = \frac{\partial}{\partial \rho_i}$ and $\mu_i = (1/m_i + 1/m_3)^{-1}$.

The quark-quark interactions used by these authors are similar in their general structure to those used by other authors, in that there is a confining term (chosen to be logarithmic) and a Coulomb-like term. There is also a ‘contact’ hyperfine term, but no tensor or spin-orbit interactions. These authors also explore the effects of interactions that arise from exchange of pseudoscalar and scalar mesons. They confine their discussion to the lowest-lying, positive parity states. In Tables 19 to 22, the

results obtained by Albertus *et al.* [334] are shown in columns 10, nine, eight and seven respectively.

Table 19. Predictions for Λ_c , Σ_c and Ω_c baryons from a number of theoretical approaches. The numbers in columns four (QM1) and five (QM2) result from ‘conventional’ quark models. Column six is the result of a relativistic model (RQM1) in which there are no excitations between the two light quarks. Column seven results from a relativistic model with instanton forces (RQM2). The numbers in column eight are from a Fadeev study (FD), while those in column nine result from relativistic three-quark equations that include dispersion techniques (RQM3). The numbers in column ten are from a nonrelativistic quark model that include heavy quark symmetry constraints (QM3), and column eleven results from a lattice simulation with 2+1+1 flavours of dynamical quarks.

Flavor	J^P	Expt. Mass	QM1 [333]	QM2 [76]	RQM1 [335]	RQM2 [336]	FD [337]	RQM3 [338] [339, 340]	QM3 [334]	Lattice [341]
Λ_c	$\frac{1}{2}^+$	2286	2268	2265	2297	2272	2292	2284	2296	2291±44
			2791	2775	2772	2769	2669			
	$\frac{3}{2}^+$		2887	2910	2874	2848	2906			
			3073	3035	3262	3100	3061			
	$\frac{5}{2}^+$		2887	2910	2883					
	$\frac{1}{2}^-$	2592	2625	2630	2598	2594	2559	2400		
			2816	2780	3017	2853	2779	2635		
Σ_c	$\frac{3}{2}^-$	2628	2636	2640	2628	2586	2559	2625		
			2830	2840	3034	2874	2779	2630		
	$\frac{5}{2}^-$		2872	2900	3061			2765		
	$\frac{1}{2}^+$	2453	2455	2440	2439	2459	2448	2458	2466	2481±29
			2958	2890	2864	2947	2793			
	$\frac{3}{2}^+$	2518	2519	2495	2518	2539	2505	2516	2548	2559±34
			2995	2985	2912	3010	2825			
Ω_c	$\frac{5}{2}^+$		3003	3065	3001					
	$\frac{1}{2}^-$		2748	2765	2795	2769	2706	2700		
			2768	2770	2805	2817	2791	2915		
	$\frac{3}{2}^-$		2763	2770	2761	2799	2706	2570		
			2776	2805	2799	2815	2791	2570		
	$\frac{5}{2}^-$		2790	2815	2790			2740		
	$\frac{1}{2}^+$	2695	2718		2698	2688	2701	2806	2681	2681±34
Ω_c			3152		3065	3169	3044			
	$\frac{3}{2}^+$	2766	2776		2768	2721	2759	3108	2755	2764±33
			3190		3119		3080			
	$\frac{5}{2}^+$		3196		3218					
	$\frac{1}{2}^-$		2977		3020		2959			
			2990		3025		3029			
	$\frac{3}{2}^-$		2986		2998		2959			
		2994		3026		3029				
$\frac{5}{2}^-$		3014		3022						

6.1.2. Relativistic Equations A number of relativistic treatments of baryons, exist in the literature. Among these are bound-state equations like the Bethe-Salpeter (BS) equation, Dyson-Schwinger (DS) treatments [316], and QCD sum rules. All of these treatments are very technical, so that a full description is well beyond the scope of this review article. However, the salient points of one of these approaches are presented here.

Table 20. Predictions for Λ_b , Σ_b and Ω_b baryons from a number of theoretical approaches. The lattice numbers are from a quenched simulation, and only the statistical uncertainties are shown. The numbers in columns four (QM1) and five (QM2) result from ‘conventional’ quark models. Column six is the result of a relativistic model (RQM1) in which there are no excitations between the two light quarks. Column seven results from a Fadeev study (FD), while column eight results from relativistic three-quark equations that include dispersion techniques (RQM2). The numbers in column nine are from a nonrelativistic quark model that include heavy quark symmetry constraints (QM3). Column ten results from a quenched lattice simulation.

Flavor	J^P	Expt. Mass	QM1 [333]	QM2 [76]	RQM1 [335]	FD [337]	RQM2 [338] [339, 340]	QM3 [334]	Lattice [342]	
Λ_b	$\frac{1}{2}^+$	5619	5612	5585	5622	5624	5624	5643	5679±71	
	$\frac{3}{2}^+$		6181	6145	6189	6246				
				6401		6540				
	$\frac{5}{2}^+$		6183	6165	6548					
	$\frac{1}{2}^-$		5912	5939	5912	5930	5890			
				6180	5780	6328	5853			
$\frac{3}{2}^-$		5920	5941	5920	5947	5890				
			6191	5840	6337	5874				
$\frac{5}{2}^-$			6206	6205	6421					
Σ_b	$\frac{1}{2}^+$	5811	5833	5795	5805	5789	5808	5851	5887±49	
	$\frac{3}{2}^+$	5832	5858	5805	5834	5844	5829	5882	5909±47	
	$\frac{1}{2}^-$		6099	6070	6108	6039				
	$\frac{3}{2}^-$		6101	6070	6076	6039				
Ω_b	$\frac{1}{2}^+$	6071	6081		6065	6037	6120	6033	6048±33	
	$\frac{3}{2}^+$		6102		6088	6090	6220	6063	6069±34	
	$\frac{1}{2}^-$		6301		6352	6278				
	$\frac{3}{2}^-$		6304		6330	6278				

The starting point in the BS approach is the six-point Green’s function (or three-fermion propagator) for three interacting fermions. This is the vacuum expectation value of the time-ordered product of three fermion field operators Ψ^i and their adjoints $\bar{\Psi}^i$:

$$G_{a_1 a_2 a_3; a'_1 a'_2 a'_3}(x_1, x_2, x_3; x'_1, x'_2, x'_3) := - \langle 0 | T \Psi_{a_1}^1(x_1) \Psi_{a_2}^2(x_2) \Psi_{a_3}^3(x_3) \bar{\Psi}_{a'_1}^1(x'_1) \bar{\Psi}_{a'_2}^2(x'_2) \bar{\Psi}_{a'_3}^3(x'_3) | 0 \rangle. \quad (6.23)$$

Here $|0\rangle$ is the physical vacuum, T is the time ordering operator and the a_i denote combined Dirac, colour and flavour indices. The integral equation that is obtained for the full three-fermion propagator is shown diagrammatically in Figure 26, and is written symbolically as

$$G = G_0 - iG_0 K G. \quad (6.24)$$

In this equation, G is the full propagator, G_0 is the propagator with no interactions

Table 21. Predictions for Ξ_c baryons from a number of theoretical approaches. The numbers in column three are from a conventional quark model (QM1). Those in column four result from a relativistic model with no excitations between the light quarks (RQM1), while those in column five are from a relativistic model in which all excitations are allowed (RQM2). Column six results from a Fadeev study (FD), while column seven results from relativistic three-quark equations that include dispersion techniques (RQM3). Column eight is from a nonrelativistic model with heavy quark symmetry constraints (QM2), and column nine is from a lattice simulation with 2+1+1 dynamical fermions.

J^P	Expt. mass	QM1 [333]	RQM1 [335]	RQM2 [336]	FD [337]	RQM3 [338] [339, 340]	QM2 [334]	Lattice [341]
$\frac{1}{2}^+$	2467	2466	2481	2469	2496	2467	2474	2439±39
	2576	2594	2578	2595	2574	2565	2578	2568±28
$\frac{3}{2}^+$	2646	2649	2654	2651	2633	2725	2655	2655±28
		3012	3030		2951			
$\frac{5}{2}^+$		3004	3042					
$\frac{1}{2}^-$	2789	2773	2801	2769	2749			
	2816?	2855	2928		2829			
$\frac{3}{2}^-$	2816?	2783	2820	2771	2749			
		2866	2900		2829			
$\frac{5}{2}^-$		2989	2921					

Table 22. Predictions for Ξ_b baryons from a number of theoretical approaches. The numbers in column three are from a conventional quark model (QM1). Those in column four result from a relativistic model with no excitations between the light quarks (RQM1). Column five results from a Fadeev study (FD), while column six results from relativistic three-quark equations that include dispersion techniques (RQM2). Column seven is from a nonrelativistic model with heavy quark symmetry constraints (QM2), and column eight is from a quenched lattice simulation, and only the statistical uncertainties are shown.

J^P	Expt. mass	QM1 [333]	RQM1 [335]	FD [337]	RQM2 [338] [339, 340]	QM2 [334]	Lattice [342]
$\frac{1}{2}^+$	5788	5806	5812	5825	5761	5808	5795±53
	5945?	5970	5806	5937	6007	5825	5968±39
$\frac{3}{2}^+$	5945?	5980	5963	5967	6066	5975	5989±39
$\frac{1}{2}^-$		6090	6119	6076			
$\frac{3}{2}^-$		6093	6130	6076			

between the quarks, and K is the sum of the full two-particle and three-particle irreducible kernels. There is a similar integral equation for the full propagator of each quark, as well as for the kernel itself. Baryon resonances are extracted as poles in the full three-particle propagator. We note here, however, that not only is the formalism very

technical, but obtaining solutions is also very challenging. More details of this formalism can be found, for instance, in the work by Löring and collaborators [317, 318, 319]. These authors used a linear confining potential with instanton-induced forces. A non-relativistic reduction of this force has the form

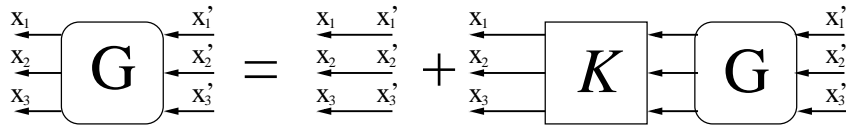
$$V_{\text{instanton}}^{\text{NR}}(\vec{x}_i - \vec{x}_j) \approx -4\mathcal{P}_{S_{ij}=0}^s \otimes (g_{nn}\mathcal{P}_A^{\mathcal{F}}(nn) + g_{ns}\mathcal{P}_A^{\mathcal{F}}(ns)) \delta^{(3)}(\vec{x}_i - \vec{x}_j), \quad (6.25)$$

where

$$\mathcal{P}_{S_{ij}=0}^s = \frac{1}{4}(\mathbf{1} \otimes \mathbf{1} - \vec{\sigma} \cdot \vec{\sigma}) \quad (6.26)$$

is the projector on quark pairs with $S_{ij} = 0$, and $\mathcal{P}_A^{\mathcal{F}}(nn)$ and $\mathcal{P}_A^{\mathcal{F}}(ns)$ denote the flavour projectors on antisymmetric nonstrange (nn) and nonstrange-strange (ns) quark pairs, respectively. g_{nn} and g_{ns} are coupling constants. Since this force acts only on flavour-antisymmetric quark pairs, it does not contribute to the spectrum of Δ resonances. However, it plays a role in the spectrum of nucleons and other states that are not fully symmetric in flavour. This is in marked contrast to the one-gluon or one-Goldstone-boson induced spin-dependent forces, which affect the spectra of both nucleons and Δ s. Further details of this calculation and others like it are beyond the scope of this manuscript.

Figure 26. Diagrammatic representation of the integral equation for the three-fermion propagator.



The results obtained in the relativistic model described above are shown in column seven of Tables 14, 15 and 18, and column six of Tables 16 and 17. This model has also been extended to treat charmed baryons [336] and the results are shown in column seven of Table 19 and column five of Table 21.

The BS formalism can be simplified somewhat when one or more of the quarks in a baryon is heavy. In the approach used by Ebert and collaborators [335], the relativistic three-body problem is reduced to a sequence of relativistic two-body problems. This is accomplished in a quasipotential approach by approximating the heavy baryon as a light diquark composed of the two light quarks that interact with each other, with a heavy quark interacting with the diquark. The diquark wave function, Ψ_d , and the baryon wave function, Ψ_B , each satisfies a quasipotential equation of the Schrödinger type

$$\left(\frac{b^2(M)}{2\mu_R} - \frac{p^2}{2\mu_R} \right) \Psi_{d,B}(\vec{p}) = \int \frac{d^3q}{(2\pi)^3} V(\vec{p}, \vec{q}; M) \Psi_{d,B}(\vec{q}), \quad (6.27)$$

where the relativistic reduced mass is

$$\mu_R = \frac{M^4 - (m_1^2 - m_2^2)^2}{4M^3}, \quad (6.28)$$

and E_1 , E_2 are given by

$$E_1 = \frac{M^2 - m_1^2 + m_2^2}{2M}, \quad E_2 = \frac{M^2 - m_1^2 + m_2^2}{2M}. \quad (6.29)$$

The bound state mass M (of the diquark or the baryon) is the sum of E_1 and E_2 . m_1 and m_2 are the masses of the two quarks in the diquark, or the mass of the diquark and the heavy quark in the baryon, and \vec{p} is their relative momentum. In the centre of mass, the relative momentum squared on shell is

$$b^2(M) = \frac{\lambda(M^2, m_1^2, m_2^2)}{4M^2}, \quad (6.30)$$

where $\lambda(a, b, c)$ is the Källén function.

The kernel $V(\vec{p}, \vec{q}; M)$ is the quasipotential operator of the quark-quark or quark-diquark interaction. Both interactions include scalar and vector confinement components, as well as an interaction arising from gluon exchange. In addition, the quarks have an anomalous chromomagnetic dipole moment. The diquarks are either scalar diquarks (with total quark spin zero) or axial-vector diquarks. In the work of Ebert *et al.* [335], no radial or orbital excitations are allowed in the light diquarks, and this has a significant effect on the spectrum they predict.

This quasipotential treatment has also been applied to baryons with two heavy quarks. In this case, the diquark is composed of the two heavy quarks that interact with each other, and the light quark interacts with the diquark. Unlike the light diquark, radial and orbital excitations are allowed in the heavy diquark, in this particular model. The interactions between the heavy quarks have the same character, namely, vector and scalar confinement and spin-dependent interactions arising from gluon exchange, but the spatial dependences of the interactions are different from those between light quarks.

The results obtained in this model for baryons containing a single heavy quark are shown in column six of Tables 19 and 20, and column four of Tables 21 and 22. The effects of the diquark approximation employed by these authors is seen in the masses of some of the Λ_c and Λ_b states shown in Tables 19 and 20. The second $\frac{3}{2}^+$, $\frac{1}{2}^-$ and $\frac{3}{2}^-$ states, as well as the only $\frac{5}{2}^-$ state shown, are significantly heavier than the corresponding states obtained in other approaches. This is because in the other approaches, the states shown include excitations of the diquark: the Ebert model assumes that states with such excitations lie much higher in mass.

6.1.3. Large N_c It was first noted by 't Hooft [343] that many features of QCD become easier to understand if the gauge group is changed from $SU(3)$ to $SU(N_c)$, in the limit $N_c \rightarrow \infty$. With this gauge group, colour-singlet mesons are still made from a quark and an antiquark, but a baryon requires N_c quarks. Thus, the mass of the baryon grows with N_c . Although $N_c \rightarrow \infty$ would appear to have little to do with the physical world, this limit provides an organization scheme in which operators and processes can be treated with '1/ N_c counting rules'. The physical limit of $N_c = 3$ is then taken, and this counting scheme works remarkably well in that limit.

Large- N_c baryon representations contain all spin and isospin representations (J, I) that are consistent with a given value of K [344], where

$$\vec{K} = \vec{J} + \vec{I}. \quad (6.31)$$

For the physical case of N_c odd, the lowest allowed baryon angular momentum is $J = 1/2$. The irreducible representation with $K = 0$ corresponds to the infinite tower of (J, I) states

$$\left(\frac{1}{2}, \frac{1}{2}\right), \left(\frac{3}{2}, \frac{3}{2}\right), \left(\frac{5}{2}, \frac{5}{2}\right), \dots \quad (6.32)$$

The irreducible representation with $K = 1/2$ corresponds to the tower

$$\left(\frac{1}{2}, 0\right), \left(\frac{1}{2}, 1\right), \left(\frac{3}{2}, 1\right), \left(\frac{3}{2}, 2\right), \left(\frac{5}{2}, 2\right), \left(\frac{5}{2}, 3\right), \dots \quad (6.33)$$

The irreducible representation with $K = 1$ corresponds to the tower

$$\begin{aligned} &\left(\frac{1}{2}, \frac{1}{2}\right), \left(\frac{1}{2}, \frac{3}{2}\right), \left(\frac{3}{2}, \frac{1}{2}\right), \left(\frac{3}{2}, \frac{3}{2}\right), \left(\frac{3}{2}, \frac{5}{2}\right), \left(\frac{5}{2}, \frac{3}{2}\right), \\ &\left(\frac{5}{2}, \frac{5}{2}\right), \left(\frac{5}{2}, \frac{7}{2}\right), \dots \end{aligned} \quad (6.34)$$

The irreducible representation with $K = 3/2$ corresponds to the tower

$$\left(\frac{1}{2}, 1\right), \left(\frac{1}{2}, 2\right), \left(\frac{3}{2}, 0\right), \left(\frac{3}{2}, 1\right), \left(\frac{3}{2}, 2\right), \left(\frac{3}{2}, 3\right), \dots \quad (6.35)$$

If the quantum number K is related to the number of strange quarks in a baryon by $K = N_s/2$, then the low-spin states in each tower have the correct spin, isospin and strangeness to be identified with the spin- $\frac{1}{2}$ octet and spin- $\frac{3}{2}$ decuplet. The $K = 0$ tower contains the strangeness-0 baryons, the nucleon, $(\frac{1}{2}, \frac{1}{2})$ and Δ , $(\frac{3}{2}, \frac{3}{2})$. The $K = \frac{1}{2}$ tower contains the strangeness -1 baryons Λ $(\frac{1}{2}, 0)$, Σ $(\frac{1}{2}, 1)$ and Σ^* $(\frac{3}{2}, 1)$. Similarly, the $K = 1$ tower contains the strangeness -2 baryons Ξ $(\frac{1}{2}, \frac{1}{2})$ and Ξ^* $(\frac{3}{2}, \frac{1}{2})$, while the $K = \frac{3}{2}$ tower contains the Ω^- $(\frac{3}{2}, 0)$.

Implementation of an analysis of baryons in the framework of the $1/N_c$ expansion requires the establishment of the counting rules associated with the different operators needed in the theory. This is most easily done in the limit where the quark masses are large enough that a non-relativistic picture becomes reliable. Since the $1/N_c$ counting is largely unaffected by the quark masses, the counting rules established should also hold when the current masses are small. Using this approach, Witten [345, 346, 347] showed that baryon masses are proportional to N_c , but that their sizes are only affected by corrections $\mathcal{O}(1/N_c)$. Thus, baryons are compact systems, allowing for rigorous usage of the effective potential approach à la Hartree.

As with the conventional quark model, the colour wave function of a baryon is completely antisymmetric, which means that the rest of the wave function must be completely symmetric in identical quarks. A convenient basis is furnished by using wave functions factorized into a spatial part and a spin-flavour part, summed over permutations. The spin-flavour wave functions belong to the irreducible representations

of $SU(2N_f)$ when N_f flavours with degenerate or nearly-degenerate masses are considered. Such wave functions therefore also belong to irreducible representations of the permutation group of the N_c quark indices. In a Hartree picture, the spatial wave function takes the form of a product of N_c one-quark wave functions. In the large N_c limit, ground state baryons have wave functions of the form [322]

$$\Psi_{\xi_1, \dots, \xi_{N_c}}^{GS}(x_1, \dots, x_{N_c}) = \chi_{\xi_1, \dots, \xi_{N_c}}^S \prod_{i=1}^{N_c} \phi(x_i), \quad (6.36)$$

where the one-quark spatial wave function $\phi(x)$ is an S -wave.

Excited baryons result from exciting one or more quarks, leaving a core of quarks in their ground states. A quark in the core has, up to corrections proportional to $1/N_c$, the same wave function as a quark in the ground state baryons. To date, only excited states with a single excited quark have been discussed in detail, but the generalization to two or more excited quarks can be carried out easily. The wave functions with one excited quark are of two types, namely symmetric (S) and mixed-symmetric (MS) in spin flavour. They take the form

$$\begin{aligned} \Psi_{\xi_1, \dots, \xi_{N_c}}^S(x_1, \dots, x_{N_c}) &= \frac{1}{\sqrt{N_c}} \chi_{\xi_1, \dots, \xi_{N_c}}^S \sum_{i=1}^{N_c} \phi(x_1) \dots \phi'(x_i) \dots \phi(x_{N_c}), \\ \Psi_{\xi_1, \dots, \xi_{N_c}}^{MS}(x_1, \dots, x_{N_c}) &= \frac{1}{\sqrt{N_c}(N_c-1)!} \sum_{\sigma} \chi_{\xi_{\sigma_1}, \dots, \xi_{\sigma_{N_c}}}^{MS} \phi(x_{\sigma_1}) \dots \\ &\quad \times \phi(x_{\sigma_{N_c-1}}) \phi'(x_{\sigma_{N_c}}), \end{aligned} \quad (6.37)$$

where $\phi'^{(x)}$ is the excited quark wave function, taken to be orthonormal to the ground state wave function $\phi(x)$. The label σ indicates the permutation: the sum in the second equation is over all possible permutations of the quarks. The generalization to states with more than one excited quark can be easily carried out.

It must be noted that these wave functions do not treat the centre-of-mass motion properly. The effects introduced by this deficiency are generally subleading in $1/N_c$ and should not affect the power countings addressed so far in this approach. Nevertheless there exists the possibility of modification to countings that are suppressed solely on the grounds of orthonormality of the single-quark wave functions used, when the centre-of-mass motion is properly treated.

With three flavours of quark, baryons are classified into $SU(6)$ multiplets. This group has 35 generators, $\{S_i, T_a, G_{ia}\}$, with $i = 1, 2, 3$ and $a = 1, \dots, 8$. The first three are the $SU(2)$ generators of spin, the second eight are the generators of flavour $SU(3)$, and the last 24 are identified as the components of an octet of axial-vector currents in the limit of zero momentum transfer. In a nonrelativistic picture, these generators are expressed in terms of the quark fields as

$$S_i = q^\dagger \frac{\sigma_i}{2} q, \quad T_a = q^\dagger \frac{\lambda_a}{2} q, \quad G_{ia} = q^\dagger \frac{\sigma_i \lambda_a}{4} q, \quad (6.38)$$

with the Gell-Mann matrices normalized to give $Tr[\lambda_a \lambda_b] = 2\delta_{ab}$.

The mass operator in the large N_c limit can be expressed as a linear combination of composite operators sorted according to their order in $1/N_c$. A basis of such operators can be constructed using the $O(3) \otimes SU(6)$ generators, with a distinction drawn between operators that act on quarks in the core, denoted $\{S_i^c, T_a^c, G_{ia}^c\}$, and those that act on the excited quark (in the case of excited baryons), denoted $\{s_i, t_a, g_{ia}\}$. Operators are also classified as n -body operators. The mass operators must be rotationally invariant, parity and time-reversal even and isospin symmetric. A generic n -body mass operator has the general structure

$$O^{(n)} = \frac{1}{N_c^{n-1}} O_\ell O_q O_c, \quad (6.39)$$

where the factors O_ℓ , O_q and O_c can be expressed in terms of products of generators of orbital angular momentum (ℓ_i), spin flavour of the excited quark (s_i, t_a and g_{ia}), and spin-flavour of the core (S_i^c, T_a^c and G_{ia}^c). The explicit $1/N_c$ factors originate in the $n - 1$ gluon exchanges required to give an n -body operator. For a given $O(3) \otimes SU(6)$ multiplet, the coefficients associated with each operator are obtained by fitting to the empirical masses of the states in the multiplet.

To a first approximation, the main features of the spectrum can be described by taking into account a few operators. These are the $\mathcal{O}(N_c)$ spin-flavour singlet operator that essentially counts the number of quarks in the baryon. The strangeness operator appears at $\mathcal{O}(N_c^0 m_s)$, and counts the number of strange quarks in the baryon. The hyperfine operator appears at $\mathcal{O}(1/N_c)$. For a few multiplets, the hyperfine $SU(3)$ breaking $\mathcal{O}(m_s/N_c)$ operator $S_i G_{i8} - \frac{1}{2\sqrt{3}} S_i S_i$ is necessary for achieving a consistent fit. Other operators play smaller roles.

By considering the leading operators as described above, mass formulae can be written for the states of a particular multiplet. For instance, for the ground state $(56, 0_0^+)$, the mass formula obtained is

$$M_{\text{GS}} = N_c c_1 \mathbb{1} + \frac{1}{N_c} C_{\text{HF}} \left(S^2 - \frac{3}{4} N_c \right) - c_S \mathcal{S} + \frac{1}{N_c} c_4 \left(I^2 - S^2 - \frac{1}{4} \mathcal{S}^2 \right), \quad (6.40)$$

where S is the spin of the baryon, I is its isospin and \mathcal{S} is the strangeness operator. The expressions for the masses of excited multiplets have similar forms, perhaps with contributions from additional operators.

The values obtained for the coefficient c_1 for the various multiplets can be fit by the form [348]

$$(3c_1)^2 = 1.179 \pm 0.003 + (1.05 \pm 0.01)\ell \quad (6.41)$$

for the $(56, \ell)$ multiplets, and

$$(3c_1)^2 = 1.34 \pm 0.02 + (1.18 \pm 0.02)\ell \quad (6.42)$$

for the $(70, \ell)$ multiplets. Thus, the leading contributions to the masses are consistent with linear Regge trajectories.

Operators that contain T_a and/or G_{ia} correspond to changes of flavour in the quarks, and may be interpreted in terms of meson exchanges. In most calculations in the large N_c

approach, there is no mixing among the multiplets of $SU(6) \times O(3)$. There is therefore also no mixing of different orbital angular components in the states. For instance, the ground-state nucleon is completely devoid of any D -wave component. More recent work has included such contributions to the masses and wave functions. They appear at different orders in the $\frac{1}{N_c}$ expansion, depending on the specific $SU(6) \otimes O(3)$ multiplets being considered.

For baryons containing one or more heavy quarks, simply extending the spin-flavour symmetry group from $SU(6)$ to include the heavier flavours of quark ($SU(8)$ for the inclusion of charm quarks, for instance) is not appropriate, as this symmetry is so badly broken. Instead, the spin-flavour symmetry group is expanded to $SU(6) \otimes SU(2)_c \otimes SU(2)_b$. There is therefore a separate spin symmetry for each heavy flavour. As far as can be determined, such an approach is yet to be applied to excited heavy baryons.

The results from the large N_c treatment of baryons are shown in Tables 14 to 18 from a number of authors. For the nucleons and Δ resonances, Tables 14 and 15, respectively, the numbers are shown in column eight. For the Λ and Σ states in Tables 16 and 17, respectively, they are shown in column seven. For the Ξ and Ω states, the number are shown in column eight of Table 18. In this approach, fits are carried out for baryons in a particular $(SU(6) \otimes O(3))$ multiplet. Masses of the $(56, 2^+)$ and the $(70, 1^-)$ are from the work by Goity and collaborators, while those for the $(70, 0^+)$, $(70, 2^+)$ and $(56, 4^+)$ are from the work by Matagne and Stancu [326, 349]. The masses for radially excited states of the $(56, 0^{+'})$ are taken from [350].

6.2. Lattice

Lattice QCD is a discretized version of QCD [351, 352]. The path integral over fields at infinitely many Minkowski space-time points is approximated by a finite number of points in a Euclidean space lattice with periodic boundary conditions. The finite lattice spacing provides an automatic ultraviolet cut-off, while the finite box-size provides an infrared cut-off, and it is crucial that any physics extracted from this technique not be affected by these cut-offs. Any results obtained on the lattice must be extrapolated to the physical limit of infinite box size and zero lattice spacing.

At present, lattice simulations are the only *ab initio* treatment of QCD in the non-perturbative regime. Advances in computer capabilities and improvements in calculational techniques have made it possible for ever more precise, unquenched extractions of hadron properties, at more and more realistic quark masses. An observable corresponding to the vacuum expectation value of an operator (\mathcal{O}) may be written

$$\langle \mathcal{O} \rangle = \frac{1}{\mathcal{Z}} \int [dU] [d\psi] [d\bar{\psi}] e^{-S_F(U, \psi, \bar{\psi}) - S_G(U)} \mathcal{O}(U, \psi, \bar{\psi}), \quad (6.43)$$

where

$$\mathcal{Z} = \int [dU] [d\psi] [d\bar{\psi}] e^{-S_F(U, \psi, \bar{\psi}) - S_G(U)}. \quad (6.44)$$

S_G is the gauge action and $S_F = \bar{\psi}M\psi$ is the fermion action with Dirac operator M . A particle of interest is created by constructing an operator with the appropriate quantum numbers. For the nucleon, for example, one possible choice is

$$\chi_N(x) = \epsilon^{abc} (u^{T,a}(x)C\gamma_5d^b(x)) u^c(x), \quad (6.45)$$

where u , d are the spinors for the u and d quark, respectively. Note that all three quarks reside at the same lattice point.

For a baryon created at a specific space-time point $y = (\vec{y}, 0)$ and annihilated at point $x = (\vec{x}, t)$, the Euclidean two-point function is

$$C^{(2)}(x, y) = \frac{1}{\mathcal{Z}} \int [dU] [d\psi] [d\bar{\psi}] e^{-S(U, \psi, \bar{\psi})} \bar{\chi}_N(x) \chi_N(y). \quad (6.46)$$

When t is large enough, the lowest-energy state dominates, and its mass can be obtained by fitting the correlator to an exponential as

$$C^{(2)}(t) \approx Ae^{-mt}. \quad (6.47)$$

Obtaining the spectrum of excited states on the lattice requires overcoming a number of challenges. First, excited-state contributions to the correlation functions decay faster than those of the ground state. Thus, at large times, the signals for excited states are swamped by signals for lower-energy states. This can be mitigated by the use of anisotropic lattices that have a finer spacing in the Euclidean time dimension than in the space dimensions. A larger basis of independent operators that allow maximum overlap with high-spin operators is also needed. Since rotational symmetry is lost on the lattice, irreducible representations of the cubic group must be used. For a chosen parity, there are two two-dimensional irreducible representations G_1 and G_2 , and one four-dimensional irreducible representation H . G_1 contains $J = \frac{1}{2}, \frac{7}{2}, \frac{9}{2}, \frac{11}{2}, \dots$, G_2 contains $J = \frac{3}{2}, \frac{5}{2}, \frac{7}{2}, \frac{9}{2}, \dots$, and H contains $J = \frac{5}{2}, \frac{7}{2}, \frac{11}{2}, \dots$. The continuum-limit angular momenta J of lattice states are identified by examining patterns of degeneracies among the different irreducible representations.

In addition to the challenges discussed briefly above, some lattice simulations are carried out with light quark-masses that lead to pions that are significantly heavier than the physical pion. For instance, the results of Edwards *et al.* [329, 330, 331] are obtained using pion masses of 524 MeV, 444 MeV and 396 MeV. For many collaborations, significant effort is placed on extrapolating the results to the physical pion mass, using techniques taken from chiral perturbation theory. Furthermore, there is the question of quenched vs unquenched simulations. For quenched calculations, quark-pair creation is forbidden, which affects the values of properties extracted. More realistic, unquenched calculations, however, are very expensive computationally. Nevertheless there has been some progress in this area. In addition, calculations with lighter quark masses come with another set of complications that stem from the resonant nature of the states being treated and the existence of nearby thresholds. It then becomes necessary to include multi-particle states in lattice simulations in order to extract the properties of the states of interest. For a discussion of this and other challenges inherent in lattice computations, see reference [352].

There are a number of lattice simulations of light baryons. Some of the more recent studies include chiral extrapolations to the physical mass of the pion, and others start with pion masses that are quite light [353]. However, to date, we know of a single collaboration that has yet examined states with $J \geq \frac{3}{2}$, and these are the results that are shown in Tables 14 to 18. For baryons composed only of u , d and s quarks, lattice results for the masses are shown in the last column of Tables 14 to 18. The results shown in those tables are from the work of Edwards and collaborators [329, 330, 331], who use improved gauge and fermion actions with 2+1 dynamical flavours. For charmed baryons, Tables 19 and 21, the lattice results are taken from the work by Briceño *et al.* [341], who use 2+1+1 flavours of dynamical quarks. For b -flavoured baryons, the results are taken from the work of Ali Khan *et al.* [342], whose calculation is a quenched one.

6.3. Other Approaches

There are a number of other approaches to baryon spectroscopy that cannot be treated in any depth in this manuscript, but which warrant a brief mention.

6.3.1. Effective Field Theories Traditionally, effective field theories have little to say about excited hadrons. The quintessential example is chiral perturbation theory, in which an expansion parameter that is small compared with Λ_{QCD} is needed. Since baryonic excitation energies are typically of the same order as Λ_{QCD} , there is no easy way to include more than one resonance in such a theory, or predict the mass differences between them. In the case of baryons containing a single heavy quark, however, the expansion parameter is the inverse mass of the heavy quark [354]. In the limit of an infinitely massive quark, all baryonic mass differences are small compared with the mass of the heavy quark, and a limited number of predictions can be made.

When one of the quarks in a baryon is very heavy ($m_Q \gg \Lambda_{\text{QCD}}$), that quark acts like a static source of colour around which the light quarks and gluons move. The spin of the heavy quark decouples from the light degrees of freedom. Consequently, states in the spectrum are arranged in nearly degenerate doublets: when the light degrees of freedom have total angular momentum and parity j^P , the possible baryons have total angular momentum $J = j \pm \frac{1}{2}$ and parity P . Since these two states are almost degenerate, the doublet is denoted $((j - \frac{1}{2})^P, (j + \frac{1}{2})^P)$. The exception occurs when $j = 0$, leading to a singlet with $J = \frac{1}{2}$.

Since the mass difference between the states of a doublet arises from the chromomagnetic interaction with the heavy quark, the effective theory that has been developed predicts that this splitting is inversely proportional to the mass of the heavy quark. If the charm and beauty quarks are treated as heavy, this implies that mass splittings within multiplets of b -flavoured baryons can be predicted once the analogous splittings within the corresponding multiplets of c -flavoured baryons are known. Furthermore, since the dynamics of the light quarks and gluons are completely

insensitive to the flavour of the heavy quark, mass differences between multiplets should also be independent of the flavour of heavy quark. This means, for instance, that the mass difference between the spin-averaged mass of the $(\frac{1}{2}^-, \frac{3}{2}^-)$ and the spin averaged mass of the ground-state $(\frac{1}{2}^+, \frac{3}{2}^+)$ should be the same for the Σ_c and the Σ_b , modulo $1/m_b$ and $1/m_c$ corrections.

The heavy quark expansion (expansion of the QCD Lagrangian in powers of $1/m_Q$) has been combined with other approaches, such as quark models and QCD sum rules, to simplify the formalisms, or to try to enhance the predictive power. On its own, this expansion can only be used in the ways already described.

6.3.2. Bag Models The bag model was originally designed to describe the confinement of quarks and gluons inside hadrons. In the original formulation, the bag is a spherical cavity with rigid walls, and the quarks move freely within the cavity. Each quark satisfies the Dirac equation for a free particle, subject to the boundary condition of a confining bag. Many variants have been proposed, including deformed bags, cloudy bags, bags with partially restored chiral symmetry, etc. In the early work of Donoghue *et al.* [355], the mass of the baryon is written

$$E(R) = \sum_i N_i (m_i^2 + x^2/R^2)^{1/2} - \frac{Z_0}{R} + B \frac{4\pi R^3}{3}, \quad (6.48)$$

where R is the radius of the bag, N_i is the number of quarks of type i and x is the quark momentum in units of $1/R$. The last term is a phenomenological bag pressure added to keep the bag from expanding to infinite radius. Equilibrium arises when $E(R)$ is minimized. Chromoelectric and chromomagnetic corrections can then be included in $E(R)$.

One challenge experienced with the bag model was the existence of a number of spurious excitations connected with the motion of the centre of mass of the system. This has been dealt with for ground state baryons, but becomes increasingly challenging for higher excitations. This is one of the main reasons why bag models have not been applied to highly excited states in the baryon spectrum. When one of the quarks in the baryon is heavy, it is treated as being anchored at the centre of the bag, with the light quarks in motion around it, but the challenge of isolating the centre-of-mass motion remains.

6.3.3. QCD Sum Rules As with lattice simulations and relativistic bound-state equations, the starting point for sum-rule calculations of baryon spectra is a correlation function

$$\Pi(q) = i \int d^4x e^{iq \cdot x} \langle 0 | T [B(x) \bar{B}(0)] | 0 \rangle, \quad (6.49)$$

where B is the interpolating field for a spin- $\frac{1}{2}$ baryon. This approach thus has the same starting point as that of the relativistic bound-state equations, and of the lattice simulations. As the angular momentum of the baryon increases, the form of the

correlation function becomes more complicated. For $J = -\frac{3}{2}$, the correlation function is [356]

$$\Pi_{\mu\nu}(q) = i \int d^4x e^{iq \cdot x} \langle 0 | T [B_\mu(x) \overline{B}_\nu(0)] | 0 \rangle, \quad (6.50)$$

where B_μ is the vector-spinor that represents a particle with spin $\frac{3}{2}$.

For the spin- $\frac{1}{2}$ baryon, the most general form for the correlation function is

$$\Pi(q) = \Pi_1(q^2) + \not{q} \Pi_2(q^2), \quad (6.51)$$

and a sum rule can be written for each of the Π_i . For the spin- $\frac{3}{2}$ case, the correlator is a tensor of rank two that can be constructed from the momentum p , the metric tensor and Dirac γ matrices. It takes the form

$$\begin{aligned} \Pi_{\mu\nu}(p) = & \lambda_{3/2}^2 \left\{ -g_{\mu\nu} \not{p} + \frac{1}{3} \gamma_\mu \gamma_\nu \not{p} - \frac{1}{3} (\gamma_\mu p_\nu - \gamma_\nu p_\mu) + \frac{2}{3} \frac{p_\mu p_\nu}{M_{3/2}^2} \not{p} \right. \\ & \left. \pm M_{3/2} \left[g_{\mu\nu} - \frac{1}{3} \gamma_\mu \gamma_\nu + \frac{1}{3M_{3/2}^2} (\gamma_\mu p_\nu - \gamma_\nu p_\mu) \not{p} - \frac{2}{3} \frac{p_\mu p_\nu}{M_{3/2}^2} \right] \right\} \\ & + \dots \end{aligned} \quad (6.52)$$

where the contributions from the spin- $\frac{1}{2}$ sector of the vector-spinor, as well as of other spin- $\frac{3}{2}$ resonances, are denoted by ‘...’ in the equation above.

The correlation for a particular spin is calculated in two ways. In the hadronic representation, a complete set of baryon states with the appropriate quantum numbers is inserted into the correlation function. For the spin- $\frac{1}{2}$ correlator, the pole terms of the lowest lying states are obtained as

$$\Pi^\pm(p) = \lambda_+^2 \frac{\not{p} + M_+}{M_+^2 - p^2} + \lambda_-^2 \frac{\not{p} + M_-}{M_-^2 - p^2} + \dots \quad (6.53)$$

On the QCD side, the correlator is calculated using a variety of field theory methods, such as the operator product expansion. Matching both sides, and using a few other mathematical tools (such as Borel transforms) allows the extraction of baryon masses.

Because the correlators for higher-spin states become increasingly complicated, this method has not been applied to states with spin beyond $\frac{3}{2}$, to the best of our knowledge. However, they have been applied to obtain a variety of properties of baryons, none of which are discussed in this manuscript.

6.3.4. Dynamical Generation A number of authors have examined the properties of a few baryons using chiral dynamics. They find that a number of states are ‘dynamically-generated’ states. That is, they arise as result of the strong interaction (chiral dynamics) between baryons and mesons, and manifest themselves as poles in the scattering amplitude [357]. This approach has been used to describe properties of scattering amplitudes in the neighbourhood of the dynamically generated states, but it has not been used to predict where such states should lie.

6.3.5. Parity Doublets Chiral symmetry predicts that there should exist approximately degenerate hadronic states of opposite parity. Along with the nucleon, there should be a state with the same mass and opposite parity. There is a very simple interpretation to this prediction. In the chiral limit, in which the pion is massless, a state containing a nucleon and a pion at rest has the same mass as a state with a single nucleon, but the two states have opposite parity. More recently, the interpretation is that there should be approximately degenerate states in the baryon spectrum, for instance, that have the same total angular momentum and opposite parity. It has been argued that the presence of such doublets is consistent with the restoration of chiral symmetry high in the baryon spectrum [358].

Löring *et al.* [318] have noted that, in their model, approximate parity doublets arise from the dynamics of the 't Hooft force that they use, with no explicit influence from chiral symmetry. In other models, such as that of Capstick and Isgur [76], pairs of approximately degenerate states with opposite parity abound, even though that model was constructed with no reference to chiral symmetry. In order to more firmly establish the idea of chiral doublets, there need to be predictions of ratios of decay amplitudes, for instance, for the states assigned to a particular doublet.

6.3.6. Holography A recent approach to quantum field theory is that has garnered some interest is the so-called AdS/CFT correspondence (Anti de Sitter/Conformal Field Theory), which establishes a duality between string theories defined on the five-dimensional AdS space-time and conformal field theories in physical space-time [359]. The strong coupling is assumed to be approximately constant in an appropriate range of momentum transfer, and that the quark masses can be neglected. With these assumptions, QCD becomes a nearly conformal field theory and the AdS/CFT correspondence can be applied. The hadron spectrum and strong interaction dynamics can then be calculated from a holographic dual string theory defined on the five-dimensional AdS space. A very useful summary of the calculation methodology and the results obtained is presented in the review by Klempt and Richard [4].

7. Discussion and Open Questions

One of the important questions to be addressed is that of the relevant degrees of freedom in a baryon. Does a baryon consist of three quarks, a quark and a diquark, or does it even have a very different, more complex structure. A better understanding of the properties of the known resonances and an improved mapping of the baryon spectra will help elucidate this question. Recent photoproduction experiments in the light-baryon sector that aim at finding new or undiscovered states have yielded a number of candidates, but none of these is yet without doubt. It is worth pointing out again that, unlike for heavy baryons, the confirmation of a new light-baryon state is more challenging since the discovery is not inferred from a direct observation.

7.1. Heavy-Quark Baryons

A glance at Tables 14 to 22 reveals that, among the light baryons, all of the theoretical approaches we have discussed in Section 6 lead to rather similar results. In the heavy sector, the predictions of the diquark model show more striking differences from the three-quark model. In the model of Ebert *et al.* [335], the lack of excitations in the diquark means that there is a single negative-parity $\frac{1}{2}^-$ state along with a single $\frac{3}{2}^-$ Λ_Q in the region of low-lying excitations. These two states form an HQET $(\frac{1}{2}^-, \frac{3}{2}^-)$ doublet. The second $\frac{1}{2}^-$ state in this model is 417 MeV heavier than the first, whereas the mass difference is between 150 and 250 MeV in other models. Similarly, there are two $\frac{1}{2}^-$ and two $\frac{3}{2}^-$ Σ_Q along with a single $\frac{5}{2}^-$ state. These form a $(\frac{1}{2}^-, \frac{3}{2}^-)$ doublet, a $(\frac{3}{2}^-, \frac{5}{2}^-)$ doublet and a $(\frac{1}{2}^-)$ singlet. In models in which all three quarks can be excited, there are three $\frac{1}{2}^-$ states, three $\frac{3}{2}^-$ states and a single $\frac{5}{2}^-$, in each isospin sector, all within 250 MeV of each other (in the mass range 2600 to 2890 MeV for the Λ_c and 2750 to 2880 MeV for the Σ_c). In each sector, these seven states constitute a $(\frac{1}{2}^-)$ singlet, two $(\frac{1}{2}^-, \frac{3}{2}^-)$ doublets, and a $(\frac{3}{2}^-, \frac{5}{2}^-)$ doublet, although spin-dependent forces induce some mixing among states with the same J^P . In the limit in which the mass of the quark becomes infinitely massive, the multiplet structure should be as described. This structure should therefore be more apparent for the b -flavoured baryons than for the charmed ones, and in the model of Roberts and Pervin [333], this is indeed found to be the case. A number of experimentally observed Λ_c states have masses between 2700 and 2900 MeV, but the quantum numbers are unknown. If any of these states are found to have negative parity, it would suggest that the basic hypothesis of the quark-diquark model would not be correct, at least for baryons containing a heavy quark.

Among the heavy baryons, it can be seen that most approaches get the masses of the ground states roughly correct, mainly because these states are often used as input to the fits to the spectra. The details of the inter-quark potential then determines where the excited states lie, and this is where differences in the predictions of the masses emerge. Nevertheless, for the low-lying excitations, most models are quite consistent, often predicting masses within a range of 50 MeV of each other. The same is true of the lattice studies. It should be noted that the lattice predictions for the b -flavoured baryons are from a quenched study, while the results for the c -flavoured baryons are from an unquenched calculation.

A number of the known charmed baryons have been omitted from Tables 19 and 21. This is because for each of these experimental states, there are a number of model candidates that are sufficiently close in mass to make an assignment ambiguous. Two examples are the $\Lambda_c(2880)^+$ and the $\Lambda_c(2940)^+$. The former is close in mass to a $\frac{3}{2}^+$ state with a predicted mass of 2887 MeV in the model by Roberts and Pervin [333], but also to a $\frac{5}{2}^+$ state with the same mass, and a $\frac{5}{2}^-$ state with a predicted mass of 2872 MeV. This is not very different from the other models shown. The state at 2940 MeV could be one of a number of positive-parity excitations. Thus, other information, such as the strong and radiative decay widths of the state, will be needed before a definite assignment can

be made. Among the b -flavoured baryons, the Ξ'_b ground-state doublet is still to be identified experimentally, if the state at 5945 MeV is indeed the $\frac{3}{2}^+$ state. In the Fadeev study of Garcilazo *et al.* for instance [337], the Ξ'_b with $J^P = \frac{1}{2}^+$ is predicted to have a mass of 5937 MeV, in very good agreement with the experimentally known state, and the $\frac{3}{2}^+$ state is predicted to be 30 MeV heavier at 5967 MeV. In Tables 20 and 21, there are experimental states that are included twice, alongside possible model states that they match. These are the $\Xi_c(2816)$ that is close in mass to model states with $J^P = \frac{1}{2}^-$ and $\frac{3}{2}^-$, and the $\Xi_b(5945)$ that could be either the Ξ'_b or the Ξ_b^* .

Examination of the multiplet structure of Figure 2 provides some guidance regarding the states that can be expected. There should be an Ω_c state for every triplet of Σ_c found. There should be a doublet of Ξ_c for every Λ_c , and another doublet for every triplet of Σ_c . Similarly, in the light sector, there should be a doublet of Ξ resonances for each quartet of Δ states, and another doublet for each doublet of nucleons. There should be an Ω for each Δ quartet. There should also be a triplet of Σ states for each nucleon and Δ isospin multiplet, and there should be more Λ states than nucleon doublets.

7.2. Light-Quark Baryons

In the light baryon sector, we first note that the lattice results of Edwards and collaborators [329, 330, 331] are significantly higher than the experimental masses for the nucleons and Δ resonances. This is primarily because the results shown correspond to a pion mass of 396 MeV. There are simulations that have been carried out with lower pion masses, but they have focused on states with $J \leq \frac{3}{2}$ to date. Among the hyperons, the predictions for the ground-state masses improve steadily as the number of strange quarks in the baryon increases. In this study, although the dependence of the results on the pion mass has been examined, no extrapolations to the physical pion mass have been carried out. At present, chiral extrapolations for excited states are not yet very reliable. In this simulation, the ordering of the states is consistent with the conventional quark model, in that the excited $\frac{1}{2}^+$ nucleon is more massive than the $\frac{1}{2}^-$ state. More generally, in all flavour sectors, the lower-lying positive-parity excitations are all more massive than the low-lying negative-parity states. We note, however, that there has been at least one lattice study in which the lowest-lying $\frac{1}{2}^+$ excitation has a mass that is lower than the lowest-lying $\frac{1}{2}^-$ state [360]. A second feature that emerges from this lattice simulation is that the number of lower-lying excitations is consistent with the conventional quark model, not the diquark version. Of course, these results may change significantly as the pion mass decreases toward the physical value. In addition, the present calculation, as well as that of [360], includes only one-particle states. The conclusions about which states are *bona fide* resonances may change when multi-particle states are included.

7.2.1. Multiplet Assignments Tables 23 and 24 show our suggestions for assignments of the known light baryons to the lowest-lying quark model spin-flavour $SU(6) \otimes O(3)$ multiplets. The assignments to the ground-state octet and decuplet of the $(\mathbf{56}, 0_0^+)$

are straightforward and have been discussed in Section 2.1, Table 2. This is the only supermultiplet that is completely filled.

The first excitation band contains one supermultiplet, $(\mathbf{70}, 1_1^-)$, and the states have one unit of orbital angular momentum and negative parity. This leads to a total of five flavour octets from coupling the orbital angular momentum, $L = 1$, with the two possible spins, $S = \frac{1}{2}$ and $S = \frac{3}{2}$. These are a doublet of total angular momentum and parity $(\frac{1}{2}^-, \frac{3}{2}^-)$ (${}^2\mathbf{8}_{\frac{1}{2}^-}$ and ${}^2\mathbf{8}_{\frac{3}{2}^-}$) and a triplet with $J^P = (\frac{1}{2}^-, \frac{3}{2}^-, \frac{5}{2}^-)$ (${}^4\mathbf{8}_{\frac{1}{2}^-}$, ${}^4\mathbf{8}_{\frac{3}{2}^-}$ and ${}^4\mathbf{8}_{\frac{5}{2}^-}$). The notation in parentheses is ${}^{2S+1}\mathbf{D}_{J^P}$ to denote the multiplets. Here S is the total spin of the three quarks in the baryon, \mathbf{D} denotes the SU(3) flavour multiplet to which it belongs, and J^P are the total angular momentum and the parity. There will also be multiplets ${}^2\mathbf{10}_{\frac{1}{2}^-}$, ${}^2\mathbf{10}_{\frac{3}{2}^-}$, ${}^2\mathbf{1}_{\frac{1}{2}^-}$ and ${}^2\mathbf{1}_{\frac{3}{2}^-}$. The $N(1535)\frac{1}{2}^-$ and $N(1520)\frac{3}{2}^-$ are members of the ${}^2\mathbf{8}_{J^-}$ doublet (with $J = \frac{1}{2}$ or $\frac{3}{2}$), and $N(1650)\frac{1}{2}^-$, $N(1700)\frac{3}{2}^-$ and $N(1675)\frac{5}{2}^-$ belong to the ${}^4\mathbf{8}_{J^-}$ triplet. $\Lambda(1670)\frac{1}{2}^-$ and $\Lambda(1690)\frac{3}{2}^-$ can be identified as members of the ${}^2\mathbf{8}_{J^-}$ doublet, while two members of the ${}^4\mathbf{8}_{J^-}$ triplet, $\Lambda(1800)\frac{1}{2}^-$ and $\Lambda(1830)\frac{5}{2}^-$ can be identified, with the third member, the state with $J^P = \frac{3}{2}^-$, missing or undiscovered. The assignments for the Σ and Ξ hyperons are more difficult because they can be members of either flavour octets or flavour decuplets. Moreover, quantum numbers for most of the few Ξ resonances known have not been measured. Only the $\Xi(1820)$ is listed with $J^P = \frac{3}{2}^-$ in the RPP [1], and there is evidence that the $\Xi(1690)$ has $J^P = \frac{1}{2}^-$ [37]. Assignments for excited Σ states remain educated guesses. In [4, 361], the authors suggest that $\Sigma(1620)\frac{1}{2}^-$ and $\Sigma(1670)\frac{3}{2}^-$ belong to the ${}^2\mathbf{8}_{J^-}$ doublet, with $\Sigma(1750)\frac{1}{2}^-$, $\Sigma(1775)\frac{5}{2}^-$ and a missing the $\Sigma(?)\frac{3}{2}^-$ belonging to the ${}^4\mathbf{8}_{J^-}$ triplet. We have included these states in Table 23. In [260], $\Sigma(1620)\frac{1}{2}^-$ was assigned to the ${}^4\mathbf{8}_{J^-}$ triplet and the $(**)$ state, $\Sigma(1560)?^?$, to the ${}^2\mathbf{8}_{J^-}$ doublet ($?^?$ indicates that the total angular momentum and the parity of the state are not known). However, as discussed in Section 5.2, the low-mass of $\Sigma(1560)?^?$ raises serious doubts about its existence.

We assign $\Lambda(1405)\frac{1}{2}^-$ and $\Lambda(1520)\frac{3}{2}^-$ to the ${}^2\mathbf{1}_{J^-}$ doublet, a classification not questioned in the literature. $\Delta(1620)\frac{1}{2}^-$ and $\Delta(1700)\frac{3}{2}^-$ belong to the ${}^2\mathbf{10}_{J^-}$. $\Sigma(1940)\frac{3}{2}^-$ could be a member of the ${}^2\mathbf{8}_{J^-}$ with $J = \frac{3}{2}$, but its high mass makes an assignment to the third excitation band more likely. We therefore consider the two Σ states to be missing. Quantum numbers for excited Ω states are unknown and we do not assign them to any of the multiplets.

The second excitation band contains several positive-parity supermultiplets. These are the first radial excitation of the ground-state octet and decuplet, $(\mathbf{56}, 0_2^+)$, along with multiplets in which either of the oscillators is excited with two units of orbital angular momentum, $(\mathbf{56}, 2_2^+)$, or where each oscillator carries one unit of orbital angular momentum and these couple to give $L = 0, 1, 2$. These states sit in the three multiplets $(\mathbf{70}, 0_2^+)$, $(\mathbf{20}, 1_2^+)$, and $(\mathbf{70}, 2_2^+)$. The $\mathbf{20}$ does not contain a decuplet (Equation (2.6)) and is therefore not listed in Table 24. The $(\mathbf{56}, 0_2^+)$ comprises a radially excited ${}^2\mathbf{8}_{\frac{1}{2}^+}$ and ${}^4\mathbf{10}_{\frac{3}{2}^+}$ multiplets. The spin-flavour momentum multiplets of the $(\mathbf{70}, 0_2^+)$ consist of ${}^2\mathbf{10}_{\frac{1}{2}^+}$, ${}^2\mathbf{8}_{\frac{1}{2}^+}$, ${}^2\mathbf{1}_{\frac{1}{2}^+}$ and ${}^4\mathbf{8}_{\frac{3}{2}^+}$. The $(\mathbf{56}, 2_2^+)$ contains ${}^4\mathbf{10}_{J^+}$, with $J^P = (\frac{1}{2}^+, \frac{3}{2}^+, \frac{5}{2}^+, \frac{7}{2}^+)$

and ${}^2\mathbf{8}_{J^+}$ with $J^P = (\frac{3}{2}^+, \frac{5}{2}^+)$. In the $(\mathbf{70}, 2_2^+)$, the spin-flavour multiplets consist of ${}^4\mathbf{8}_{J^+}$ with $J^P = (\frac{1}{2}^+, \frac{3}{2}^+, \frac{5}{2}^+, \frac{7}{2}^+)$, as well as ${}^2\mathbf{8}_{J^+}$, ${}^2\mathbf{10}_{J^+}$ and ${}^2\mathbf{1}_{J^+}$, each with $J^P = (\frac{3}{2}^+, \frac{5}{2}^+)$.

The ${}^2\mathbf{8}_{\frac{1}{2}^+}$ multiplet of the $(\mathbf{56}, 0_2^+)$ includes the states $N(1440)_{\frac{1}{2}^+}$, $\Lambda(1600)_{\frac{1}{2}^+}$, and $\Sigma(1660)_{\frac{1}{2}^+}$, while the $\Delta(1600)_{\frac{3}{2}^+}$ resonance is a member of the ${}^4\mathbf{10}_{\frac{3}{2}^+}$. The ${}^2\mathbf{8}_{\frac{1}{2}^+}$ spin-flavour multiplet of the $(\mathbf{70}, 0_2^+)$ contains $N(1710)$, $\Lambda(1810)$, and presumably $(*)\Sigma(1770)$. The Λ state may also be the ${}^2\mathbf{1}_{\frac{1}{2}^+}$ state. Evidence for the ${}^2\mathbf{10}_{\frac{1}{2}^+}$ members of the $(\mathbf{70}, 0_2^+)$ is poor. These could be $(*)\Delta(1750)$ and $(**) \Sigma(1880)$, but the latter state could also be a member of the ${}^2\mathbf{8}_{\frac{1}{2}^+}$. However, its mass makes a decuplet assignment more likely, and the $\Sigma(1770)_{\frac{1}{2}^+}$ has already been assigned as a ${}^2\mathbf{8}_{\frac{1}{2}^+}$ state in this supermultiplet.

For the members of the $(\mathbf{56}, 2_2^+)$ we suggest $(N(1720)_{\frac{3}{2}^+}, N(1680)_{\frac{5}{2}^+})$, $(\Lambda(1890)_{\frac{3}{2}^+}, \Lambda(1820)_{\frac{5}{2}^+})$, and $((*)\Sigma(1840)_{\frac{3}{2}^+}, \Sigma(1915)_{\frac{5}{2}^+})$. These assignments are speculative and all these states could also be assigned to the ${}^2\mathbf{8}_{J^+}$ in the $(\mathbf{70}, 2_2^+)$ (Table 23). The masses of the Σ states are too low to make them likely ${}^2\mathbf{10}_{J^+}$ members. The group of Δ s below 2 GeV, $\Delta(1910)$, $\Delta(1920)$, $\Delta(1905)$, and $\Delta(1910)$, with $J = \frac{1}{2}, \frac{3}{2}, \frac{5}{2}, \frac{7}{2}$, respectively, are ideal candidates for the ${}^4\mathbf{10}_{J^+}$. The corresponding Σ resonances are missing.

The $(\mathbf{70}, 2_2^+)$ multiplet contains ${}^4\mathbf{8}_{J^+}$, ${}^2\mathbf{8}_{J^+}$, ${}^2\mathbf{10}_{J^+}$ and ${}^2\mathbf{1}_{J^+}$. Assuming the existence of the new nucleon resonances listed in the RPP [1], we assign $(**) N(1860)_{\frac{5}{2}^+}$ to ${}^2\mathbf{8}_{J^+}$ with the $J = \frac{3}{2}$ state missing, and the four states, $(**) N(1880)_{\frac{1}{2}^+}$, $N(1900)_{\frac{3}{2}^+}$, $(**) N(2000)_{\frac{5}{2}^+}$, and $(**) N(1990)_{\frac{7}{2}^+}$ to the ${}^4\mathbf{8}_{J^+}$. The two Λ s, $\Lambda(2110)_{\frac{5}{2}^+}$ and $(*)\Lambda(2020)_{\frac{7}{2}^+}$ are also likely members of this spin-flavour multiplet, with two Λ members missing. The assignment of the $\Lambda(2110)$ is not certain, as it could also be the $J = \frac{5}{2}$ ${}^2\mathbf{1}_{J^+}$ state. The corresponding Σ resonances are expected with similar masses and the three states, $(**) \Sigma(2080)_{\frac{3}{2}^+}$, $(*)\Sigma(2070)_{\frac{5}{2}^+}$, and $\Sigma(2030)_{\frac{7}{2}^+}$ are ideal candidates with the $J = \frac{1}{2}$ state missing. However, the assignment of the Σ states is also ambiguous since they can be members of the ${}^4\mathbf{10}_{J^+}$ in the $(\mathbf{56}, 2_2^+)$ supermultiplet (this is the assignment made in the large N_c calculation, and in [4]). We finally assign $(*) N(2100)_{\frac{1}{2}^+}$ and $(*) N(2040)_{\frac{3}{2}^+}$ to the ${}^2\mathbf{8}_{J^+}$ in the $(\mathbf{20}, 1_2^+)$ supermultiplet but evidence for these states is poor. The ${}^4\mathbf{1}_{J^+}$ of the $(\mathbf{20}, 1_2^+)$ with $J^P = (\frac{1}{2}^+, \frac{3}{2}^+, \frac{5}{2}^+)$ are all missing.

In the higher excitation bands the number of multiplets increases substantially and the classification of resonances is very ambiguous. We refer to our assignments in Tables 23 and 24. We assign the two new, lower-mass nucleon resonances listed in the RPP [1], namely $(**) N(1895)_{\frac{1}{2}^-}$ and $(**) N(1875)_{\frac{3}{2}^-}$, to the $(\mathbf{56}, 1_3^-)$ with $S = \frac{1}{2}$ in the third excitation band. The likely partners of these states are the group of three Δ s, $(**) \Delta(1900)$, $(**) \Delta(1940)$, and $\Delta(1930)$ with $J = \frac{1}{2}^-, \frac{3}{2}^-, \frac{5}{2}^-$, respectively. Some of the higher-spin Δ resonances find clear assignments but all partners are missing.

The evidence for many states is still weak and the assignments of the known states to multiplets is certainly ambiguous. The ground-state octet and decuplet are completely filled. In the first excitation band with negative parity, the octet multiplet with $S = \frac{3}{2}$

Table 23. (Colour online) Tentative assignments of the known light baryons to the lowest-lying $SU(6) \otimes O(3)$ singlets and octets. States marked with \dagger are merely educated guesses because the evidence for their existence is poor or they can be assigned to other multiplets. A hyphen indicates that the state does not exist, an empty box that it is missing. For the higher multiplets, Nx gives the number of expected states.

N	(D, L_N^P)	S	J^P	Octet Members				Singlets
0	$(56, 0_0^+)$	$\frac{1}{2}$	$\frac{1}{2}^+$	$N(939)$	$\Lambda(1116)$	$\Sigma(1193)$	$\Xi(1318)$	–
1	$(70, 1_1^-)$	$\frac{1}{2}$	$\frac{1}{2}^-$	$N(1535)$	$\Lambda(1670)$	$\Sigma(1620)$	$\Xi(1690)$	$\Lambda(1405)$
			$\frac{3}{2}^-$	$N(1520)$	$\Lambda(1690)$	$\Sigma(1670)$	$\Xi(1820)$	$\Lambda(1520)$
			$\frac{5}{2}^-$	$N(1650)$	$\Lambda(1800)$	$\Sigma(1750)$		–
			$\frac{7}{2}^-$	$N(1700)$				–
			$\frac{9}{2}^-$	$N(1675)$	$\Lambda(1830)$	$\Sigma(1775)$		–
2	$(56, 0_2^+)$	$\frac{1}{2}$	$\frac{1}{2}^+$	$N(1440)$	$\Lambda(1600)$	$\Sigma(1660)$		–
	$\frac{3}{2}^+$		$N(1710)$	$\Lambda(1810)^\dagger$	$\Sigma(1770)^\dagger$		–	
	$(70, 0_2^+)$	$\frac{3}{2}$	$\frac{1}{2}^+$					–
	$\frac{3}{2}^+$						–	
	$(56, 2_2^+)$	$\frac{1}{2}$	$\frac{1}{2}^+$	$N(1720)^\dagger$	$\Lambda(1890)^\dagger$	$\Sigma(1840)^\dagger$		–
			$\frac{3}{2}^+$	$N(1680)$	$\Lambda(1820)^\dagger$	$\Sigma(1915)^\dagger$		–
	$(70, 2_2^+)$	$\frac{1}{2}$	$\frac{1}{2}^+$	$N(1860)$				–
			$\frac{3}{2}^+$	$N(1880)$				–
			$\frac{5}{2}^+$	$N(1900)^\dagger$		$\Sigma(2080)^\dagger$		–
			$\frac{7}{2}^+$	$N(2000)$	$\Lambda(2110)^\dagger$	$\Sigma(2070)^\dagger$		–
$\frac{9}{2}^+$			$N(1990)$	$\Lambda(2020)$	$\Sigma(2030)^\dagger$		–	
$\frac{11}{2}^+$			$N(2100)^\dagger$				–	
$(20, 1_2^+)$	$\frac{1}{2}$	$\frac{1}{2}^+$	$N(2040)^\dagger$	–	–	–	–	
3	$(56, 1_3^-)$	$\frac{1}{2}$	$\frac{1}{2}^-$	$N(1895)^\dagger$				–
			$\frac{3}{2}^-$	$N(1875)^\dagger$		$\Sigma(1940)^\dagger$		–
	$(70, 1_3^-)$	$\frac{1}{2}$	$\frac{1}{2}^-$	5 x				–
			$\frac{3}{2}^-$	5 x				–
	$(70, 1_3^-)$	$\frac{1}{2}$	$\frac{1}{2}^-$	2 x				–
	$\frac{3}{2}^-$		6 x				–	
	$(20, 1_3^-)$	$\frac{1}{2}$	$\frac{1}{2}^-$	2 x				–
	$\frac{3}{2}^-$		2 x				–	
$(56, 3_3^-)$	$\frac{1}{2}$	$\frac{1}{2}^-$	$N(2190)^\dagger$	$\Lambda(2100)^\dagger$			–	
$\frac{3}{2}^-$		$N(2250)$				–		
$(70, 3_3^-)$	$\frac{1}{2}$	$\frac{1}{2}^-$	2 x				–	
$(20, 3_3^-)$	$\frac{1}{2}$	$\frac{1}{2}^-$					–	
4			$\frac{9}{2}^+$	$N(2220)$	$\Lambda(2350)$			
5			$\frac{11}{2}^-$	$N(2600)$				

Table 24. (Colour online) Tentative assignments of the known light baryons to the lowest-lying $SU(6) \otimes O(3)$ decuplets. States marked with \dagger are merely educated guesses because the evidence for their existence is poor or they can be assigned to other multiplets. A hyphen indicates that the state does not exist, an empty box that it is missing. For the higher multiplets, Nx gives the number of expected states.

N	(D, L_N^P)	Spin, S	J^P	Decuplet Members			
0	$(56, 0_0^+)$	$\frac{3}{2}$	$\frac{3}{2}^+$	$\Delta(1232)$	$\Sigma(1385)$	$\Xi(1530)$	$\Omega(1672)$
1	$(70, 1_1^-)$	$\frac{1}{2}$	$\frac{1}{2}^-$ $\frac{3}{2}^-$	$\Delta(1620)$ $\Delta(1700)$			
2	$(56, 0_2^+)$	$\frac{3}{2}$	$\frac{3}{2}^+$	$\Delta(1600)$	$\Sigma(1880)^\dagger$		
	$(70, 0_2^+)$		$\frac{1}{2}^+$	$\Delta(1750)^\dagger$			
	$(56, 2_2^+)$		$\frac{1}{2}^+$	$\Delta(1910)^\dagger$			
			$\frac{3}{2}^+$	$\Delta(1920)^\dagger$			
			$\frac{5}{2}^+$	$\Delta(1905)$			
		$\frac{7}{2}^+$	$\Delta(1950)$				
	$(70, 2_2^+)$	$\frac{1}{2}$	$\frac{3}{2}^+$ $\frac{5}{2}^+$	$\Delta(2000)$			
3	$(56, 1_3^-)$	$\frac{3}{2}$	$\frac{1}{2}^-$	$\Delta(1900)^\dagger$			
			$\frac{3}{2}^-$	$\Delta(1940)^\dagger$			
			$\frac{5}{2}^-$	$\Delta(1930)^\dagger$			
	$(70, 1_3^-)$	$\frac{1}{2}$		2 x			
			$\frac{1}{2}$	2 x			
			$\frac{1}{2}$	2 x			
$(56, 3_3^-)$	$\frac{3}{2}$		4 x				
$(70, 3_3^-)$		$\frac{1}{2}$	2 x				
4	$(56, 4_4^+)$	$\frac{3}{2}$	$\frac{11}{2}^+$	$\Delta(2420)$			
5			$\frac{13}{2}^-$	$\Delta(2750)$			
6			$\frac{15}{2}^+$	$\Delta(2950)$			

and $J = \frac{3}{2}$ appears to be empty. Some doubt has recently emerged about the existence of the $N(1700)$ as will be discussed briefly in the next section. Looking over Table 23, it is interesting to note that in the second excitation band with positive parity, many multiplets with $J = \frac{3}{2}$ are either completely empty or have many missing members, which puts into question the already poor evidence of the assigned states.

From a theoretical point of view, the only multiplet which is completely inconsistent with the quark-diquark picture discussed in Section 6 is the **20**. The evidence for the two (*) N^* states which we assigned to the $(\mathbf{20}, 1_2^+)$ supermultiplet is weak. If the

evidence for these states grows stronger in the future, the missing states in the table will have to be regarded as simply undiscovered states, not forbidden ones. Therefore, these states spell trouble for diquark models. We also note that the predictions from the diquark model [315] in Table 14 include only one low-mass $\frac{5}{2}^+$ state and no $\frac{7}{2}^+$ state. However, beyond the well-established $N(1680)\frac{5}{2}^+$, two further $N\frac{5}{2}^+$ candidates and one $N\frac{7}{2}^+$ candidate are currently known at and below 2 GeV (Table 9). Solid evidence for these candidates is still missing, but it appears that the dynamics inside of a baryon go beyond the quark-diquark picture.

A comparison of the results from the different models does not indicate that any of the other models is significantly better than any of the others in predicting the masses of the light (or heavy) excited baryons. Apart from the diquark model, all the models predict roughly the same number of states, in roughly the same ordering with some variation in the masses. From the results shown, it is not glaringly obvious that the relativistic models provide a better description of the baryon spectrum than the nonrelativistic ones (or vice versa), for instance. More significant differences between the models will emerge if they are used to examine other properties of the baryons, such as their strong and electromagnetic decay widths.

7.2.2. Does the $N(1700)\frac{3}{2}^-$ really exist? In recent years, some doubts have been raised about the existence of $N(1700)\frac{3}{2}^-$. The various analyses do not agree very well and support has mostly come from the Bonn-Gatchina group. The latest analysis by the SAID group [217] finds no evidence for this resonance. Moreover, the EBAC group reported negative evidence in their latest analysis [223, 225]. It is also interesting to note that the $N(1700)\frac{3}{2}^-$ appears to be the only low-lying, “well established” resonance with $J \leq \frac{3}{2}$ which is not observed by the BES collaboration in J/ψ decays. Interestingly, experimental evidence for the other strange members of the $J^P = \frac{3}{2}^-$ multiplet is also currently non-existent, although all other octets of $(\mathbf{70}, 1_1^-)$ appear to be filled with the exception of the doubly-strange Ξ baryons. All models predict a group of $\frac{3}{2}^-$ baryons with masses around 1700 MeV and the non-observation of these states would pose an interesting challenge for quark models.

7.2.3. Has a second $N(1720)\frac{3}{2}^+$ been discovered? The CLAS collaboration has reported indications for a second nucleon resonance with $J^P = \frac{3}{2}^+$ and a mass of about 1720 MeV [264] based on $\gamma^*p \rightarrow p\pi^+\pi^-$ data [121]. While a second low-mass $\frac{3}{2}^+$ resonance is needed to completely fill the $(\mathbf{70}, 0_2^+)$ and $(\mathbf{56}, 2_2^+)$ supermultiplets of the second excitation band, quark models typically predict a further $\frac{3}{2}^+$ state with a mass about 150-200 MeV higher (Table 14). The new CLAS state requires a large $\Delta\pi$ coupling and a suppressed $N\rho$ coupling, very different from the RPP listings of recent years. An alternative hypothesis is that, the well known $\frac{3}{2}^+$ resonance is much broader than originally thought, with the additional width coming from a large $\Delta\pi$ partial width. The $N(1720)$ Breit-Wigner width reported in the RPP was changed from $\Gamma = 150\text{-}300$ MeV (2010 edition) to $\Gamma = 150\text{-}400$ MeV (2012 edition).

The question of a second $N(1720) \frac{3}{2}^+$ resonance with a mass around 1700 MeV is certainly interesting. If it exists, such a state could be a candidate for a resonance beyond the quark model with structure different from the conventional (qqq) picture. One possibility would be a hybrid baryon.

7.3. Exotic Baryons and the Interpretation of $N(1685)$

The prediction of exotic mesons – states beyond the conventional quark model with three quark degrees of freedom – has inspired the search for hybrid mesons and glueballs for many decades, see e.g. [362] for a very comprehensive review. These states receive strong contributions to their overall quantum numbers from gluonic components and some have J^P assignments which are not allowed for a conventional $q\bar{q}$ system. Candidates have been identified through overpopulation of some conventional quark-model multiplets [363, 364].

Hybrid baryons are also expected to exist, but no candidates for baryonic hybrids currently exist. Some lattice simulations have examined baryon states with significant gluon components in their correlation functions [329] and additional nucleons with $J^P = \frac{1}{2}^+, \frac{3}{2}^+, \frac{5}{2}^+$ and Δ resonances with $J^P = \frac{1}{2}^+, \frac{3}{2}^+$, having significant hybrid components in their wave functions, have resulted from such simulations. For the most part, these have been found to lie above the lowest band of excited, positive-parity, three-quark baryons. However, there are a few instances in which the hybrids penetrate into the band of conventional baryons. In the case of the Λ resonances, there are $\frac{1}{2}^+$ hybrids at 2213 ± 19 MeV and 2452 ± 40 MeV. Among the Σ , the lightest hybrid is again $\frac{1}{2}^+$, and has a mass of 2364 ± 54 MeV. Generally, though, the hybrids do have masses that are significantly larger than the first band of positive-parity excitations, particularly those with higher total angular momenta. We also note that where the hybrids sit in the spectrum is sensitive to the pion mass used. For a pion mass of 524 MeV, none of the hybrid masses fall within the band of conventional positive-parity excitations.

It will be challenging to identify hybrid baryons experimentally as there are no obviously exotic signals as is the case with exotic mesons. Since all J^P can be accessed by conventional three-quark baryons, there are no exotic quantum numbers for exotic baryons. The extraction of helicity amplitudes in electroproduction experiments can help our understanding of the structure of baryon resonances. Recent results from the CLAS collaboration [261] have ruled out the Roper resonance, $N(1440) \frac{1}{2}^+$, as a q^3G hybrid state. Other baryons have received attention owing to their unusual properties and have been interpreted beyond the regular quark model. For example, the nucleon resonance, $N(1535) \frac{1}{2}^-$, has an unusually large coupling to the $N\eta$ decay mode and the hyperon resonance, $\Lambda(1405) \frac{1}{2}^-$, is very low in mass compared to predictions. An interpretation of these states as dynamically-generated resonances has been proposed, e.g. [274, 275, 365, 366, 367].

A different group of exotic baryons are those which are composed of more than three constituent quarks. The idea of such multiquark hadrons is intriguing and was further

nourished in 2003 by the announcement of a pentaquark candidate, the $\Theta(1540)^+$, in photoproduction, see e.g. the review in [368]. The observed candidate triggered much excitement because its mass appeared to be almost exactly as predicted: the chiral soliton model of [369] predicted an antidecuplet of narrow $qqqq\bar{q}$ baryons. The $\Theta(1540)^+$ was initially confirmed by several (low-statistics) experiments but the experimental evidence has mostly died out in recent years. We refer to the literature for a more detailed discussion of this state.

In its latest (2012) edition, the RPP lists a nucleon resonance, $N(1685)$, with unknown quantum numbers and a one-star rating. This new state is associated with a narrow peak discovered in the reaction $\gamma n \rightarrow n\eta$ [164, 166, 370]. While the experimental evidence for this narrow state appears solid, its interpretation as a pentaquark is extremely weak. Other explanations appear more likely and may even rule out the particle as an excited nucleon state. As discussed in Section 5.4.2, an interference effect was proposed involving the two low-lying S_{11} states, $N(1535)\frac{1}{2}^-$ and $N(1650)\frac{1}{2}^-$. Alternatively, a threshold effect has been discussed which explains the observed structure in $n\eta$ by a strong (resonant or non-resonant) $\gamma p \rightarrow p\omega$ coupling in the S_{11} partial wave. The measurement of polarization observables in $\gamma n \rightarrow n\eta$ will help elucidate the origin of this new structure.

7.4. Future Experiments

Baryon spectroscopy remains an active and lively field. Many more results on heavy-flavour baryons can be expected from the LHC experiments and new surprises are just a matter of time. In the light-flavour sector, programs to extract polarization observables in electromagnetically-induced reactions will continue at the ELSA and MAMI facilities. At the time of this writing, the recording of new data at Jefferson Lab has been suspended owing to the energy upgrade of the CEBAF accelerator from 6 to 12 GeV. Data taking will likely resume in 2014/15 and hadron spectroscopy will continue at the GlueX and CLAS12 experiments. The scientific focus of the future excited baryon programs is on the spectroscopy of doubly- and triply-strange baryons, Ξ_s and Ω_s . The properties of these multi-strange states are poorly known as discussed earlier and only the J^P of the $\Xi(1820)\frac{3}{2}^-$ has been (directly) determined experimentally. Future experiments will provide better statistics and improved detector acceptance, which are considered the prime limitations of previous experiments.

The Ξ hyperons have the unique feature of double strangeness: the quark content is ssu and ssd . If the confining potential is independent of quark flavour, the energy of spatial excitations of a given pair of quarks decreases as their reduced mass is increased in many theoretical approaches. This means that the lightest excitations in each partial wave occur between the two strange quarks. In a spectator decay model, such states will not decay to the ground state Ξ and a pion because of orthogonality of the spatial wave functions of the two strange quarks in the excited state and the ground state. This removes the decay channel with the largest phase space for the lightest states in each

partial wave, substantially reducing their widths. Typically, Γ_{Ξ^*} is about 10-20 MeV for the known lower-mass resonances, which is 5-30 times narrower than for N^* , Δ^* , Λ^* , and Σ^* states.

These features, combined with their isospin of $\frac{1}{2}$, render possible the study of the Ξ and its excited states in reactions such as $\gamma p \rightarrow KY^* \rightarrow K(\bar{K}Y)_{\Xi^*}K$, complementary to the challenging study of broad and overlapping N^* states. This reaction will also render possible the study of excited Σ and Λ states [372]. At GSI, the PANDA collaboration has developed plans to study multi-strange hyperons in proton-antiproton annihilations in reactions such as $p\bar{p} \rightarrow \bar{Y}Y^*$. Compared to photoproduction, the associated production of kaons is not required in $p\bar{p}$ reactions and the predicted Ξ and Ω cross sections are large.

It has been well known that rescattering effects play an important role in photoproduction processes. This means that in a particular reaction, the baryon and meson in an intermediate state are not necessarily the same as those in the final state and the reaction can proceed through different resonances. The ideal analysis of experimental data needs to be performed in the framework of a coupled-channel analysis since different channels feed into each other. For the same reason, it is necessary to carry out a combined search for nucleon resonances using both hadronic and photoproduction data. A coupled-channel analysis is theoretically very challenging and has led to the formation of the Excited Baryon Analysis Center (EBAC) at Jefferson Lab. However, challenges also remain on the experimental side since the data on πN and KN reactions is scarce. As discussed in Section 5.1, a fair amount of data is available on $\pi N \rightarrow \pi N$, but statistics for reactions such as $\pi N \rightarrow \pi\pi N$ and $\pi p \rightarrow KY$ are very poor and stem from a few decades ago. New possibilities for studying reactions using hadronic probes are being discussed for the Japan Proton Accelerator Research Complex (J-PARC) in Tokai, Japan.

Acknowledgments

We acknowledge useful discussions with Jose Goity, Jozef Dudek, Robert Edwards, Simon Capstick, Reinhard Beck, Ulrike Thoma, Victor Mokeev, Vitaliy Shklyar, Daniel Mohler and Igor Strakovsky. Special thanks to Jozef Dudek and Robert Edwards for providing the numbers from their simulations. This work was partially supported by the Department of Energy, Office of Nuclear Physics, under contracts DE-AC05-06OR23177 and DE-FG02-92ER40735.

References

- [1] J. Beringer *et al.* [Particle Data Group Collaboration], Phys. Rev. D **86**, 010001 (2012).
- [2] K. Nakamura *et al.* [Particle Data Group Collaboration], J. Phys. GG **37**, 075021 (2010).
- [3] B. T. Meadows, In *Toronto 1980, Proceedings, Baryon 1980*, 283-300.
- [4] E. Klempt and J. -M. Richard, Rev. Mod. Phys. **82**, 1095 (2010).
- [5] A. J. G. Hey and R. L. Kelly, Phys. Rept. **96**, 71 (1983).

- [6] S. Capstick and W. Roberts, *Prog. Part. Nucl. Phys.* **45**, S241 (2000).
- [7] B. Krusche and S. Schadmand, *Prog. Part. Nucl. Phys.* **51**, 399 (2003).
- [8] D. Drechsel and T. Walcher, *Rev. Mod. Phys.* **80**, 731 (2008).
- [9] L. Tiator *et al.*, *Eur. Phys. J. ST* **198**, 141 (2011).
- [10] I. G. Aznauryan and V. D. Burkert, *Prog. Part. Nucl. Phys.* **67**, 1 (2012).
- [11] N. Isgur and M. B. Wise, *Phys. Rev. Lett.* **66**, 1130 (1991).
- [12] R. Aaij *et al.* [LHCb Collaboration], arXiv:1302.1072 [hep-ex].
- [13] R. Aaij *et al.* [LHCb Collaboration], *Phys. Rev. Lett.* **109**, 172003 (2012).
- [14] S. Chatrchyan *et al.* [CMS Collaboration], *Phys. Rev. Lett.* **108**, 252002 (2012).
- [15] M. Mattson *et al.* [SELEX Collaboration], *Phys. Rev. Lett.* **89**, 112001 (2002).
- [16] A. Ocherashvili *et al.* [SELEX Collaboration], *Phys. Lett. B* **628**, 18 (2005).
- [17] S. E. Kopp [CLEO Collaboration], *Nucl. Instrum. Meth. A* **384**, 61 (1996).
- [18] P. Avery *et al.* [CLEO Collaboration], *Phys. Rev. Lett.* **62**, 863 (1989).
- [19] K. W. Edwards *et al.* [CLEO Collaboration], *Phys. Rev. Lett.* **74**, 3331 (1995).
- [20] P. Avery *et al.* [CLEO Collaboration], *Phys. Rev. Lett.* **75**, 4364 (1995).
- [21] L. Gibbons *et al.* [CLEO Collaboration], *Phys. Rev. Lett.* **77**, 810 (1996).
- [22] C. P. Jessop *et al.* [CLEO Collaboration], *Phys. Rev. Lett.* **82**, 492 (1999).
- [23] J. P. Alexander *et al.* [CLEO Collaboration], *Phys. Rev. Lett.* **83**, 3390 (1999).
- [24] D. Cronin-Hennessy *et al.* [CLEO Collaboration], *Phys. Rev. Lett.* **86**, 3730 (2001).
- [25] S. E. Csorna *et al.* [CLEO Collaboration], *Phys. Rev. Lett.* **86**, 4243 (2001).
- [26] M. Artuso *et al.* [CLEO Collaboration], *Phys. Rev. Lett.* **86**, 4479 (2001).
- [27] R. Ammar *et al.* [CLEO Collaboration], *Phys. Rev. Lett.* **86**, 1167 (2001).
- [28] S. B. Athar *et al.* [CLEO Collaboration], *Phys. Rev. D* **71**, 051101 (2005).
- [29] J. P. Alexander *et al.* [CLEO Collaboration], *Phys. Rev. D* **82**, 092002 (2010).
- [30] B. Aubert *et al.* [BABAR Collaboration], *Nucl. Instrum. Meth. A* **479**, 1 (2002).
- [31] B. Aubert *et al.* [BABAR Collaboration], *Phys. Rev. D* **72**, 052006 (2005).
- [32] B. Aubert *et al.* [BABAR Collaboration], *Phys. Rev. Lett.* **97**, 232001 (2006).
- [33] B. Aubert *et al.* [BABAR Collaboration], *Phys. Rev. D* **74**, 011103 (2006).
- [34] B. Aubert *et al.* [BABAR Collaboration], *Phys. Rev. Lett.* **98**, 012001 (2007).
- [35] B. Aubert *et al.* [BABAR Collaboration], *Phys. Rev. D* **77**, 012002 (2008).
- [36] B. Aubert *et al.* [BABAR Collaboration], *Phys. Rev. D* **78**, 112003 (2008).
- [37] B. Aubert *et al.* [BABAR Collaboration], *Phys. Rev. D* **78**, 034008 (2008).
- [38] T. Iijima *et al.* [Belle Collaboration], *Nucl. Instrum. Meth. A* **446**, 75 (2000).
- [39] R. Mizuk *et al.* [Belle Collaboration], *Phys. Rev. Lett.* **94**, 122002 (2005).
- [40] N. Gabyshev *et al.* [Belle Collaboration], *Phys. Rev. Lett.* **97**, 242001 (2006).
- [41] R. Chistov *et al.* [Belle Collaboration], *Phys. Rev. Lett.* **97**, 162001 (2006).
- [42] K. Abe *et al.* [Belle Collaboration], *Phys. Rev. Lett.* **98**, 262001 (2007).
- [43] E. Solovieva *et al.* [Belle Collaboration], *Phys. Lett. B* **672**, 1 (2009).
- [44] T. Lesiak *et al.* [Belle Collaboration], *Phys. Lett. B* **665**, 9 (2008).
- [45] V. M. Abazov *et al.* [D0 Collaboration], *Phys. Rev. Lett.* **94**, 102001 (2005).
- [46] V. M. Abazov *et al.* [D0 Collaboration], *Phys. Rev. Lett.* **99**, 052001 (2007).
- [47] V. M. Abazov *et al.* [D0 Collaboration], *Phys. Rev. Lett.* **99**, 142001 (2007).
- [48] V. M. Abazov *et al.* [D0 Collaboration], *Phys. Rev. Lett.* **99**, 182001 (2007).
- [49] V. M. Abazov *et al.* [D0 Collaboration], *Phys. Rev. Lett.* **101**, 232002 (2008).
- [50] V. M. Abazov *et al.* [D0 Collaboration], *Phys. Rev. D* **84**, 031102 (2011).
- [51] D. Acosta *et al.* [CDF Collaboration], *Phys. Rev. D* **71**, 032001 (2005).
- [52] D. Acosta *et al.* [CDF Collaboration], *Phys. Rev. D* **66**, 112002 (2002).
- [53] D. Acosta *et al.* [CDF Collaboration], *Phys. Rev. D* **72**, 051104 (2005).
- [54] D. Acosta *et al.* [CDF Collaboration], *Phys. Rev. Lett.* **96**, 202001 (2006).
- [55] A. Abulencia *et al.* [CDF Collaboration], *Phys. Rev. Lett.* **98**, 122001 (2007).
- [56] A. Abulencia *et al.* [CDF Collaboration], *Phys. Rev. Lett.* **98**, 122002 (2007).

- [57] T. Aaltonen *et al.* [CDF Collaboration], Phys. Rev. Lett. **99**, 052002 (2007).
- [58] T. Aaltonen *et al.* [CDF Collaboration], Phys. Rev. Lett. **99**, 202001 (2007).
- [59] T. Aaltonen *et al.* [CDF Collaboration], Phys. Rev. D **79**, 032001 (2009).
- [60] T. Aaltonen *et al.* [CDF Collaboration], Phys. Rev. D **80**, 072003 (2009).
- [61] T. Aaltonen *et al.* [CDF Collaboration], Phys. Rev. Lett. **103**, 031801 (2009).
- [62] T. Aaltonen *et al.* [CDF Collaboration], Phys. Rev. Lett. **104**, 102002 (2010).
- [63] T. Aaltonen *et al.* [CDF Collaboration], Phys. Rev. Lett. **107**, 102001 (2011).
- [64] T. Aaltonen *et al.* [CDF Collaboration], Phys. Rev. D **84**, 012003 (2011).
- [65] T. Aaltonen *et al.* [CDF Collaboration], Phys. Rev. D **85**, 092011 (2012).
- [66] A. A. Alves, Jr. *et al.* [LHCb Collaboration], JINST **3**, S08005 (2008).
- [67] S. Chatrchyan *et al.* [CMS Collaboration], JINST **3**, S08004 (2008).
- [68] R. Aaij *et al.* [LHCb Collaboration], Phys. Lett. B **708**, 241 (2012).
- [69] B. Knapp *et al.*, Phys. Rev. Lett. **37**, 882 (1976).
- [70] M. Jezabek *et al.*, Acta Phys. Polon. B **23**, 771 (1992).
- [71] P. L. Frabetti *et al.* [E687 Collaboration], Phys. Rev. Lett. **72**, 961 (1994).
- [72] P. L. Frabetti *et al.* [E687 Collaboration], Phys. Lett. B **365**, 461 (1996).
- [73] H. Albrecht *et al.* [ARGUS Collaboration], Phys. Lett. B **317**, 227 (1993).
- [74] H. Albrecht *et al.* [ARGUS Collaboration], Phys. Lett. B **402**, 207 (1997).
- [75] A. E. Blechman, A. F. Falk, D. Pirjol, J. M. Yelton, Phys. Rev. D **67**, 074033 (2003).
- [76] S. Capstick and N. Isgur, Phys. Rev. D **34**, 2809 (1986).
- [77] H. Y. Cheng and C. K. Chua, Phys. Rev. D **75**, 014006 (2007).
- [78] S. F. Biagi *et al.*, Phys. Lett. B **122**, 455 (1983).
- [79] S. F. Biagi *et al.*, Z. Phys. C **28**, 175 (1985).
- [80] M. I. Adamovich *et al.* [WA89 Collaboration], Phys. Lett. B **358**, 151 (1995).
- [81] P. L. Frabetti *et al.* [E687 Collaboration], Phys. Lett. B **338**, 106 (1994).
- [82] C. Amsler *et al.* [Particle Data Group Collaboration], Phys. Lett. B **667**, 1 (2008).
- [83] G. Bari *et al.*, Nuovo Cim. A **104**, 571 (1991).
- [84] G. Bari *et al.*, Nuovo Cim. A **104**, 1787 (1991).
- [85] D. Buskulic *et al.* [ALEPH Collaboration], Phys. Lett. B **384**, 449 (1996).
- [86] J. L. Rosner, Phys. Rev. D **75**, 013009 (2007).
- [87] P. Abreu *et al.* [DELPHI Collaboration], Z. Phys. C **68**, 541 (1995).
- [88] J. Abdallah *et al.* [DELPHI Collaboration], Eur. Phys. J. C **44**, 299 (2005).
- [89] W. Roberts and T. Oed, Phys. Rev. C **71**, 055201 (2005).
- [90] <http://hepdata.cedar.ac.uk/>.
- [91] <http://gwdac.phys.gwu.edu/>.
- [92] A. Starostin *et al.*, Phys. Rev. C **72**, 015205 (2005).
- [93] H. Denz *et al.*, Phys. Lett. B **633**, 209 (2006).
- [94] R. Meier *et al.*, Phys. Lett. B **588**, 155 (2004).
- [95] J. Breitschopf *et al.*, Phys. Lett. B **639**, 424 (2006).
- [96] I. G. Alekseev *et al.*, Eur. Phys. J. C **45**, 383 (2006).
- [97] I. G. Alekseev *et al.* [ITEP-PNPI Collaboration], Eur. Phys. J. A **39**, 163 (2009).
- [98] A. Mokhtari *et al.*, Phys. Rev. D **35**, 810 (1987).
- [99] C. J. Seftor *et al.*, Phys. Rev. D **39**, 2457 (1989).
- [100] A. Starostin *et al.* [Crystal Ball Collaboration], Phys. Rev. C **64**, 055205 (2001).
- [101] N. G. Kozlenko *et al.*, Phys. Atom. Nucl. **66**, 110 (2003) [Yad. Fiz. **66**, 112 (2003)].
- [102] A. Starostin *et al.* [Crystal Ball Collaboration], Phys. Rev. C **67**, 068201 (2003).
- [103] M. Borgh *et al.* [Crystal Ball Collaboration], Phys. Rev. C **68**, 015206 (2003).
- [104] J. Olmsted *et al.* [Crystal Ball Collaboration], Phys. Lett. B **588**, 29 (2004).
- [105] K. Craig *et al.* [Crystal Ball Collaboration], Phys. Rev. Lett. **91**, 102301 (2003).
- [106] M. E. Sadler *et al.* [Crystal Ball Collaboration], Phys. Rev. C **69**, 055206 (2004).
- [107] S. Prakhov *et al.* [Crystal Ball Collaboration], Phys. Rev. C **69**, 045202 (2004).

- [108] S. Prakhov *et al.* [Crystal Ball Collaboration], Phys. Rev. C **69**, 042202 (2004).
- [109] S. Prakhov *et al.* [Crystal Ball Collaboration], Phys. Rev. C **70**, 034605 (2004).
- [110] S. Prakhov *et al.* [Crystal Ball Collaboration], Phys. Rev. C **72**, 015203 (2005).
- [111] S. Prakhov *et al.*, Phys. Rev. C **80**, 025204 (2009).
- [112] D. Mekterovic *et al.* [Crystal Ball Collaboration], Phys. Rev. C **80**, 055207 (2009).
- [113] G.-F. Chew *et al.*, Phys. Rev. **106**, 1345 (1957).
- [114] G. Knochlein *et al.*, Z. Phys. A **352**, 327 (1995).
- [115] W. T. Chiang and F. Tabakin, Phys. Rev. C **55**, 2054 (1997).
- [116] I. S. Barker *et al.*, Nucl. Phys. B **95**, 347 (1975).
- [117] I. Aznauryan *et al.*, J. Phys. Conf. Ser. **299**, 012008 (2011).
- [118] B. A. Mecking *et al.* [CLAS Collaboration], Nucl. Instrum. Meth. A **503**, 513 (2003).
- [119] R. Thompson *et al.* [CLAS Collaboration], Phys. Rev. Lett. **86**, 1702 (2001).
- [120] K. Joo *et al.* [CLAS Collaboration], Phys. Rev. Lett. **88**, 122001 (2002).
- [121] M. Ripani *et al.* [CLAS Collaboration], Phys. Rev. Lett. **91**, 022002 (2003).
- [122] K. Joo *et al.* [CLAS Collaboration], Phys. Rev. C **68**, 032201 (2003).
- [123] K. Joo *et al.* [CLAS Collaboration], Phys. Rev. C **70**, 042201 (2004).
- [124] H. Egiyan *et al.* [CLAS Collaboration], Phys. Rev. C **73**, 025204 (2006).
- [125] M. Ungaro *et al.* [CLAS Collaboration], Phys. Rev. Lett. **97**, 112003 (2006).
- [126] H. Denizli *et al.* [CLAS Collaboration], Phys. Rev. C **76**, 015204 (2007).
- [127] K. Park *et al.* [CLAS Collaboration], Phys. Rev. C **77**, 015208 (2008).
- [128] A. S. Biselli *et al.* [CLAS Collaboration], Phys. Rev. C **78**, 045204 (2008).
- [129] G. V. Fedotov *et al.* [CLAS Collaboration], Phys. Rev. C **79**, 015204 (2009).
- [130] D. S. Carman *et al.* [CLAS Collaboration], Phys. Rev. C **79**, 065205 (2009).
- [131] K. Park *et al.* [CLAS Collaboration], Eur. Phys. J. A **49**, 16 (2013).
- [132] V. I. Mokeev *et al.* [CLAS Collaboration], Phys. Rev. C **86**, 035203 (2012).
- [133] R. Bradford *et al.* [CLAS Collaboration], Phys. Rev. C **73**, 035202 (2006).
- [134] R. K. Bradford *et al.* [CLAS Collaboration], Phys. Rev. C **75**, 035205 (2007).
- [135] I. Hleiqawi *et al.* [CLAS Collaboration], Phys. Rev. C **75**, 042201 (2007) [Erratum-ibid. C **76**, 039905 (2007)].
- [136] M. Dugger *et al.* [CLAS Collaboration], Phys. Rev. C **76**, 025211 (2007).
- [137] M. Battaglieri *et al.* [CLAS Collaboration], Phys. Rev. Lett. **102**, 102001 (2009).
- [138] M. Battaglieri *et al.* [CLAS Collaboration], Phys. Rev. D **80**, 072005 (2009).
- [139] M. Dugger *et al.* [CLAS Collaboration], Phys. Rev. C **79**, 065206 (2009).
- [140] M. Williams *et al.* [CLAS Collaboration], Phys. Rev. C **80**, 065209 (2009).
- [141] M. Williams *et al.* [CLAS Collaboration], Phys. Rev. C **80**, 065208 (2009).
- [142] M. Williams *et al.* [CLAS Collaboration], Phys. Rev. C **80**, 045213 (2009).
- [143] M. E. McCracken *et al.* [CLAS Collaboration], Phys. Rev. C **81**, 025201 (2010).
- [144] B. Dey *et al.* [CLAS Collaboration], Phys. Rev. C **82**, 025202 (2010).
- [145] O. Bartholomy *et al.* [CB-ELSA Collaboration], Phys. Rev. Lett. **94**, 012003 (2005).
- [146] H. van Pee *et al.* [CB-ELSA Collaboration], Eur. Phys. J. A **31**, 61 (2007).
- [147] V. Crede *et al.* [CB-ELSA Collaboration], Phys. Rev. Lett. **94**, 012004 (2005).
- [148] O. Bartholomy *et al.* [CB-ELSA Collaboration], Eur. Phys. J. A **33**, 133 (2007).
- [149] U. Thoma *et al.* [CB-ELSA Collaboration], Phys. Lett. B **659**, 87 (2008).
- [150] I. Horn *et al.* [CB-ELSA Collaboration], Phys. Rev. Lett. **101**, 202002 (2008).
- [151] I. Horn *et al.* [CB-ELSA Collaboration], Eur. Phys. J. A **38**, 173 (2008).
- [152] J. Junkersfeld *et al.* [CB-ELSA Collaboration], Eur. Phys. J. A **31**, 365 (2007).
- [153] E. Aker *et al.* [Crystal Barrel Collaboration], Nucl. Instrum. Meth. A **321**, 69 (1992).
- [154] D. Elsner *et al.* [CBELSA/TAPS Collaboration], Eur. Phys. J. A **33**, 147 (2007).
- [155] R. Castelijns *et al.* [CBELSA/TAPS Collaboration], Eur. Phys. J. A **35**, 39 (2008).
- [156] F. Klein *et al.* [CBELSA/TAPS Collaboration], Phys. Rev. D **78**, 117101 (2008).
- [157] M. Nanova *et al.* [CBELSA/TAPS Collaboration], Eur. Phys. J. A **35**, 333 (2008).

- [158] D. Elsner *et al.* [CBELSA/TAPS Collaboration], *Eur. Phys. J. A* **39**, 373 (2009).
- [159] E. Gutz *et al.* [CBELSA/TAPS Collaboration], *Phys. Lett. B* **687**, 11 (2010).
- [160] V. Crede *et al.* [CBELSA/TAPS Collaboration], *Phys. Rev. C* **80**, 055202 (2009).
- [161] N. Sparks *et al.* [CBELSA/TAPS Collaboration], *Phys. Rev. C* **81**, 065210 (2010).
- [162] V. Crede *et al.* [CBELSA/TAPS Collaboration], *Phys. Rev. C* **84**, 055203 (2011).
- [163] R. Ewald *et al.* [CBELSA/TAPS Collaboration], *Phys. Lett. B* **713**, 180 (2012).
- [164] I. Jaegle *et al.* [CBELSA/TAPS Collaboration], *Phys. Rev. Lett.* **100**, 252002 (2008).
- [165] I. Jaegle *et al.* [CBELSA/TAPS Collaboration], *Eur. Phys. J. A* **47**, 11 (2011).
- [166] I. Jaegle *et al.* [CBELSA/TAPS Collaboration], *Eur. Phys. J. A* **47**, 89 (2011).
- [167] A. Thiel *et al.* [CBELSA/TAPS Collaboration], *Phys. Rev. Lett.* **109**, 102001 (2012).
- [168] W. J. Schuille *et al.*, *Nucl. Instrum. Meth. A* **344**, 470 (1994).
- [169] M. Q. Tran *et al.* [SAPHIR Collaboration], *Phys. Lett. B* **445**, 20 (1998).
- [170] K. H. Glander *et al.*, *Eur. Phys. J. A* **19**, 251 (2004).
- [171] J. Barth *et al.*, *Eur. Phys. J. A* **17**, 269 (2003).
- [172] J. Barth *et al.*, *Eur. Phys. J. A* **18**, 117 (2003).
- [173] R. Lawall *et al.*, *Eur. Phys. J. A* **24**, 275 (2005).
- [174] C. Wu *et al.*, *Eur. Phys. J. A* **23**, 317 (2005).
- [175] B. Krusche *et al.*, *Phys. Rev. Lett.* **74**, 3736 (1995).
- [176] R. Beck, *Eur. Phys. J. A* **28S1**, 173 (2006).
- [177] M. Weis *et al.* [A1 Collaboration], *Eur. Phys. J. A* **38**, 27 (2008).
- [178] J. Ahrens *et al.* [GDH Collaboration], *Eur. Phys. J. A* **34**, 11 (2007).
- [179] D. Krambrich *et al.* [Crystal Ball at MAMI Collaboration], *Phys. Rev. Lett.* **103**, 052002 (2009).
- [180] E. F. McNicoll *et al.* [Crystal Ball at MAMI Collaboration], *Phys. Rev. C* **82**, 035208 (2010) [Erratum-ibid. *C* **84**, 029901 (2011)].
- [181] V. L. Kashevarov *et al.*, *Phys. Lett. B* **693**, 551 (2010).
- [182] F. Zehr *et al.*, *Eur. Phys. J. A* **48**, 98 (2012).
- [183] V. L. Kashevarov *et al.*, *Phys. Rev. C* **85**, 064610 (2012).
- [184] O. Bartalini *et al.* [GRAAL Collaboration], *Eur. Phys. J. A* **26**, 399 (2005).
- [185] O. Bartalini *et al.* [GRAAL Collaboration], *Eur. Phys. J. A* **33**, 169 (2007).
- [186] F. Renard *et al.* [GRAAL Collaboration], *Phys. Lett. B* **528**, 215 (2002).
- [187] J. Ajaka *et al.*, *Phys. Rev. Lett.* **96**, 132003 (2006).
- [188] Y. Assafiri *et al.*, *Phys. Rev. Lett.* **90**, 222001 (2003).
- [189] J. Ajaka *et al.*, *Phys. Lett. B* **651**, 108 (2007).
- [190] O. Bartalini *et al.* [GRAAL Collaboration], *Phys. Lett. B* **544**, 113 (2002).
- [191] E. Hourany [GRAAL Collaboration], *Nucl. Phys. A* **755**, 447 (2005).
- [192] A. Lleres *et al.*, *Eur. Phys. J. A* **31**, 79 (2007).
- [193] A. Lleres *et al.* [GRAAL Collaboration], *Eur. Phys. J. A* **39**, 149 (2009).
- [194] J. Ajaka *et al.*, *Phys. Rev. Lett.* **100**, 052003 (2008).
- [195] A. Fantini *et al.* [GRAAL Collaboration], *Phys. Rev. C* **78**, 015203 (2008).
- [196] R. Di Salvo *et al.*, *Eur. Phys. J. A* **42**, 151 (2009).
- [197] T. Mibe *et al.* [LEPS Collaboration], *Phys. Rev. Lett.* **95**, 182001 (2005).
- [198] M. Sumihama *et al.* [LEPS Collaboration], *Phys. Rev. C* **73**, 035214 (2006).
- [199] M. Sumihama *et al.* [LEPS Collaboration], *Phys. Rev. C* **80**, 052201 (2009).
- [200] Z. Zhao [BESIII Collaboration], *AIP Conf. Proc.* **1432**, 92 (2012).
- [201] M. Ablikim *et al.* [BESIII Collaboration], *Nucl. Instrum. Meth. A* **614**, 345 (2010).
- [202] J. Z. Bai *et al.* [BES Collaboration], *Phys. Lett. B* **510**, 75 (2001).
- [203] M. Ablikim *et al.* [BES Collaboration], *Phys. Rev. Lett.* **97**, 062001 (2006).
- [204] M. Ablikim *et al.* [BES Collaboration], *Phys. Rev. D* **71**, 072006 (2005).
- [205] M. Ablikim *et al.* [BES Collaboration], *Phys. Rev. D* **74**, 012004 (2006).
- [206] M. Ablikim *et al.* [BES Collaboration], *Phys. Rev. D* **76**, 092003 (2007).
- [207] M. Ablikim *et al.* [BES Collaboration], *Eur. Phys. J. C* **53**, 15 (2008).

- [208] M. Ablikim *et al.* [BES Collaboration], Phys. Rev. D **80**, 052004 (2009).
- [209] Y. Liang [BESIII Collaboration], AIP Conf. Proc. **1432**, 387 (2012).
- [210] M. Ablikim *et al.* [BESIII Collaboration], Phys. Rev. Lett. **110**, 022001 (2013).
- [211] M. Ablikim *et al.* [BES II Collaboration], Chin. Phys. C **36**, 1031 (2012).
- [212] M. E. B. Franklin *et al.*, Phys. Rev. Lett. **51**, 963 (1983).
- [213] S. Ceci *et al.*, Phys. Lett. B **659**, 228 (2008).
- [214] R. L. Workman *et al.*, Phys. Rev. C **79**, 038201 (2009).
- [215] R. A. Arndt *et al.*, Int. J. Mod. Phys. A **18**, 449 (2003).
- [216] R. L. Workman *et al.*, Phys. Rev. C **85**, 025201 (2012).
- [217] R. A. Arndt *et al.*, Phys. Rev. C **74**, 045205 (2006).
- [218] <http://www.kph.uni-mainz.de/MAID/>.
- [219] D. Drechsel *et al.*, Eur. Phys. J. A **34**, 69 (2007).
- [220] T. Mart and A. Sulaksono, Phys. Rev. C **74**, 055203 (2006).
- [221] A. Matsuyama *et al.*, Phys. Rept. **439**, 193 (2007).
- [222] H. Kamano, PoS QNP **2012**, 011 (2012).
- [223] B. Julia-Diaz *et al.*, Phys. Rev. C **76**, 065201 (2007).
- [224] J. Durand *et al.*, Phys. Rev. C **78**, 025204 (2008).
- [225] H. Kamano *et al.*, Phys. Rev. C **79**, 025206 (2009).
- [226] B. Julia-Diaz *et al.*, Phys. Rev. C **77**, 045205 (2008).
- [227] B. Julia-Diaz *et al.*, Phys. Rev. C **80**, 025207 (2009).
- [228] H. Kamano *et al.*, Phys. Rev. C **80**, 065203 (2009).
- [229] T. Sato and T. S. H. Lee, J. Phys. G **36**, 073001 (2009).
- [230] M. Doring *et al.*, Phys. Lett. B **681**, 26 (2009).
- [231] M. Doring *et al.*, Nucl. Phys. A **829**, 170 (2009).
- [232] G. Y. Chen *et al.*, Phys. Rev. C **76**, 035206 (2007).
- [233] S. Sarkar *et al.*, Nucl. Phys. A **750**, 294 (2005) [Erratum-ibid. A **780**, 78 (2006)].
- [234] G. Penner and U. Mosel, Phys. Rev. C **66**, 055211 (2002).
- [235] G. Penner and U. Mosel, Phys. Rev. C **66**, 055212 (2002).
- [236] V. Shklyar *et al.*, Eur. Phys. J. A **21**, 445 (2004).
- [237] V. Shklyar *et al.*, Phys. Rev. C **71**, 055206 (2005) [Erratum-ibid. C **72**, 019903 (2005)].
- [238] V. Shklyar *et al.*, Phys. Rev. C **72**, 015210 (2005).
- [239] R. Shyam *et al.*, Phys. Rev. C **81**, 015204 (2010).
- [240] V. Shklyar *et al.*, Phys. Rev. C **87**, 015201 (2013).
- [241] A. Anisovich *et al.*, Eur. Phys. J. A **24**, 111 (2005).
- [242] A. V. Anisovich and A. V. Sarantsev, Eur. Phys. J. A **30**, 427 (2006).
- [243] A. V. Anisovich *et al.*, Eur. Phys. J. A **44**, 203 (2010).
- [244] A. V. Anisovich *et al.*, Eur. Phys. J. A **47**, 27 (2011).
- [245] A. V. Anisovich *et al.*, Eur. Phys. J. A **47**, 153 (2011).
- [246] <http://pwa.hiskp.uni-bonn.de/>
- [247] A. V. Anisovich *et al.*, Eur. Phys. J. A **48**, 15 (2012).
- [248] M. Clajus and B. M. K. Nefkens, PiN Newslett. **7**, 76 (1992).
- [249] I. G. Alekseev *et al.* [EPECUR Collaboration], arXiv:1204.6433 [hep-ex].
- [250] G. Höhler, *Pion-Nucleon Scattering*, Landoldt-Börnstein Vol. **I/9b2** (1983), edited by H. Schopper, Springer-Verlag.
- [251] R. E. Cutkosky *et al.*, Phys. Rev. D **20**, 2839 (1979).
- [252] A. V. Sarantsev *et al.*, Phys. Lett. B **659**, 94 (2008).
- [253] D. Aston *et al.*, Phys. Lett. B **215**, 799 (1988).
- [254] D. Berley *et al.*, Phys. Rev. Lett. **15**, 641 (1965).
- [255] D. M. Manley *et al.* [Crystal Ball Collaboration], Phys. Rev. Lett. **88**, 012002 (2001).
- [256] R. Koniuk and N. Isgur, Phys. Rev. D **21**, 1868 (1980) [Erratum-ibid. D **23**, 818 (1981)].
- [257] P. Gao *et al.*, Phys. Rev. C **86**, 025201 (2012).

- [258] R. A. Arndt *et al.*, Phys. Rev. C **69**, 035213 (2004).
- [259] B. M. K. Nefkens *et al.* [Crystal Ball Collaboration], nucl-ex/0202007.
- [260] T. Melde *et al.*, Phys. Rev. D **77**, 114002 (2008).
- [261] I. G. Aznauryan *et al.* [CLAS Collaboration], Phys. Rev. C **80**, 055203 (2009).
- [262] S. Fubini *et al.*, Phys. Rev. **111**, 329 (1958).
- [263] D. Drechsel *et al.*, Nucl. Phys. A **645**, 145 (1999).
- [264] V. I. Mokeev *et al.*, Phys. Rev. C **80**, 045212 (2009).
- [265] T. Sato and T. S. H. Lee, Phys. Rev. C **63**, 055201 (2001).
- [266] S. S. Kamalov *et al.*, Phys. Rev. C **64**, 032201 (2001).
- [267] C. Alexandrou *et al.*, Phys. Rev. D **77**, 085012 (2008).
- [268] S. Capstick and B. D. Keister, Phys. Rev. D **51**, 3598 (1995).
- [269] I. G. Aznauryan, Phys. Rev. C **76**, 025212 (2007).
- [270] G. Ramalho *et al.*, Phys. Rev. D **81**, 074020 (2010).
- [271] Z. P. Li, Phys. Rev. D **44**, 2841 (1991).
- [272] Z. P. Li *et al.*, Phys. Rev. D **46**, 70 (1992).
- [273] N. Kaiser *et al.*, Phys. Lett. B **362**, 23 (1995).
- [274] D. Jido *et al.*, Nucl. Phys. A **725**, 181 (2003).
- [275] D. Jido *et al.*, Phys. Rev. C **77**, 065207 (2008).
- [276] K. Helbing, Prog. Part. Nucl. Phys. **57**, 405 (2006).
- [277] S. B. Gerasimov, Conf. Proc. C **690923**, 367 (1969).
- [278] S. D. Drell and A. C. Hearn, Phys. Rev. Lett. **16**, 908 (1966).
- [279] J. Ahrens *et al.* [GDH and A2 Collaboration], Phys. Rev. Lett. **84**, 5950 (2000).
- [280] J. Ahrens *et al.* [GDH and A2 Collaboration], Phys. Rev. Lett. **87**, 022003 (2001).
- [281] J. Ahrens *et al.*, Phys. Rev. Lett. **97**, 202303 (2006).
- [282] H. Dutz *et al.* [GDH Collaboration], Phys. Rev. Lett. **91**, 192001 (2003).
- [283] H. Becks *et al.*, Nucl. Phys. B **60**, 267 (1973).
- [284] W. Brefeld *et al.*, Nucl. Phys. B **100**, 93 (1975).
- [285] D. M. Manley and E. M. Saleski, Phys. Rev. D **45**, 4002 (1992).
- [286] A. Sibirtsev *et al.*, Eur. Phys. J. A **46**, 359 (2010).
- [287] P. J. Bussey *et al.*, Phys. Lett. B **61**, 479 (1976).
- [288] R. Beck, <http://www.slac.stanford.edu/econf/C110613/>.
- [289] A. V. Anisovich *et al.*, Eur. Phys. J. A **41**, 13 (2009).
- [290] V. Shklyar *et al.*, Phys. Lett. B **650**, 172 (2007).
- [291] M. Doring and K. Nakayama, Phys. Lett. B **683**, 145 (2010).
- [292] F. Huang *et al.*, arXiv:1208.2279 [nucl-th].
- [293] T. Corthals *et al.*, Phys. Lett. B **656**, 186 (2007).
- [294] T. Mart and C. Bennhold, Phys. Rev. C **61**, 012201(R) (1999).
- [295] V. A. Nikonov *et al.*, Phys. Lett. B **662**, 245 (2008).
- [296] K. Schilling *et al.*, Nucl. Phys. B **15**, 397 (1970) [Erratum-ibid. B **18**, 332 (1970)].
- [297] Q. Zhao *et al.*, Phys. Rev. C **71**, 054004 (2005).
- [298] B. Dey and C. A. Meyer, AIP Conf. Proc. **1388**, 242 (2011).
- [299] P. Collins *et al.* [CLAS Collaboration], Contribution at the Eleventh Conference on the Intersections of Particle and Nuclear Physics (CIPANP 2012), St. Petersburg, USA (2012).
- [300] A. Fix and H. Arenhovel, Eur. Phys. J. A **25**, 115 (2005).
- [301] L. Roca, Nucl. Phys. A **748**, 192 (2005).
- [302] J. C. Nacher *et al.*, Nucl. Phys. A **695**, 295 (2001).
- [303] A. Fix *et al.*, Phys. Rev. C **82**, 035207 (2010).
- [304] M. Doring *et al.*, Eur. Phys. J. A **46**, 315 (2010).
- [305] V. Crede, AIP Conf. Proc. **1343**, 123 (2011).
- [306] C. Bookwalter, PhD thesis, Florida State University, Tallahassee, Florida (2012).
- [307] J. Z. Bai *et al.* [BES Collaboration], Phys. Rev. D **63**, 032002 (2001).

- [308] M. Ablikim *et al.* [BES Collaboration], Phys. Lett. B **632**, 181 (2006).
- [309] M. Ablikim *et al.* [BES Collaboration], Phys. Lett. B **648**, 149 (2007).
- [310] M. Ablikim *et al.* [BES Collaboration], Phys. Rev. D **78**, 092005 (2008).
- [311] M. Ablikim *et al.* [BESIII Collaboration], Phys. Rev. D **86**, 032014 (2012).
- [312] W. Rarita and J. Schwinger, Phys. Rev. **60**, 61 (1941).
- [313] W. H. Liang *et al.*, J. Phys. G **28**, 333 (2002).
- [314] S. Capstick and W. Roberts, Phys. Rev. D **47**, 1994 (1993).
- [315] J. Ferretti *et al.*, Phys. Rev. C **83**, 065204 (2011).
- [316] See, for example, C. Chen *et al.*, Few Body Syst. **53**, 293 (2012), and references therein.
- [317] U. Loring *et al.*, Eur. Phys. J. A **10**, 309 (2001).
- [318] U. Loring *et al.*, Eur. Phys. J. A **10**, 395 (2001).
- [319] U. Loring *et al.*, Eur. Phys. J. A **10**, 447 (2001).
- [320] J. L. Goity *et al.*, Phys. Rev. D **66**, 114014 (2002).
- [321] J. L. Goity *et al.*, Phys. Lett. B **564**, 83 (2003).
- [322] J. L. Goity, Phys. Atom. Nucl. **68**, 624 (2005) [Yad. Fiz. **68**, 655 (2005)].
- [323] J. L. Goity and N. Matagne, JLAB-THY-08-860.
- [324] C. L. Schat *et al.*, Phys. Rev. Lett. **88**, 102002 (2002).
- [325] C. E. Carlson *et al.*, Phys. Rev. D **59**, 114008 (1999).
- [326] N. Matagne and F. Stancu, Phys. Rev. D **71**, 014010 (2005).
- [327] N. Matagne and F. Stancu, Phys. Rev. D **83**, 056007 (2011).
- [328] N. Matagne and F. Stancu, Phys. Rev. D **85**, 116003 (2012).
- [329] R. G. Edwards *et al.*, Phys. Rev. D **84**, 074508 (2011).
- [330] R. G. Edwards *et al.*, arXiv:1212.5236 [hep-ph].
- [331] J. J. Dudek and R. G. Edwards, Phys. Rev. D **85**, 054016 (2012).
- [332] D. B. Lichtenberg, Phys. Rev. **178**, 2197 (1969).
- [333] W. Roberts and M. Pervin, Int. J. Mod. Phys. A **23**, 2817 (2008).
- [334] C. Albertus *et al.*, Nucl. Phys. A **740**, 333 (2004).
- [335] D. Ebert *et al.*, Phys. Lett. B **659**, 612 (2008).
- [336] S. Migura *et al.*, Eur. Phys. J. A **28**, 41 (2006).
- [337] H. Garcilazo *et al.*, J. Phys. G **34**, 961 (2007).
- [338] S. M. Gerasyuta and D. V. Ivanov, Nuovo Cim. A **112**, 261 (1999).
- [339] S. M. Gerasyuta and E. E. Matskevich, Int. J. Mod. Phys. E **17**, 585 (2008).
- [340] S. M. Gerasyuta and E. E. Matskevich, Int. J. Mod. Phys. E **18**, 1785 (2009).
- [341] R. A. Briceno *et al.*, Phys. Rev. D **86**, 094504 (2012).
- [342] A. Ali Khan *et al.*, Phys. Rev. D **62**, 054505 (2000).
- [343] G. 't Hooft, Nucl. Phys. B **72**, 461 (1974).
- [344] E. E. Jenkins, Ann. Rev. Nucl. Part. Sci. **48**, 81 (1998).
- [345] E. Witten, Nucl. Phys. B **160**, 57 (1979).
- [346] E. Witten, Nucl. Phys. B **149**, 285 (1979).
- [347] E. Witten, Nucl. Phys. B **145**, 110 (1978).
- [348] J. L. Goity and N. Matagne, Phys. Lett. B **655**, 223 (2007).
- [349] N. Matagne and F. Stancu, Phys. Rev. D **74**, 034014 (2006).
- [350] C. E. Carlson and C. D. Carone, Phys. Lett. B **484**, 260 (2000).
- [351] For a recent review, see Z. Fodor and C. Hoelbling, Rev. Mod. Phys. **84**, 449 (2012).
- [352] See the review by S. Hashimoto, J. Laiho and S. R. Sharpe in [1].
- [353] See, for example, G. P. Engel, C. B. Lang, D. Mohler and A. Schafer, arXiv:1303.4198 [hep-lat].
- [354] See, for example, M. Neubert, Phys. Rept. **245**, 259 (1994).
- [355] J. F. Donoghue *et al.*, Phys. Rev. D **12**, 2875 (1975).
- [356] F. X. Lee, Nucl. Phys. A **791**, 352 (2007).
- [357] J. A. Oller *et al.*, Prog. Part. Nucl. Phys. **45**, 157 (2000).
- [358] T. D. Cohen and L. Y. Glozman, Phys. Rev. D **65**, 016006 (2001).

- [359] S. J. Brodsky, Eur. Phys. J. A **31**, 638 (2007).
- [360] F. X. Lee, JLAB-THY-02-88.
- [361] E. Klempt and B. C. Metsch, Eur. Phys. J. A **48**, 127 (2012).
- [362] E. Klempt and A. Zaitsev, Phys. Rept. **454**, 1 (2007).
- [363] V. Crede and C. A. Meyer, Prog. Part. Nucl. Phys. **63**, 74 (2009).
- [364] C. A. Meyer and Y. Van Haarlem, Phys. Rev. C **82**, 025208 (2010).
- [365] T. Hyodo and D. Jido, Prog. Part. Nucl. Phys. **67**, 55 (2012).
- [366] E. Oset and A. Ramos, Nucl. Phys. A **635**, 99 (1998).
- [367] J. A. Oller and U. G. Meissner, Phys. Lett. B **500**, 263 (2001).
- [368] K. H. Hicks, Prog. Part. Nucl. Phys. **55**, 647 (2005).
- [369] D. Diakonov, V. Petrov and M. V. Polyakov, Z. Phys. A **359**, 305 (1997).
- [370] V. Kuznetsov *et al.*, Phys. Lett. B **647**, 23 (2007).
- [371] V. Kuznetsov *et al.*, Phys. Rev. C **83**, 022201 (2011).
- [372] J. K. S. Man *et al.*, Phys. Rev. C **83**, 055201 (2011).